



National Library
of Canada

Bibliothèque nationale
du Canada

Canadian Theses Service

Service des thèses canadiennes

Ottawa, Canada
K1A 0N4

NOTICE

The quality of this microform is heavily dependent upon the quality of the original thesis submitted for microfilming. Every effort has been made to ensure the highest quality of reproduction possible.

If pages are missing, contact the university which granted the degree.

Some pages may have indistinct print especially if the original pages were typed with a poor typewriter ribbon or if the university sent us an inferior photocopy.

Reproduction in full or in part of this microform is governed by the Canadian Copyright Act, R.S.C. 1970, c. C-30, and subsequent amendments.

AVIS

La qualité de cette microforme dépend grandement de la qualité de la thèse soumise au microfilmage. Nous avons tout fait pour assurer une qualité supérieure de reproduction.

S'il manque des pages, veuillez communiquer avec l'université qui a conféré le grade.

La qualité d'impression de certaines pages peut laisser à désirer, surtout si les pages originales ont été dactylographiées à l'aide d'un ruban usé ou si l'université nous a fait parvenir une photocopie de qualité inférieure.

La reproduction, même partielle, de cette microforme est soumise à la Loi canadienne sur le droit d'auteur, SRC 1970, c. C-30, et ses amendements subséquents.

UNIVERSITY OF ALBERTA

Susceptibility of 420 Martensitic Stainless Steel to Cracking
in H₂S/CO₂/Cl⁻ Environments

BY

Tarek Milleti

A thesis submitted to the Faculty of Graduate Studies and Research in partial fulfillment of the requirements for the degree of Master of Science.

IN

Metallurgical Engineering

DEPARTMENT OF MINING, METALLURGICAL AND
PETROLEUM ENGINEERING

EDMONTON, ALBERTA
SPRING 1992



National Library
of Canada

Bibliothèque nationale
du Canada

Canadian Theses Service Service des thèses canadiennes

Ottawa, Canada
K1A 0N4

The author has granted an irrevocable non-exclusive licence allowing the National Library of Canada to reproduce, loan, distribute or sell copies of his/her thesis by any means and in any form or format, making this thesis available to interested persons.

The author retains ownership of the copyright in his/her thesis. Neither the thesis nor substantial extracts from it may be printed or otherwise reproduced without his/her permission.

L'auteur a accordé une licence irrévocable et non exclusive permettant à la Bibliothèque nationale du Canada de reproduire, prêter, distribuer ou vendre des copies de sa thèse de quelque manière et sous quelque forme que ce soit pour mettre des exemplaires de cette thèse à la disposition des personnes intéressées.

L'auteur conserve la propriété du droit d'auteur qui protège sa thèse. Ni la thèse ni des extraits substantiels de celle-ci ne doivent être imprimés ou autrement reproduits sans son autorisation.

ISBN 0-315-73089-7

Canada

UNIVERSITY OF ALBERTA
RELEASE FORM

NAME OF AUTHOR: Tarek Milleti

TITLE OF THESIS: Susceptibility of 420 Martensitic Stainless Steel to Cracking
in H₂S/CO₂/Cl⁻ Environments

DEGREE: Master of Science in Metallurgical Engineering

YEAR THIS DEGREE GRANTED: Spring 1992

Permission is hereby granted to the University of Alberta Library to reproduce single copies of this thesis and to lend or sell such copies for private, scholarly or scientific research purposes only.

The author reserves all other publication and other rights in association with the copyright in the thesis, and except as hereinbefore provided neither the thesis nor any substantial portion thereof may be printed or otherwise reproduced in any material form whatever without the authors prior written permission.

(SIGNED)

PERMANENT ADDRESS:

P.O. Box 3460.

TRIPOLI - LIBYA.

Date *23 April* 1992

UNIVERSITY OF ALBERTA

FACULTY OF GRADUATE STUDIES AND RESEARCH

The undersigned certify that they have read, and recommend to the Faculty of Graduate Studies and Research for acceptance, a thesis entitled SUSCEPTIBILITY OF 420 MARTENSITIC STAINLESS STEEL TO CRACKING IN H₂S/CO₂/Cl⁻ ENVIRONMENTS submitted by TAREK MILLETI in partial fulfillment of the requirements for the degree of MASTER OF SCIENCE in METALLURGICAL ENGINEERING.

Supervisor: S.A. Bradford
S.A. Bradford

Committee: B.M. Patchett
B.M. Patchett

H. Hencin
H. Hencin

F. Ellyin
F. Ellyin

J.M. Whiting
J.M. Whiting

Date 21 April 1992

Dedication

To my parents

Abstract

The commercial, high strength steels developed for sour well services are mostly quenched and tempered steels. The purpose of this study was to determine the effect of tempering temperature, P_{H_2S} and P_{CO_2} on sulfide stress corrosion (SSC) cracking and/or stress corrosion cracking (SCC) resistance of AISI 420 martensitic stainless steel. Slow strain rate tests were used to evaluate the SSC and/or SCC susceptibility at 22°C in 0.5% acetic acid - 5% NaCl solutions saturated with N_2 , with 90% H_2S /10% CO_2 , with 50% H_2S /50% CO_2 , with 10% H_2S /90% CO_2 and with 100% CO_2 .

It was found that the susceptibility to SSC and/or SCC is strongly affected by tempering temperature. Tempering at 750°C produces the most favourable microstructure for SSC resistance, that is a well-recovered substructure with fine carbides. Moreover, the predominant intergranular cracking of (0.38%C) 420 steel was directly related to the precipitation of the closely spaced carbide particles along the prior austenite grain boundaries.

Regardless of the tempering temperature, high susceptibility to SSC was evidenced in H_2S -containing solutions, where above 10% H_2S the degree of susceptibility is only slightly dependent on the H_2S concentration. The addition of CO_2 to H_2S -containing solutions does not affect the acidity of the solutions, but it slightly lowers the aggressiveness of the test solutions. Also, superior SSC cracking resistance of this steel in CO_2/Cl^- environment over that in $H_2S/CO_2/Cl^-$ was evidenced, due to the absence of hydrogen embrittlement. On the other hand, the steel showed much better SCC resistance in CO_2 -free and H_2S -free chloride solutions.

Acknowledgement

I would like to express my appreciation for the guidance and help of, my supervisor, Dr. S.A. Bradford.

The assistance of the following staff members of the department is gratefully acknowledged: Bob Konzuk, Bob Smith, Doug Booth, Henryk Skrzypek, Rob Stefaniuk, Shiraz Merali and Tina Barker.

This thesis was financially assisted by the Mining, Petroleum and Metallurgical Engineering Department, University of Alberta. The support and help of the department chairman Dr. J. Whiting is greatly appreciated.

TABLE OF CONTENTS

| CHAPTER | PAGE |
|---|------|
| 1. INTRODUCTION | 1 |
| 2. ROLES OF H ₂ S IN DEGRADATION OF Fe-BASE ALLOYS | 3 |
| 2.1 HYDROGEN SULFIDE CORROSION | 3 |
| 2.2 SULFIDE STRESS CORROSION CRACKING | 5 |
| 2.3 MECHANISMS OF SULFIDE STRESS CRACKING | 6 |
| 2.3.1 HYDROGEN EMBRITTLEMENT CRACKING MECHANISMS | 7 |
| 2.3.2 STRESS CORROSION CRACKING MECHANISMS | 7 |
| 2.4 FACTORS INFLUENCING SULFIDE STRESS CORROSION CRACKING | 8 |
| 2.4.1 ENVIRONMENTAL FACTORS | 9 |
| 2.4.2 METALLURGICAL FACTORS | 10 |
| 2.5 HYDROGEN-INDUCED (STEPWISE) CRACKING (HIC) | 14 |
| 2.6 FACTORS INFLUENCING HIC | 15 |
| 2.6.1 ENVIRONMENTAL FACTORS | 15 |
| 2.6.2 METALLURGICAL FACTORS | 16 |
| 3. ROLES OF CO ₂ IN DEGRADATION OF Fe-BASE ALLOYS | 19 |
| 3.1 CO ₂ CORROSION MECHANISM | 20 |
| 3.2 ENVIRONMENTAL FACTORS INFLUENCING CO ₂ CORROSION | 21 |
| 3.3 PREVENTION OF CO ₂ CORROSION | 25 |

| | | |
|-----------|---|-----------|
| 4. | CORROSION AND SSC IN H₂S/CO₂/Cl⁻ ENVIRONMENT | 26 |
| 4.1 | SSC OF MARTENSITIC STAINLESS STEEL IN H ₂ S/CO ₂ /Cl ⁻ SYSTEMS | 27 |
| 4.2 | HYDROGEN EMBRITTLEMENT OF MARTENSITIC STAINLESS STEEL IN H ₂ S/CO ₂ /Cl ⁻ ENVIRONMENTS | 28 |
| 5. | CORROSION RESISTANT MATERIALS | 30 |
| 5.1 | 9Cr - 1Mo STEEL | 31 |
| 5.2 | 13Cr STEELS | 33 |
| | 5.2.1 AISI 410 | 35 |
| | 5.2.2 AISI 420 | 37 |
| 5.3 | α - γ DUPLEX STAINLESS STEEL | 38 |
| 6. | HEAT TREATMENT OF STAINLESS STEEL | 40 |
| 6.1 | C-Cr-Fe PHASE DIAGRAM | 40 |
| 6.2 | MARTENSITIC STAINLESS STEELS | 41 |
| 6.3 | HEAT TREATMENT OF MARTENSITIC STAINLESS STEELS | 42 |
| 7. | SCC AND SSC TEST METHODS | 45 |
| 7.1 | CONSTANT STRAIN AND CONSTANT LOAD TEST METHODS | 45 |
| 7.2 | SLOW STRAIN RATE TEST | 46 |

| | | |
|--------------------------|--|-----------|
| Experimental Part | | |
| 8. | MATERIAL AND SOLUTIONS | 48 |
| 8.1 | MATERIAL | 48 |
| 8.2 | TEST SOLUTIONS | 48 |
| 9. | EXPERIMENTAL PROCEDURES | 48 |
| 9.1 | MICROSTRUCTURE OF THE STEEL | 48 |
| 9.1.1 | SPECIMEN PREPARATION | 49 |
| 9.1.2 | SPECIMEN HEAT TREATING | 49 |
| 9.1.3 | HARDNESS MEASUREMENT | 49 |
| 9.1.4 | EXAMINATION WITH THE MICROSCOPE | 50 |
| 9.1.5 | X-RAY DIFFRACTION | 51 |
| 9.2 | SLOW STRAIN RATE TESTS (SSRT) | 51 |
| 9.2.1 | SPECIMEN PREPARATION | 51 |
| 9.2.2 | SPECIMEN HEAT TREATING | 51 |
| 9.2.3 | EQUIPMENT | 52 |
| 9.2.3.1 | THE MATERIAL TEST SYSTEM | 52 |
| 9.2.3.2 | TESTING CELL | 53 |
| 9.2.3.3 | RECIRCULATION SYSTEM | 53 |
| 9.2.4 | TEST PROCEDURE | 54 |
| 9.2.5 | VISUAL AND MICROSCOPIC FRACTURE EXAMINATION | 55 |
| 10. | RESULTS AND DISCUSSION | 56 |
| 10.1 | MICROSTRUCTURE AND HARDNESS | 56 |
| 10.2 | STRESS-TIME CURVES | 59 |
| 10.2.1 | STEEL QUENCHED AND TEMPERED AT 550°C | 59 |
| 10.2.2 | STEEL QUENCHED AND TEMPERED AT 650°C | 60 |

| | | |
|------------|--|------------|
| 10.2.3 | STEEL QUENCHED AND TEMPERED AT 750°C | 61 |
| 10.2.4 | STEEL QUENCHED AND TEMPERED AT 850°C | 63 |
| 10.3 | FRACTURE APPEARANCE | 64 |
| 10.3.1 | STEEL QUENCHED AND TEMPERED AT 550°C | 64 |
| 10.3.2 | STEEL QUENCHED AND TEMPERED AT 650°C | 64 |
| 10.3.3 | STEEL QUENCHED AND TEMPERED AT 750°C | 65 |
| 10.3.4 | STEEL QUENCHED AND TEMPERED AT 850°C | 66 |
| 10.4 | EVALUATION OF SLOW STRAIN RATE TEST (SSRT) RESULTS | 67 |
| 10.4.1 | INDICATION OF SSC SUSCEPTIBILITY | 67 |
| 10.4.2 | MEASUREMENT OF SSC SEVERITY | 67 |
| 10.4.3 | CHLORIDE STRESS CORROSION CRACKING | 68 |
| 10.4.4 | SSC CRACKING IN H ₂ S/CO ₂ SOLUTIONS | 71 |
| 10.4.5 | SCC IN CO ₂ SOLUTIONS | 73 |
| 11. | CONCLUSIONS | 75 |
| | REFERENCES | 138 |

List of Tables

| Table | Page |
|---|------|
| 1. A Short History of Investigations on CO ₂ Corrosion | 76 |
| 2. SCC of 13Cr Steel Test Conditions | 76 |
| 3. The Results of SCC Tests in CO ₂ / H ₂ S Environments | 77 |
| 4. Typical High-Alloy Materials Being Considered for Corrosive Oilfield Service | 77 |
| 5. Chemical Composition of Selected Alloy Steels | 78 |
| 6. The Chemical Composition of Steel Used | 78 |
| 7. Test Conditions | 78 |
| 8. Slow Strain Rate Test Results | 79 |
| 9. Severity of the Slow Strain Rate Tests | 80 |

List of Figures

| Figure | Page |
|---|------|
| 1. Mechanism of Pitting Corrosion in a Sour Gas System | 81 |
| 2. Weight-Loss Corrosion of Low-Alloy Steel versus pH in Solution of Water and H ₂ S-CC ₂ Gas Mixture | 81 |
| 3. Failure Times as a Function of pH, with and without H ₂ S | 82 |
| 4. Effect of H ₂ S and pH on Sulfide Stress Cracking of P-110 Casing | 82 |
| 5. Temperature for Sulfide Stress Cracking Resistance Behavior versus Material Yield Strength for API Casing Steels | 83 |
| 6. Time to Failure for Sulfide Stress Cracking versus Temperature for a HSLA (C-Mn) Steel | 83 |
| 7. Equilibrium Potential pH Diagram with Stress Corrosion Results on 12 Mo -V Stainless in 3% NaCl Solution | 84 |
| 8. Formation of Hydrogen Blister in Steel | 84 |
| 9. A Schematic of Stepwise Cracking in Line-Pipe Steel | 85 |
| 10. A Schematic Diagram of Factors Affecting Hydrogen Sulfide Induced Cracking | 85 |
| 11. Effect of pH value on Stepwise -Cracking Behavior for API Line-Pipe Steel | 86 |
| 12. Effect of Temperature on Stepwise-Cracking Behavior for API Line-Pipe Steels with Various Modifications | 87 |
| 13. Effect of CO ₂ Partial Pressure and Temperature on Corrosion Rate of Cr Steel | 88 |
| 14. Effect of Cl ⁻ Ion Concentration on the Corrosion Rate of Cr Steel at 150°C | 89 |
| 15. Effect of Temperature and a Small Amount of H ₂ S on Corrosion Rate (Cr Steel) | 89 |

| Figure | Page |
|--|------|
| 16. Stress-Time to Failure Curves of a 0.2%C-13%Cr Steel Under Conditions iv, v, vi and vii Shown in Table (2) | 90 |
| 17. Effect of Yield Strength on SCC Susceptibility of 13Cr Steels | 90 |
| 18. Effect of Current Density for Hydrogen Charging on Degree of Hydrogen Embrittlement, $(E_{I_H}/E_{I_{air}})$, Measured by SSRT Testing | 91 |
| 19. Comparison of (a) Anodic Stress Corrosion Cracking and (b) Hydrogen-Embrittlement Cracking | 91 |
| 20. Effect of H ₂ S Partial Pressure and Temperature on Susceptibility to SSC | 92 |
| 21. Effect of H ₂ S Partial Pressure and Strength of 9Cr-1Mo and 13Cr Steels on Susceptibility to SSC | 93 |
| 22. The Relationship Between Tempering Temperature and Tensile Properties | 94 |
| 23. The Relationship Between Tempering Temperature, Yield Strength, Tensile Strength and Impact Resistance | 94 |
| 24. Effect of H ₂ S Partial Pressure and pH on SSC Susceptibility of L-80 Grade 13Cr Steel | 95 |
| 25. Effect of Tempering Temperature on the Mechanical Properties of Type 410 Stainless Steel | 96 |
| 26. Effect of Rockwell Hardness on Time-to-Failure of Type 410 and 416 Stainless Steels | 97 |
| 27. Intergranular Cracking of Type 410 Stainless Steel | 97 |
| 28. Transgranular Cracking of Type 410 Stainless Steel | 98 |
| 29. SSC and Three Martensitic Stainless Steels | 98 |
| 30. Effect of H ₂ S Partial Pressure and Temperature on Susceptibility to SSC of 22-25Cr α - γ Duplex Stainless Steel | 99 |

| Figure | Page |
|--|------|
| 31. The Iron-Chromium Equilibrium Diagram | 100 |
| 32. Vertical Section at 13% Chromium | 100 |
| 33. Effect of Carbon on the Fe-Cr Diagram (0.4%C) | 101 |
| 34. Effect of Chromium Additions on the Temperature and Carbon Content of the $\gamma \leftrightarrow \alpha + M_3C$ Eutectoid | 101 |
| 35. The Effect of Carbon on the Hardness of Martensite and Austenite | 102 |
| 36. The Effect of Chromium on the Tempering of a 0.35 C Steel | 103 |
| 37. Effect of Tempering Temperature on Tensile Properties and Hardness of Type 420 Martensitic Stainless Steels | 104 |
| 38. Tensile Test Specimen | 105 |
| 39. Material Test System | 105 |
| 40. Data Acquisition System | 106 |
| 41. Test Cell | 107 |
| 42. Attached Nylon Sleeves | 108 |
| 43. Recirculation System | 108 |
| 44. The Microstructure of As-Received Material | 109 |
| 45. The Microstructure of the 420 Steel after Air Cooling from 1150°C | 109 |
| 46. The General Microstructure of 420 Steel Tempered at 550°C | 110 |
| 47. The General Microstructure of 420 Steel Tempered at 650°C | 110 |
| 48. The General Microstructure of 420 Steel Tempered at 750°C | 111 |
| 49. Carbide Distribution in 420 Steel Tempered at 550°C | 111 |
| 50. Carbide Distribution in 420 Steel Tempered at 650°C | 112 |

| Figure | Page |
|---|------|
| 51. Carbide Distribution in 420 Steel Tempered at 750°C | 112 |
| 52. The Microstructure of 420 Steel Tempered at 800°C | 113 |
| 53. Carbide Distribution in 420 Steel Tempered at 800°C | 113 |
| 54. Martensite Hardness versus Carbon Content | 114 |
| 55. The General Microstructure of 420 Steel Tempered at 850°C | 114 |
| 56. Carbide Distribution in 420 Steel Tempered at 850°C | 115 |
| 57. Stress versus Time Curve for Specimen 1 SSRT | 115 |
| 58. Stress versus Time Curve for Specimen 2 SSRT | 116 |
| 59. Stress versus Time Curve for Specimen 3 SSRT | 116 |
| 60. Stress versus Time Curve for Specimen 4 SSRT | 117 |
| 61. Secondary Cracks in the Reduced Section of Specimen Failed with SSC | 117 |
| 62. Stress versus Time Curve for Specimen 5 SSRT | 118 |
| 63. Stress versus Time Curve for Specimen 6 SSRT | 118 |
| 64. Stress versus Time Curve for Specimen 7 SSRT | 119 |
| 65. Stress versus Time Curve for Specimen 8 SSRT | 119 |
| 66. Stress versus Time Curve for Specimen 9 SSRT | 120 |
| 67. Stress versus Time Curve for Specimen 10 SSRT | 120 |
| 68. Stress versus Time Curve for Specimen 11 SSRT | 121 |
| 69. Stress versus Time Curve for Specimen 12 SSRT | 121 |
| 70. Stress versus Time Curve for Specimen 13 SSRT | 122 |
| 71. Stress versus Time Curve for Specimen 14 SSRT | 122 |
| 72. Stress versus Time Curve for Specimen 15 SSRT | 123 |
| 73. Stress versus Time Curve for Specimen 16 SSRT | 123 |

| Figure | Page |
|---|------|
| 74. Stress versus Time Curve for Specimen 17 SSRT | 124 |
| 75. Stress versus Time Curve for Specimen 18 SSRT | 124 |
| 76. Stress versus Time Curve for Specimen 19 SSRT | 125 |
| 77. SEM Fractograph of Specimen 1 | 125 |
| 78. SEM Fractograph of Specimen 2 (Brittle Fracture Zone) | 126 |
| 79. SEM Fractograph of Specimen 2 (Ductile Fracture Zone) | 126 |
| 80. SEM Fractograph of Specimen 3 | 127 |
| 81. SEM Fractograph of Specimen 4 | 127 |
| 82. SEM Fractograph of Specimen 5 | 128 |
| 83. SEM Fractograph of Specimen 6 | 128 |
| 84. SEM Fractograph of Specimen 7 | 129 |
| 85. SEM Fractograph of Specimen 8 | 129 |
| 86. SEM Fractograph of Specimen 9 | 130 |
| 87. SEM Fractograph of Specimen 9 | 130 |
| 88. SEM Fractograph of Specimen 10 | 131 |
| 89. SEM Fractograph of Specimen 11 | 131 |
| 90. SEM Fractograph of Specimen 12 | 132 |
| 91. SEM Fractograph of Specimen 13 | 132 |
| 92. SEM Fractograph of Specimen 14 | 133 |
| 93. SEM Fractograph of Specimen 15 | 133 |
| 94. SEM Fractograph of Specimen 16 | 134 |
| 95. SEM Fractograph of Specimen 17 | 134 |
| 96. SEM Fractograph of Specimen 18 | 135 |

| Figure | Page |
|--|------|
| 97. SEM Fractograph of Specimen 19 | 135 |
| 98. SEM Fractograph Shows the Quasicleavage and the Brittle Fracture | 136 |
| 99. Stress versus Time Curves for 420 Stainless Steel Tempered at 650°C | 136 |
| 100. Stress versus Time Curves for 420 Stainless Steel Tempered at 750°C | 137 |
| 101. Stress versus Time Curves for 420 Stainless Steel Tempered at 850°C | 137 |

1. INTRODUCTION

The production of oil and gas from the reservoirs that contain significant amounts of hydrogen sulfide (H_2S) and carbon dioxide (CO_2) has been promoted as the demand for energy increases. Deep sour oil wells involve an environment containing hydrogen sulfide so that corrosion of equipment and failures due to sulfide stress cracking are usually encountered.

Likewise, enhanced recovery using carbon dioxide injection, as well as the production of CO_2 wells, is expected to encounter some corrosion problems¹. The corrosion problems would not be as severe as those encountered and/or anticipated in deep sour gas wells. However, the high pressure and temperature, along with the presence of H_2S and chloride ions in the CO_2 environments, can induce severe corrosion attack in the forms of high corrosion rates, localized corrosion and/or stress corrosion cracking (SCC).

Over the years, intensive research efforts have been aimed at examining the behavior of low alloy steels in H_2S environments. In contrast, the highly alloyed stainless steels were not studied extensively, due to their higher cost, as a result very little information is readily available on the performance of a variety of highly alloyed stainless steels in H_2S/CO_2 environments that contain chlorides.

The materials technology has centered around the need for high strength and corrosion resistant materials that can withstand the high temperatures, high pressures and the presence of significant quantities of corrosive gases such as H_2S and CO_2 and aggressive species such as chlorides and sulphur compounds. 13% chromium (Cr) stainless steels have attracted attention for application in these areas, particularly where the oil and gas contain high levels of CO_2 along with low levels of H_2S , because they offer improved corrosion resistance in comparison with low alloy steels². 13% Cr steels have performed satisfactorily in such applications when used in a quenched and tempered condition with hardness below Rc 22. However,

a main concern in the use of 13% Cr steels is their susceptibility to localized corrosion and sulfide stress corrosion (SSC) cracking in the presence of H₂S. Furthermore, increased corrosion resistance is required when gas or oil wells have high CO₂ concentrations which lower the pH of well brines and make them more corrosive.

It has been recognized that 13% Cr steels are sensitive to SSC more than quenched and tempered low alloy steels, but there are few works on this matter^{3,4}. Until recently, low alloy steel tubulars have been used in combination with corrosion inhibitors in gas or oil wells containing H₂S, CO₂ and salt water. This practice is very expensive, however. Moreover, the efficiency of inhibitors is reduced in high temperature wells. Under these conditions, the alternative of using special corrosion-resistant alloy tubulars has been considered. Some data from field and laboratory tests are available regarding the corrosion and environmental cracking behavior of 13% Cr martensitic stainless steels, such as AISI 410 in H₂S/CO₂/Cl⁻ environments⁴. However, relatively little data exist regarding the performance of higher carbon grades of 13% Cr martensitic steels such as AISI 420.

A characteristic feature of 13% Cr steel is that the microstructure is affected significantly by the chemical composition, especially the carbon content. Increasing the carbon content generally increases the SSC cracking susceptibility; this is due to the influence that carbon has on the microstructure and on the hardness. From the point of view that the SSC resistance of these steels is expected to be affected by the change in microstructure, the effect of tempering temperature on the susceptibility of 13% Cr steel, AISI 420, to SSC and the effect of CO₂ additions to H₂S/Cl⁻/H₂O environments on the resistance of this type of steel is investigated in this thesis.

2. ROLES OF H₂S IN DEGRADATION OF IRON BASE ALLOYS

A consideration which has remained paramount over the past several decades of research has been the role of H₂S in the degradation of engineering materials. In addition to being extremely toxic, H₂S is responsible for corrosion and environmental embrittlement in common materials of construction in industry. Consequently, it has been necessary to develop special materials and processing methods which minimize the effects of corrosive degradation and maximize the integrity of oil and gas production systems.

2.1 HYDROGEN SULFIDE CORROSION

The corrosion of steel by aqueous hydrogen sulfide is a significant technical problem in two major industrial areas. In oil refineries and/or oil production and in natural gas treatment facilities, the process conditions vary widely due to natural causes. It is well known that hydrogen sulfide accelerates the anodic dissolution of iron. Upon the addition of H₂S, the corrosion potential becomes more noble and the current density at a given potential increases.

The initial corrosion of iron or carbon steel by H₂S-saturated water at low temperatures is complex. There is a considerable confusion regarding corrosion product identity in the earlier literature, but it is now established that the initial corrosion involves the formation of up to three iron monosulfide phases⁵: mackinawite (tetragonal FeS_{1-x}), cubic ferrous sulfide and troilite (stoichiometric hexagonal FeS). The order of stability is troilite > mackinawite > cubic ferrous sulfide⁸.

Corrosion rates of low alloy steels in H₂S-containing production environments can be high (> 2.5 mm/y) with the attack commonly exhibiting pitting or other manifestations of localized corrosion. Such attack has been observed under FeS corrosion product as shown in Figure 1. Mechanisms for this type of corrosion

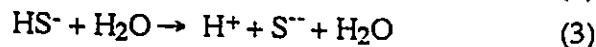
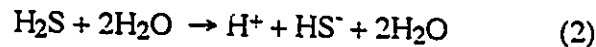
attack have been proposed which involve galvanic interaction between the steel and FeS surface in the presence of FeCl₂ ⁶.

Corrosion rates of low alloy steels in H₂S-containing environments tend to increase with decreasing pH of the aqueous solution, Figure 2. Hydrogen sulfide is stable as a dissolved species in aqueous solutions only at low pH levels (pH≤6), whereas, at higher pH levels, other S-containing species (HS⁻ and S²⁻) are stable. The corrosion of iron in the presence of H₂S and H₂O is dependent upon the dissociation of the H₂S molecule. Iron is oxidized to the ferrous form at the anode and the H₂S undergoes a two-step dissociation at the cathode. The prospective equilibrium reactions are outlined below⁷:

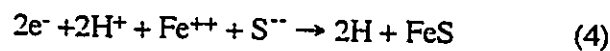
Anode



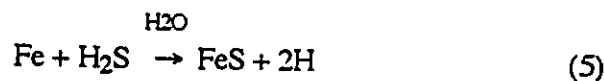
Cathode



Product combination



Net reaction



Reactions (4) and (5) indicate that ferrous sulfide or "troilite" is formed as one of the reaction products. This is not strictly correct as iron sulfide can exist in a number of molecular forms. The other forms are FeS₂, known as pyrite, Fe₇S₈, pyrrhotite, and Fe₉S₈, referred to as kansite. The kansite crystal lattice structure is much more imperfect than the pyrite or troilite; consequently, the increase in the kansite concentration leads to an increase in the corrosion rate. The particular product that is formed depends upon the operating conditions¹⁰, e.g. H₂S concentration, pH, and presence of other reactants such as chlorides and CO₂.

In conjoint action with dissolved oxygen, H_2S can be highly corrosive, both of itself and by reason of complex reaction products such as polythionic acids.

At lower pH values, it can be argued that iron ions are in large excess compared to sulfide ions, and therefore the sulfide ions in the vicinity of the metal surface are soon exhausted so that iron ions move to the bulk of the solution where iron sulfide is precipitated. In this case, no passivating sulfide film forms on the surface. On the other hand, at high pH values, the sulfide ions are in excess compared to iron ions and therefore the location of sulfide precipitation shifts to the metal surface leading to passivation. The type of sulfide film which is protective is a matter of debate⁸.

2.2 SULFIDE STRESS CORROSION (SSC) CRACKING

One of the major materials problems facing the petroleum industry is stress corrosion cracking (SCC), the failure of a material induced by the joint action of tensile stresses and a corrosive environment. The brittle fracture of high strength steels in H_2S environments and of austenitic stainless steels in chloride environments are two of the better known examples of SCC. While no one mechanism for SCC has been defined, it is generally accepted that cracking will not occur unless surface tensile stresses exceed some critical value⁹.

In many alloy systems, SCC failures of smooth surfaces occur in three distinct phases. The first phase is the incubation period in which a pit or a slip step is formed and a crack is initiated. The second phase is a state of subcritical crack growth in which the crack propagates under the joint influence of stress and environment. Assuming that the stress is maintained at a sufficiently high level, the third phase is fast fracture when the crack reaches a critical size⁹.

It is generally accepted that SSC is a form of Hydrogen Embrittlement (HE) Cracking¹⁰. However, direct evidence to this effect is limited. SSC has been found to be induced in susceptible materials by the simultaneous presence of tensile stresses and a corrosive environment containing a sufficient level of H_2S . The role

of H_2S in this phenomenon is generally considered to be two-fold : (i) it increases the rate of corrosion of steel in aqueous solutions, and (ii) it poisons the hydrogen evolution reaction. Consequently, H_2S aids in the effectiveness of hydrogen charging¹¹.

SSC is characterized by an initial, single, straight transgranular or intergranular fracture mode¹², that develops under the application of a tensile stress, either applied or residual. It occurs at right angles to the direction of the applied stress. Frequently, initiating at corrosion pits, it propagates, branches and stops¹³. Branching tends to be related to the tensile strength of the steel; low strength steels show little branching while there is considerable in high strength steels. Another feature of SSC is that it occurs frequently in association with welds^{14,15,16}. The cracks may be in the weld metal itself or in the heat affected zone.

Rc 22 and BHN 235 are most used as the hardness figures approximating the safe limits for alloys in sour service. These values have been established through field experience and are those contained in most sour service material standards. Alloys with hardness up to Rc 29 may be used successfully, depending on alloying additions and on the heat treatments¹⁷. In other cases, cracking occurred in sour environments at hardness well below Rc 22¹⁸. Probably the microstructure, not the alloy composition, governs a material's response to sulfide solutions¹⁹.

2.3 MECHANISM OF SULFIDE STRESS CRACKING

From the above discussion, it would appear that hydrogen is intimately connected with SSC failure. Most of the attributions of the role of hydrogen in SSC are based on similar cracking tendencies observed in SSC and HE tests on low-alloy steels. However, differences in SSC in Ni-containing low-alloy steels have been observed which suggest that an anodic SSC mechanism is also possible.

2.3.1 HYDROGEN EMBRITTLEMENT CRACKING MECHANISMS

The susceptibility of low alloy steels to SSC was found to be directly related to the amount of hydrogen available--not the presence or absence of H_2S ¹⁵. In the case where hydrogen embrittlement mechanism prevails, hydrogen atoms (H) are produced on the metal surface by the H_2S -steel corrosion reaction. These hydrogen atoms can combine to form molecular hydrogen at the metal surface or can diffused into the metal. Once in the materials, atomic hydrogen readily diffuses at ambient temperatures to sites of high internal stress (like grain boundaries, inclusions, regions of triaxial stress and at notches). These atoms have to migrate to the crack tip either by surface diffusion or by bulk diffusion. The hydrogen atoms have to react with the metal at the crack tip either chemically or physically to weaken the metallic bond. Generally the action of the atoms in the metal is still open to question²⁰.

In the presence of tensile stresses, the sites of high internal stress become sites for embrittlement and the initiation of brittle cracking failure. It is generally observed that SSC in high-strength steels, >100 ksi (690MPa) yield strength, appears predominantly as intergranular cracking; lower strength steels have predominantly transgranular mode but may also have a mixed intergranular/transgranular fracture mode²¹.

2.3.2 STRESS CORROSION CRACKING MECHANISMS

It has been found that nickel-containing steels exhibit different SCC and SSC tendencies than those of nickel-free steels²². Also, it has been reported that the presence of nickel as an alloying element in steel promotes increased susceptibility to cracking²³, and specifications have been issued²⁴ limiting this element from material for service in sour conditions. The effect of nickel on the stress corrosion cracking behaviour of ferritic steel weld metal has been studied by Gooch²⁵. He found that nickel (0 - 2.2%Ni) had no adverse effect on SCC resistance of ferritic

steel weld metal under NACE conditions. In addition, these nickel-containing steels show a reduced tendency to SSC with applied cathodic potentials²⁶. This is opposite to the effect expected if hydrogen embrittlement cracking mechanisms were operating and also indicative of the behavior that would persist if anodic mechanisms were present. However, some controversy still exists regarding this matter.

2.4 FACTORS INFLUENCING SSC

Cracking of high-strength steels in H₂S environments has been a serious problem in the oil industry for a number of years. Owing to the absence of economical alternative alloys, considerable effort has been devoted to studying factors controlling SSC so as to define as accurately as possible the safe limits for use of high-strength steels in oil field and refinery applications.

The five major factors on which the SSC process depend are²⁷:

- (1) absorption of sufficient quantity of nascent hydrogen,
- (2) a total tensile stress of sufficient or critical magnitude,
- (3) a susceptible metallurgical condition in the steel, and
- (4) time.
- (5) temperature

In other words, a critical combination of these five factors is required for SSC of steel. If any of these factors is absent, or is of insufficient or critical magnitude, failure will not occur.

There is increasing evidence that nascent hydrogen absorbed by steel under stress may be the major, if not the sole, factor responsible for the failure process when it occurs in a very short period of time^{28,29}. It is true that corrosion of the metal by aqueous H₂S is the source of the nascent hydrogen absorbed by the steel. Of course corrosion can contribute to the failure process by developing sites (pits) for concentration of stresses so that fracturing may occur under circumstances

where the failure would not have occurred in steel charged with hydrogen if the corrosion had not taken place.

2.4.1 ENVIRONMENTAL FACTORS

The three paramount environmental variables are solution pH, environmental temperature, and H₂S concentration.

2.4.1.1 pH

The effect of pH has been examined by Hudgins et al.³⁰, Treseder and Swanson²³, Dvoracek³¹, and Miller and Van Rosenberg³². Hudgins performed time to failure experiments on 33 Rc hardness material in two environments, (Figure 3). He found that H₂S-containing solutions were much more potent cracking environments than those containing HCl or HCl + CO₂. Dvoracek used fatigue-precracked samples of API P-110 to study both pH and H₂S concentration effects, Figure 4. Increasing pH alleviates SSC; however, stronger steels require higher pHs for safe operation. The reason for this behavior appears to be the decrease in ability to charge hydrogen into steels in aqueous media with increasing pH³³.

2.4.1.2 TEMPERATURE

Sulfide stress cracking is a highly temperature-dependent phenomenon and this has been used effectively in the design of downhole tubular components used in sour gas applications. As shown in Figure 5, SSC susceptibility decreases with increasing temperature over the range 25-200°C³⁴. Hudgins³⁵ showed that a marked reduction in cracking susceptibility occurred in the region between 22° and 66°C with a maximum no-failure hardness increasing from 15 Rc at 24°C to 35 Rc at 93°C. Using this relationship, high-strength steels which would normally be expected to exhibit SSC at ambient temperatures can be utilized without cracking failure when continually exposed to elevated temperatures which exist downhole. It

has also been observed that SSC susceptibility is greatest at about 25°C, Figure 6³⁶. The decreased susceptibility at low temperatures is due to decrease in corrosion or diffusion rate but decreased susceptibility at high temperatures remains to be explained, although observed repeatedly.

2.4.1.3 HYDROGEN SULFIDE CONCENTRATION

Hydrogen sulfide concentration studies have been made by Hudgins et al.³⁰, Treseder and Swanson²³, McGlasson and Greathouse³⁷, and Greco and Brickell³⁸. It has been commonly observed that SSC susceptibility of steel alloys increases with increasing H₂S concentration. Where the level of H₂S at which high strength steels can be used without exhibiting failures at less than their yield strength is a function of both strength level of the materials and the H₂S concentration. In general, it was found that weaker solutions take longer to promote cracking and require stronger material before cracking begins. In field applications, it is common practice to use only those steels manufactured to restricted strength ranges and hardness levels when the concentration of H₂S in the production processes exceeds 350 Pa (H₂S partial pressure) or 50 ppm H₂S²⁶.

2.4.1.4 APPLIED POTENTIAL

Both anodic and cathodic applied potentials have been shown to affect SSC, Figure 7. Cathodic polarization is used to charge samples with hydrogen and as such could be expected to promote hydrogen embrittlement. Anodic polarization causes corrosion and might be expected to promote an active path corrosion cracking failure. SSC is considered to be closely related to hydrogen embrittlement, and cathodic protection would be expected to worsen the SSC resistance of high-strength steel²⁷.

It is now well established that SSC and/or SCC in any metal-environment system only occurs within a specific range of potentials. The potential range in which cracking occurs depends upon solution composition and temperature.

2.4.2 METALLURGICAL FACTORS

There are a number of important metallurgical variables which affect the susceptibility of steel alloys to SSC. Some of these factors are discussed below.

2.4.2.1 MICROSTRUCTURE

Although hardness is used as the criterion for determining an alloy's resistance to cracking in sour environments, microstructure is an aspect that should be given as much attention. Many recent SSC investigations involving hardness or strength are now concerned with changes in susceptibility as a result of microstructure changes. For instance, fine grained acicular ferrite has greater resistance to cracking than does a tempered martensitic structure of the same hardness due to the relatively low strength of ferrite phase^{39,40}.

Tempered structures with spheroidized carbides present the greatest resistance to cracking. In high strength, low alloy materials, evidence of the superiority of quenched and tempered (Q & T) martensitic microstructures over normalized (N) or normalized and tempered (N & T) structures has become massive⁴¹. Brickell et al.⁴² found hydrogen penetration to be slower in martensitic structures than in normalized structures, also they found that untempered martensite had a lower penetration rate than tempered martensite.

Retained austenite and/or austenite phase, under stress, can transform very slowly to untempered martensite which is extremely susceptible to cracking. Thus, soft materials can sometimes exhibit poor resistance to SSC; in other words, hardness can be a poor indicator of SSC performance⁴³.

Heat treatment, therefore, must involve, first, temperatures high enough to affect the structure and, second, rapid cooling. Care must be exercised in controlling tempering temperatures as a fully quenched and tempered martensitic structure must be obtained.

2.4.2.2 ALLOYING ELEMENTS

Alloying elements must be selected carefully to prevent weak structures or excessive hard zones.

The carbon content of steels used in sour environments can have a great influence on the SSC resistance. Increasing the carbon content generally increases the SSC cracking susceptibility⁴³. This is due to the influence that carbon has on the microstructure and on the hardness. As the carbon content increases, there is a greater potential for retaining low transformation-temperature structures upon cooling from heat treating conditions. Consequently, tempering is extremely critical. The influence of carbon is usually determined, in welding, through use of an empirical relationship termed the carbon equivalent (CE). This seeks to establish the hardenability characteristics of a steel based upon its chemistry. Field tests suggest that materials with CE less than 0.35 may be highly resistant to SSC provided the effects of all other alloying elements are considered⁴⁴.

An investigation done by Damie et al.⁴⁵, showed that supplementary addition of chromium (Cr) and molybdenum (Mo) and a relative decrease in the carbon content improve the corrosion resistance in the presence of CO₂ and chlorides. Chromium additions appear to have mixed effects on low alloy steels with respect to SSC. In solutions with a pH 5.0 or higher, chromium additions reduce hydrogen entry into the steel, probably through formation of chromium oxide which is a protective scale⁴⁶. As the pH decreases, the beneficial effect of Cr decreases. The positive effect disappears at a pH around 4.0. Some investigators^{47,48} showed that in solutions with a pH lower than 4.0, Cr additions produce an increase in the amount of diffusible hydrogen in the steel.

2.4.2.3 HARDNESS

The hardness versus tensile strength relationship is employed to select steels resistant to cracking. Rc 22 is considered the maximum safe hardness limit, although failure in materials with lower values has been encountered, particularly in

welds which are usually associated with high residual stresses. The failure is related to the severity of the environment and to high stresses. However, an alloy with hardness above Rc 22 can be used successfully in sour environments, provided the structure has been tempered properly.

2.4.2.4 CRACK MORPHOLOGY

SSC includes crack initiation and crack propagation phases. Cracking occurs only after an incubation period but this period may be very short. The crack initiation may be governed by the corrosivity of the environment, the presence of protective scales, and the alloy composition. Crack propagation is a function of the corrosive environment and the stress. Cracks that form under sulfide conditions generally propagate to failure in a brittle manner. Frequently, the final failure is a ductile overload fracture when the cross-section has been reduced enough to allow plastic deformation under the applied load. Fracture surfaces, therefore, tend to show both a brittle and, to a lesser extent, a ductile mode⁴⁹.

2.4.2.5 COLD WORK

When steel is bent or straightened cold, hardness can increase and residual stresses up to the yield strength of the metal may be present²³. It is very difficult to predict the magnitude and direction of these residual stresses which may be additive to service and applied stresses. Hudson et al.⁵⁰ showed that cold work would increase both the hydrogen solubility and permeability in steel.

2.4.2.6 SULFIDE CONTENT AND SHAPE

The control of sulfide content and shape is a promising area for improvement of SSC resistance. It is well known that inclusions act as good trap sites for hydrogen and that elongated inclusions in particular have a detrimental effect in promoting HE in steels. Therefore, recognizing the influence of inclusions in promoting hydrogen induced cracking (HIC) and/or SSC in sour environments,

Pressouyre⁵¹ found that steels immune to HIC in sour environments can be produced by keeping the sulfur content in the steel below 0.002% and the phosphorus content below 0.003%. Below these critical values, found for this particular desulfurization process, the sulfide inclusions become globular and more evenly distributed.

2.5 HYDROGEN-INDUCED (STEPWISE) CRACKING (HIC)

HIC of steels is as complex as SSC and many of the same variables are involved. Whereas SSC occurs only under the application of an external stress and the crack propagates at right angles to this stress, HIC can occur in the absence, or presence, of an external stress.

Resistance to HIC does not necessary mean resistance to SSC^{52,53}. In fact, it has been suggested that decreased resistance to HIC can be correlated with increased resistance to SSC⁵⁴. However, it is generally said that a steel that resists blistering also has a microstructure that may be resistant to cracking due to the controlled inclusion shapes or to the reduction of harmful alloying elements such as sulfur⁵⁵.

HIC occurs when monatomic hydrogen, generated at the steel surface by corrosion, penetrates the steel. The hydrogen is able to diffuse through the steel until it is trapped at internal discontinuities such as non-metallic inclusions, laminations, or regions of anomalous microstructure⁵⁶. The hydrogen collects at these voids as molecular hydrogen. As hydrogen continues to diffuse to these voids, gas pressure builds until the fracture stress of the alloy is reached and a blister forms⁵⁷, or a series of thin, stepped cracks. Figures 8 and 9 show schematics of the formation of a hydrogen blister in steel and stepwise cracking in line-pipe steel, respectively^{58,59}. Parallel cracks may link up and propagate in a steplike manner until catastrophic failure occurs when the effective thickness of the material is sufficiently reduced. This phenomenon is commonly referred to as stepwise or blister cracking.

It has been established that hard steels, typically steels with Rc above 22 in industrial application, are susceptible to HIC⁶⁰. Qualitatively this phenomenon is to be explained as follows: hard steel, in itself, means steel hardened by introducing crystal defects by alloy addition, heat treatment, cold working, and so forth; the steel then becomes susceptible to aggression by hydrogen which has entered the steel by any means.

On the other hand, soft steels are resistant to HIC, in part because of sufficiently low crystal defect density. However, soft steels suffer from hydrogen induced blistering, external or internal, when exposed to hydrogenating environments of sufficiently high hydrogen fugacity.

2.6 FACTORS INFLUENCING HIC

The factors affecting HIC are shown schematically in Figure 10. The major factors will be discussed below.

2.6.1 ENVIRONMENTAL FACTORS

The three paramount environmental variables in determining stepwise cracking behavior of linepipe steels have been found to be:

- (1) pH of the aqueous solution,
- (2) hydrogen sulfide concentration, and
- (3) environment temperature.

In aqueous environments containing H₂S, the corrosion rate of line-pipe steels increases with decreasing pH in the range pH 3-6. It has also been observed that susceptibility to stepwise cracking (SWC) also increases with decreasing pH in this pH range⁶¹, Figure 11. The reason for this behavior is that the hydrogen entry rate into the steel is higher in the lower pH environments, thus promoting SWC.

Hydrogen entry rate also increases with the H₂S concentration of the environment, as does SWC susceptibility. Ikeda et al.⁶² found that there appears to be a critical H₂S partial pressure (P_{H_2S}) required to generate SWC in line-pipe steels. Generally, the steels which have sulfide inclusion shape control exhibited cracking-free behavior up to high values of H₂S partial pressure.

Laboratory studies have shown that susceptibility to SWC decreases with increasing temperature over the range 25-100°C as shown in Figure 12.

2.6.2 METALLURGICAL FACTORS

Metallurgical variables are perhaps the most important consideration in the selection of steels to resist hydrogen induced cracking.

2.6.2.1 CASTING PRACTICE

One of the most important metallurgical factors influencing HIC of steel is the segregation of impurities and alloying elements during casting. Segregation of impurities leads to concentrations of non-metallic inclusions and these are favoured sites for the initiation of HIC. In addition, segregation of alloying elements, such as phosphorus, tends to result in banded structures with a resultant high hardness.

2.6.2.2 DEOXIDATION PRACTICE

Deoxidation with aluminum promotes HIC as alumina particles are active initiation sites for blistering. Since semi-killed steel contains fewer non-metallic inclusions and/or these inclusions are rounded in shape, it is more resistant to blistering than fully killed steels.

2.6.2.3 MICROSTRUCTURE

It is generally considered that susceptibility to HIC in steels is highest in what are termed discontinuous and/or banded structures⁶³. Cracks tend to initiate at elongated manganese sulfide (MnS) inclusions, propagating along the low temperature transformation structures of bainite and martensite⁶⁴. Isolated islands of untempered martensite apparently cause no problem, as long as they are below the 30% level normally considered necessary for cracking. For high alloys, martensitic stainless steel is more susceptible than other alloys and should be used in the quench-and tempered condition²¹. The choice of heat treatment depends on the structure of the steel. Although quenched and tempered steels are reported to be structures most resistant to HIC⁶⁵, the ideal structure appears to be spheroidized carbides in a ferrite matrix. Normalized and tempered structures are considerably more resistant than untempered martensite⁶⁶.

2.6.2.4 NON-METALLIC INCLUSIONS AND SULFUR CONTENT

Lowering the sulfur content to 0.001% remarkably reduces the HIC susceptibility because the non-metallic inclusions are reduced in number. Also, elongated non-metallic inclusions tend to increase the HIC susceptibility compared to round inclusions⁶⁶⁻⁶⁷.

2.6.2.5 ALLOYING ELEMENTS

Alloying elements are frequently added to the melt to help control HIC by preventing corrosion and, hence, the generation of hydrogen. Corrosion is reduced through a film formation. However, this effect occurs only under relatively mild conditions with a pH over 5.0.

Copper has a beneficial effect upon HIC resistance under certain pH conditions. The benefit is thought to be derived from the formation of a surface film

in conjunction with mackinawite. In low pH solutions, copper additions to the steel should be avoided as they result in increased general corrosion rates⁶⁶.

Chromium is said to have a positive effect on the HIC resistance of steels as it lowers the overall corrosion rate, particularly if the pH is over 5.0⁶⁴. Since high chromium levels can result in structures prone to SSC, a balance in chemistry must be attained.

Nickel appears to be controversial in its effect on HIC. It has been reported that nickel had no effect upon HIC resistance²⁵. However, as it may promote hardening and subsequent SSC, NACE standards²⁴ restricted the content of nickel to the 1% level.

Manganese in alloys may increase the resistance of the steel to HIC but this effect may depend on the pH of the environment. Generally, manganese reduces the susceptibility to HIC in moderate environments. This result would be consistent with the formation of a surface scale.

3. ROLES OF CO₂ IN DEGRADATION OF Fe -BASE ALLOYS

Increasingly, drilling, completion and production operations encounter high temperatures, high pressures, and corrosive species, especially carbon dioxide (CO₂) and hydrogen sulfide (H₂S). Significant amounts of CO₂ exist in offshore reservoirs. And enhanced oil recovery methods employing CO₂ floods are being utilized to increase the efficiency of hydrocarbon extraction from existing formations. All of these production efforts, and much more, share a common problem, namely CO₂ corrosion or sweet corrosion. This material degradation phenomenon is aggravated by increases in temperature, partial pressure of carbon dioxide (P_{CO₂}), chloride ion content, and presence of H₂S when Fe-base alloys are used for production equipment. The presence of H₂S may lead to SSC in susceptible materials.

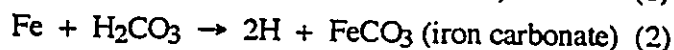
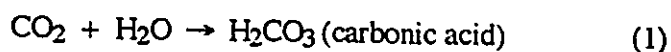
Sweet corrosion is both an old and new corrosion problem. Through the 1950's, active investigations were carried out on both CO₂ corrosion phenomena and their prevention. Recently, the resistance of materials to CO₂ corrosion has come to be important again as a result of the application of CO₂ injection for enhanced oil recovery, the active exploitation of deep natural gas reservoirs containing CO₂ and the development of geothermal wells. A short history of investigations on CO₂ corrosion phenomena is shown in table 1⁶⁷. Characteristic features of CO₂ corrosion of iron and carbon steels are its high corrosion rate even in relatively weak acid media and its specific configuration observed on corroded materials, i.e. mesa corrosion and ringworm corrosion. The former is related to dissolved CO₂ being a reservoir for H⁺ ion. The latter is closely related to corrosion products, i.e. FeCO₃ and Fe₃O₄. In order to prevent CO₂ corrosion, the addition of chromium in the steel is effective, because a Cr enriched passivation film is formed on the surface⁶⁷.

Stress corrosion cracking was not found to occur in water containing only CO₂⁶⁸. In this case, H₂CO₃ is formed in the solution and general corrosion is accelerated. Although it is recognized that carbonic acid can be more corrosive

than a completely dissociated acid at the same pH, a satisfactory mechanistic explanation of this fact has not yet been given.

3.1 CARBON DIOXIDE CORROSION MECHANISMS

Carbon dioxide corrosion can be attributed to the formation of carbonic acid and subsequent iron dissolution by the acid. The reactions given below outline the general sequence that occurs in CO₂ treatment equipment⁷.

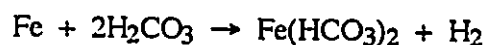


It has long been known that the corrosion rate of iron increases rapidly as the pH of the environment decreases. The presence of carbonic acid lowers the pH of the environment and thus provides hydrogen ions as electron acceptors. The reduction in pH or the amount of carbonic acid that forms is dependent primarily upon the pressure at which the system is being operated. As the partial pressure is increased, the corrosion rates increase. A general rule in the pipeline industry has been that serious corrosion can be expected if the partial pressure of CO₂ exceeds 30 psia (0.2 MPa), but corrosion will be low at a CO₂ partial pressure below 7 psia (0.05 MPa), but there is no agreement with field experience⁶⁸.

Generally, CO₂ corrosion behavior is closely related to both nucleation and growth of FeCO₃. Iron carbonate (FeCO₃) is not a very protective film and thus, corrosion is not stifled. Frequently, patches of semi-protective FeCO₃ develop and a mesa-like pitting type attack results. Carbonic acid contributes to the cathodic reaction on the surface of corroding steel, where the corrosion rate of carbon steel in waters containing CO₂ is controlled not only by the cathodic reaction but also by the anodic reaction. In the low pH region, the corrosion rate is determined by the cathodic reaction, i.e., reduction of H₂CO₃ and HCO₃⁻. However, in the high pH region, the corrosion rate is reduced by the formation of a FeCO₃ film on the

surface. The corrosion rate in the high pH region is controlled by the stability of the FeCO_3 film.

An alternative explanation might be that the undissociated carbonic acid catalyzes the hydrogen evolution reaction in equation (2) and in the intermediate reaction given below⁶⁹:



3.2 ENVIRONMENTAL FACTORS INFLUENCING CO_2 CORROSION

It has been demonstrated, by both field and laboratory experience, that environmental variables have a profound effect on the response of an alloy to carbon dioxide corrosion.

3.2.1 CARBON DIOXIDE PARTIAL PRESSURE (P_{CO_2}):

The influence of CO_2 partial pressure (P_{CO_2}) on corrosion rate of 9, 13 and 25% Cr steels was investigated by Ikeda et al.⁷⁰. The corrosion rates of 9 and 13% Cr steels increase dramatically with increasing P_{CO_2} at relatively high temperature. Also, as the P_{CO_2} increases, the critical temperature at which corrosion resistance is achieved, via a protective film, decreases. The type of corrosion product in such environments depends on the temperature and P_{CO_2} , where the tendency is for Fe_3O_4 to form in high temperature/ low CO_2 conditions and for FeCO_3 to form in low temperature / high CO_2 .

P_{CO_2} could affect both the cathodic and the anodic reactions. For the former, an increase in P_{CO_2} is accompanied by increasing the diffusion limiting current density⁶⁸. On the other hand, the anodic reaction may be enhanced through increasing instability of the Cr-Fe-O-H passivation film because an increase of P_{CO_2} lowers the pH value of the solution^{8,71}.

In comparing corrosion behavior at 0.1 MPa P_{CO_2} with that at 3.0 MPa P_{CO_2} , the corrosion rate in the former is less than in the latter, and the critical temperature to corrosion resistance is higher than in the latter, as shown in Figure 13. This would be caused by the stability of the passivation film, because the pH value of the solution is higher in the former than in the latter. In addition, it has been shown that the corrosion resistance of 25%Cr steel is independent of temperature up to 250°C and P_{CO_2} up to 3.0 MPa^{70,72}.

3.2.2 CHLORIDE IONS (Cl⁻)

The influence of Cl ion concentration on the corrosion rate of Cr steel has not been sufficiently clarified. Bryant and Chitwood⁷³ reported that NaCl concentration up to 16 wt% has a slight effect on the corrosion rate of 9% Cr and 12% Cr steels in 175°C, 7 atm CO₂.

There is less influence at low temperature (65°C) than at high temperature (175°C). Masamura et al.⁷⁴ reported that the increase of NaCl content from 10 to 20% increases the corrosion rate of 13% Cr in high temperature, high pressure CO₂ (55 to 65 atm, 150 to 200°C) while the effect of Cl ion concentration on corrosion rate is not significant in 22% Cr α - γ duplex-phase stainless steel, Figure 14.

The corrosion rates of both 9% Cr and 13% Cr steels at 150°C increase slightly with increasing Cl⁻ content over 300 ppm. At 150°C, 25% Cr steel shows an excellent corrosion resistance in Cl⁻ concentrations of up to 1.25×10^5 ppm⁶⁷. Thus, it could be concluded that the Cl⁻ concentration would hardly affect CO₂ corrosion behavior of Cr-steel at temperatures below the critical temperature, below which the corrosion resistance is stable, although it would be detrimental to corrosion resistance of Cr steel at temperatures over the critical temperature.

3.2.3 TEMPERATURE

There is a synergistic influence of Cl^- content and temperature on the general corrosion rate in any given aqueous CO_2 environment. In general, corrosion rates in excess of 10 mpy are observed at temperatures above 150°C . The higher the P_{CO_2} , the higher the corrosion rate. In addition, as the temperature increases, the solubility of CO_2 in the aqueous solutions decreases, but the net effect is to increase the rate of attack on steel⁷⁵.

The influence of temperature and P_{CO_2} on corrosion behavior of 9 to 25% Cr steels is shown in Figure 13. At low temperatures, the corrosion rate decreases as the Cr content increases, also the Cr content concentrates in the corrosion product, and it increases with increasing Cr content of the matrix. Even in 12% Cr steel, the Cr content in the film could attain concentrations of up to about 15 wt%⁷⁶. The corresponding temperatures for maximum corrosion rate move to higher temperatures with increasing Cr content in steel.

Each 9% Cr, 13% Cr and 25% Cr steel shows a stable corrosion resistance at temperatures below 100°C , 150°C and 250°C , respectively. At high temperatures over these critical temperatures, the corrosion loss of each material is approximately proportional to immersion time⁷⁰. Thus, corrosion of steel by $\text{CO}_2/\text{H}_2\text{O}$ occurs over a broad spectrum of partial pressures and temperatures.

3.2.4 HYDROGEN SULFIDE CONTAMINATION

Hydrogen sulfide is extremely detrimental to the corrosion resistance of Cr-steels, as can be noticed in Figure 15. Both 9% Cr and 13% Cr steels show a general corrosion mode in every temperature region, even in H_2S contamination of 3.3 ppm. At 3.3 ppm, 25% Cr steel suffers general corrosion at temperatures higher than 80°C ⁷⁷.

Because H_2S makes the corrosion potential noble, the passivation film of Cr-steel is easily destroyed. FeS easily forms at ambient temperature where general corrosion occurs. Thus it is necessary, for securing corrosion resistance in H_2S - CO_2 - Cl^- , to change the structure of the passivation film by means of co-addition of other alloying elements, such as nickel⁷⁸.

Kudo et al.⁷⁹ showed that even high chromium steel such as 30%Cr - 1%Mo steel would suffer high corrosion rates and SCC in CO_2 - Cl^- environment contaminated with as low as 0.01 MPa H_2S .

3.2.5 OXYGEN CONTAMINATION

It has been found that oxygen contamination below 1670 ppm hardly affects CO_2 corrosion behavior of Cr-steel with Cr content more than 9% at temperatures below $150^\circ C$ ⁶⁵. As concerns 13% Cr steel, a slight coexistence of oxygen with CO_2 tends to decrease the corrosion rate slightly. Ikeda et al.⁷⁰ observed a little pitting corrosion at the side surface of both 13% Cr and 25% Cr steels specimens, only in the condition of 1670 ppm oxygen at $80^\circ C$. It should be taken into account that oxygen contamination is slightly detrimental to localized corrosion resistance of Cr steel.

3.2.6 INFLUENCE OF FLOW VELOCITY

At temperatures below the critical temperature, below which the corrosion resistance is stable, the flow velocity hardly affects corrosion behavior of Cr-steel. Even in gas solutions, with the phase flowing as fast as 25 m/s, this tendency is maintained. As a result, both the 13% Cr steel and 25% Cr steel are significantly resistant to CO_2 corrosion at temperatures below $100^\circ C$ and below $150^\circ C$ respectively regardless of flow velocity.

3.3 PREVENTION OF CO₂ CORROSION

Studies^{75,80,81} were made of the composition of corrosion products on carbon steel subjected to CO₂ corrosion in water. A two-layer product was formed, the one next to the metal named corrossite, and the outer layer corresponded to siderite. This two-layer carbonate film had good protective properties as a result of the strength and low solubility of the corrossite (FeO . FeCO₃) and the reduced solubility of the siderite resulting from the restricted diffusion in fine pores. Artificial formation of such two-layer oxide films could be a method of protecting carbon steel equipment from CO₂ corrosion.

As for the prevention of CO₂ corrosion, 9% Cr - 1% Mo, 13% Cr and 22-25% Cr α - γ duplex stainless steels are commercially available with a couple of application limits. First, the critical application temperature for each application is 100°C for 9% Cr - 1% Mo steel, 150°C for 13% Cr steel and about 250°C for 22 - 25% Cr steel. Second, the coexistence of hydrogen sulfide with carbon dioxide would contribute significantly to the degradation of their corrosion resistance. The limit concentration of H₂S for no evidence of degradation is 0.0001 MPa for 9% Cr - 1% Mo and 13% Cr steels and 0.001 MPa for 22 - 25% Cr duplex steel⁶⁷. From the viewpoint of application to oil and gas production, 13% Cr and 22 - 25%Cr α - γ duplex steels are useful. When each steel is tempered above each specific temperature, it becomes completely immune to SCC. This specific tempering temperature was designated as the critical tempering temperature (CTT). Under these conditions, the SCC susceptibility of 13% Cr steels was considered to be dependent on their microstructure and strength. In many instances, the problems of downhole corrosion of low-alloy steels can be handled with chemical inhibition. Unfortunately, corrosion inhibition is not as reliable as properties like the strength or microstructure of the steel. It require people and machines for application. In addition, under severe conditions, the success of inhibitors is not guaranteed and the process of inhibition is very expensive. For these reasons most companies do not rely solely on inhibition to prevent SSC in particular.

4. CORROSION AND SSC IN H₂S/CO₂/Cl⁻ ENVIRONMENTS

Hydrogen sulfide as well as carbon dioxide can be dissolved in aqueous environments to form acid solutions. From this property they derive their commonly used name of acid gases.

One of the greatest problems that the oil industry is presently being faced with is to find a satisfactory solution for the availability of steels and then resistance in environments with high H₂S content. Where high content of CO₂ and Cl⁻ is found, another problem of an adequate resistance to general, pitting corrosion and/or SSC will arise.

Sardisco et al.⁸² studied the corrosion of mild steel in the H₂S/CO₂/H₂O system. According to the authors, the protectivity of the formed sulfide film depends upon the partial pressure of H₂S and the pH of the solution. When a small amount of H₂S was added to the CO₂-H₂O system, the corrosion rate dropped indicating that the H₂S became the controlling parameter instead of CO₂. In addition, a change in physical properties of the film was very noticeable.

The influence of H₂S concentration and temperature on corrosion of steel in 5% NaCl solution has been investigated by Rogne⁸³. He found that at high temperatures and high H₂S concentrations, formation of FeS film reduces the initial high corrosion rates. In H₂S/CO₂ mixtures compared to H₂S/N₂ mixtures, CO₂ increases the corrosion rate when the H₂S content is > 4%. Even a small amount of H₂S down to 0.03% H₂S in mixture with CO₂, seems to have an inhibiting effect on CO₂ corrosion of steel.

There are several inconsistencies among various investigators' results, e. g., the effect of chloride ion on SSC and/or SCC, the effect of CO₂ and H₂S partial pressure, the effect of temperature, pH and microstructure.

In order to mitigate CO₂ corrosion as well as SSC and/or SCC in the CO₂/H₂S/Cl⁻ environments, 9Cr-1Mo, AISI 420 (13%Cr) martensitic steel, and 22-25%Cr duplex stainless steel have been widely used; however, application criteria have still not been clearly defined. Recently, their performance properties have been widely investigated. However, there are a couple of important conflicting points in published research⁷⁰. One of them is SSC resistance of 13%Cr steel and the other is SCC resistance of duplex phase stainless steel in an CO₂/H₂S/Cl⁻ system. These differences would result mostly from the difference of experimental technique.

4.1 SSC OF MARTENSITIC STAINLESS STEEL IN H₂S/CO₂/Cl⁻ SYSTEMS

The SCC or pitting susceptibility of chromium stainless steels in an H₂S environment has been discussed for a long time^{23,84,85}. The influence of H₂S contamination in a CO₂-Cl⁻ environment on the corrosion behavior of martensitic stainless steels was investigated by Ikeda et al.⁷⁶ who reported that 9Cr-1Mo and 13Cr stainless steels with the martensitic microstructure are essentially CO₂ corrosion resistant alloys. The former could be applied up to 100°C and the latter could be applied up to 150°C.

The criteria for partial pressure of H₂S is one of the most important problems under investigation. The effect of the pressure of H₂S and CO₂, in H₂O-H₂S and H₂O-CO₂ systems, on the corrosion of tubular steels was investigated by Koval et al.⁸⁶ who found that generally, in the liquid phase the corrosion rates increased with pressure of H₂S and CO₂.

U-bend SCC tests of 13Cr steel in CO₂ environments containing H₂S have been made in conditions III, IV and V as shown in table 2⁸⁹. The specimen strengths were adjusted to API L-80 and C-90. The results are tabulated in table 3, which also shows tensile properties and corrosion rates.

The effects of alloying elements on the Ni-type SCC resistance showed the same inclination as the results of SCC tests in the pure CO₂ environment. This indicates that both the SCC in the pure CO₂ environment and the SCC in the CO₂ + H₂S environments involve the same phenomena and that H₂S accelerates SCC.

The failure time in the NACE solution (pH=3.5), measured by the constant load tensile tests, was considerably shorter than that of the other conditions (pH≥4.7), and the threshold stress was much smaller. The experimental results are shown in Figure 16⁸⁷. In addition, in NACE solution, the average corrosion rate of the 13%Cr stainless steel was greater than that of Ni-type alloys and low alloy steels. However, NACE solution has been widely used to study SCC in H₂S environments by different types of tests. The results agreed with the often-proved fact that the susceptibility of 13Cr steels to SCC in H₂S environments is inferior to that of low alloy steels having the same strength.

The effects of strength (s_y) on the failure time measured under an applied stress of $0.6 s_y$ are shown in Figure 17⁸⁷. When the yield strength of 13Cr steels exceeded 58 kg/mm², the time to failure was very short. In most investigations, the fracture mode of 13Cr steels was intergranular.

4.2 HYDROGEN EMBRITTLEMENT OF MARTENSITIC STAINLESS STEELS IN H₂S/CO₂/CL⁻ ENVIRONMENTS

It is generally agreed that SCC of low alloy steels in H₂S environments is caused by hydrogen embrittlement (HE)^{10,88}.

The degree of HE is usually evaluated in terms of the ratio of elongation under hydrogen charging (El_H) to elongation in air (El_{air}). The smaller ratio indicates that HE is enhanced.

Generally, low alloy steel is not significantly subject to embrittlement, but the embrittlement of 13Cr stainless steel (martensitic) is significant. As mentioned

before, the SCC resistance of low alloy steels in CO₂-H₂S environments is higher than that of 13Cr steels. Thus it is reasonable to hypothesize that the SCC is caused by HE. Furthermore, the susceptibility of 13Cr steels to HE is greatly dependent on the tempering temperature. From Figure 18⁸⁷, although the strength of Ni-type steel tempered at 710°C was higher than of that tempered at 600°C, the 13Cr steels which were tempered at 710°C exhibited less HE susceptibility compared to those which were tempered at 600°C. It is generally believed that at relatively high temperatures, the HE mechanism is less intense, because the hydrogen diffusion rate increases so the quantity of hydrogen which remains in the structure is lower.

5. CORROSION RESISTANT MATERIALS

In some cases, chemical inhibition is not effective in preventing the engineering alloys from degradation in sweet and/or sour environments because of either environmental or engineering limitations. This has recently brought about the use of corrosion-resisting alloys in a number of applications from downhole tubular to valve and specialty components. Some of the materials being considered for these applications are given in table 4⁸⁹.

High-alloy stainless steel and Ni-base alloys offer great potential in revolutionizing well completion design by increasing allowable stress levels, removing inhibitor systems, and basically making it possible to do operations not possible using conventional technology. However, it must be realized that these materials can act very differently than steels, are affected differently by H₂S, and are subject to a different set of engineering limitations.

High-alloy material for deep-well production must have high strength to ensure resistance to tensile failure under high axial load as well as resistance to collapse and burst. In addition, these materials must overcome the detrimental effects of H₂S, CO₂, sulfur compounds and concentrated brine solutions.

To obtain high strength and mitigate corrosion, there has been increased use of materials containing high levels of chromium, nickel and molybdenum. The behavior of these materials in oil field environments containing H₂S, CO₂, and chlorides, however, is an essential factor. Two important areas of concern are corrosion and cracking, where the behavior of stainless steel alloys is more complex than that for conventional steels. For example, stainless alloys may be susceptible to cracking by either a hydrogen embrittlement-cracking process or by stress corrosion cracking. The mechanisms involved in these two processes are shown in Figure 19⁴⁶.

To understand the behavior of high-alloy materials in oil field production environment, four classifications of materials need to be made. They are:

- (1) martensitic stainless steels,
- (2) duplex stainless steels,
- (3) high-alloy austenitic stainless steels, and
- (4) Ni-base alloys.

Each classification has different ranges of composition, microstructure, strengthening mechanism, and performance in corrosive production environments. As a rule, these materials do not behave as one class of materials. This must be realized when selecting these materials for oil field service.

In the next two sub-sections, the properties, performance, and applicability of 9-13% Cr martensitic stainless steels and α - γ duplex stainless steel in H₂S-CO₂-Cl⁻ environments will be discussed in that order.

5.1 9Cr - 1 Mo STEEL

This alloy is a martensitic intermediate alloy steel generally recommended for wet CO₂ environments with moderate to low chloride concentrations and moderate temperature⁹⁰. The typical chemical composition of 9Cr - 1Mo is given in table 5⁹¹.

While successful use of 9Cr - 1Mo has been reported for sweet wells⁹², it suffers pitting and SCC in certain CO₂ environments⁹³. 9Cr - 1Mo has the advantage over duplex of being strengthened by heat treatment and also it has better chloride stress corrosion cracking resistance⁹⁴, 9Cr - 1Mo being essentially immune if properly heat treated. In addition, 9Cr - 1Mo has slightly better H₂S cracking resistance than 13Cr, as reported by Phelps⁹⁵.

The corrosion behavior of 9Cr - 1Mo steel in a wet CO₂ environment and the influence of H₂S contamination was investigated in detail⁷⁰. It was confirmed

that one of the most important factors in CO₂ corrosion of Cr steel was temperature. However, the corrosion behavior of 9Cr - 1Mo at relatively high temperature, above 100 and 150°C as shown in Figure 13, suggests that the P_{CO₂} is another important factor. P_{CO₂} could affect both the cathodic and the anodic reactions. For the former, an increase in P_{CO₂} is accompanied by increasing diffusion limiting current density⁷⁶. On the other hand, the anodic reaction is enhanced through increasing instability of the Cr-Fe-O-H passivation film because an increase of P_{CO₂} lowers the pH value of the solution⁷¹.

In Figure 20, the effects of temperature and P_{H₂S} are shown. The 9Cr - 1Mo steel of C-95 grade is very susceptible to SSC. Even at 1x10⁻⁴ MPa P_{H₂S}, SSC occurs. In the CO₂-Cl⁻ environment contaminated with a small amount of H₂S, the dependence of SSC susceptibility of 9Cr - 1Mo on the strength level is clearly shown in Figure 21.

The influence of Cl ion concentration on the corrosion rate of Cr steel has been reported by Ikeda et al.⁷⁰ as shown in Figure 14. The NaCl concentration up to 16 wt% has a slight effect on the corrosion rate of 9Cr and 12Cr steels in 175°C, 7 atm CO₂.

9Cr - 1Mo with a maximum hardness of Rc 23 was selected as the most practical tubing material for the Brown-Bassett field⁹⁶, Ellenberger formation. The wells' conditions were 18,000 to 21,000 feet deep, temperature 375°F (190°C), pressure 14,000 to 16,000 psi (96 to 110 MPa), CO₂ 50 wt%, H₂S 20 -30 ppm and Cl ion up to 35,000 ppm. Today 9Cr - 1Mo is still in service in many of the field's wells. In the Puckett-Ellenberger field, in Texas, two wells were completed with 9Cr - 1Mo having a maximum hardness of Rc 26. These two wells are still in service more than 25 years later. The conditions were similar to the one mentioned before, never needing a corrosion inhibition program.

5.2 13Cr STEELS

Of all corrosion resistant martensitic alloys, 13Cr martensitic steel is the least expensive. Its strength can be changed by adjusting the carbon content and/or tempering temperature. The corrosion and SCC behavior of 13Cr steel are more significantly affected by environmental factors than those of stainless steels containing more than 13%Cr.

It has been known that 13Cr steels are highly resistant to CO₂ corrosion, but they are more susceptible to SCC in environments containing H₂S than the low alloy steels are^{4,22,97}. Therefore, they should be used in gas and oil fields with higher CO₂ concentrations and lower H₂S concentrations. As a result, it is necessary to clarify the critical H₂S concentration at which 13Cr steels undergo SCC. This critical H₂S concentration is affected by the chemical composition, strength, and microstructure of the steel.

13Cr stainless steel has perhaps the longest history of application in a wide variety of oil and gas-producing environments containing CO₂. Compared to the 9Cr - 1Mo and α - γ duplex stainless steels, 13Cr stainless steel ranks highest of the three in amount of tubular in actual use.

The above fact is due to the higher resistance of 13Cr stainless steel to general corrosion and pitting in CO₂ environments compared to that of 9Cr - 1Mo and it can tolerate higher chloride contents and temperature. Field experience has shown that 13Cr can also resist corrosion and SSC in the presence of small amounts of H₂S.

The high hardenability of 13Cr stainless steel permits a complete transformation from austenite to martensite by simply air cooling from the austenitizing temperature. A uniform martensitic microstructure is desirable from an SSC point of view and special efforts, such as internal-external quenching, are usually expended for low alloy steel in this regard.

Following hardening (air cooling), 13Cr stainless steel is tempered within a specific temperature range to achieve the desired mechanical properties. Figure 22 shows the relationship between tempering temperature and tensile properties; the tensile strength along with the yield strength decrease as the tempering temperature increases. Figure 23 presents the mechanical properties as well as corrosion resistance as a function of tempering temperature for 13Cr stainless steel. In addition to yield and tensile strengths, impact resistance is plotted in Figure 23 as a function of tempering temperature in terms of Izod energy. Also, corrosion resistance of 13Cr stainless is shown as weight loss in 3% NaCl. This figure shows that tempering at about 550°C results in maximum corrosion rate and minimum ductility.

It is clear that corrosion resistance and impact properties improve only if tempering temperatures are above, say, 620°C. The poor corrosion resistance of 13Cr stainless steel when tempered in the range 500 - 600°C is due to the precipitation of carbides and Cr depletion from specific zones, a process akin to sensitization in austenitic stainless steels.

When one considers the responses to tempering temperatures as shown in Figures 2 and 3, it becomes evident that the maximum yield strength levels attainable for 13Cr without adversely affecting the impact and corrosion resistance are limited to within 100 ksi. This fact has a bearing on the 13Cr grades commercially available, in that the product is limited to an equivalent of API C-95. Hence, 13Cr manufacturers can supply 13Cr stainless steel tubular conforming to API C-75, L-80, and C-95, as well as non-API grades, such as C-85 and C-90.

The corrosion behavior of 13Cr steels in wet CO₂ environment was investigated by Ikeda et al.⁷⁰. The 13Cr steel is corrosion resistant in a CO₂ - Cl⁻ solution below 150°C; in such conditions, corrosion resistance does not depend heavily on Cl⁻ concentration, (if less than 20% NaCl) or on P_{CO₂}, if less than 3.0 MPa at 25°C. Corrosion does, however, increase with increasing CO₂ and Cl⁻ levels.

Ikeda and Mukai⁹⁸ presented the corrosion behavior of type 420 13Cr steel in CO₂ - Cl⁻ contaminated with H₂S, where 13Cr steel would suffer primarily weight loss corrosion at temperatures over 150°C, severe pitting corrosion at intermediate temperatures between 60 and 120°C, and SSC near ambient temperature. Recently, Mukai et al.⁹⁹ showed that SSC susceptibility of martensitic 13Cr steel depended upon a notch effect in the specimen and the pH value of the solution as shown in Figure 24. The presence of H₂S accelerates the general corrosion rate and increases the tendency of pitting. H₂S also makes 13Cr stainless steel susceptible to SCC. The mechanism of corrosion of 13Cr stainless steel is distinctly different from that of low alloy steels by virtue of the resultant corrosion products that are observed. Sulfide inclusions are a likely source of initiation of pitting corrosion.

The results of the corrosion tests of AISI 410, AISI 420, and 4130 low alloy steel in NACE solution (H₂S/CO₂/Cl⁻) performed by Ishizawa et al.⁹⁷ indicate that the corrosion rate becomes higher with the increase of chromium content. The reason for this effect of chromium is not completely clear, but it can be said that the corrosion resistance of 13% Cr steel is not too high in such a corrosive environment as NACE solution.

5.2.1 AISI 410

The 12% Cr steels are general-purpose stainless steels with adequate chromium content for many corrosion and heat resisting applications. Because the hardenable 12% Cr steels furnish an effective combination of strength, relatively high hardness, and corrosion resistance, they are used in a wide variety of applications. The typical chemical composition is given in table 5. Exemplified by AISI 410, this class of steel is ferritic in the annealed condition, but it can be heat treated by rapidly cooling from 980 to 1010°C (1800 to 1850°F) followed by tempering. Figure 25 shows typical mechanical properties resulting from tempering at different temperatures. On the basis of reported laboratory tests and service experience, annealed ferritic stainless steels are the only commercial steels that is

not susceptible to SCC. Conversely, hardened (martensitic) type 410 stainless steel is susceptible to SCC under certain conditions^{100,101}.

Although AISI type 410 is used in many applications without the occurrence of SCC, this kind of attack is encountered on occasion. The 410 alloy does not offer adequate corrosion resistance to the CO₂/H₂S saturated hot brines which simulate deep well environments. This martensitic stainless steel fails by H₂S stress cracking at room temperature and suffers accelerated corrosive attack at elevated temperatures¹.

Tempering temperature is a very important factor in controlling the susceptibility of martensitic type 410 stainless to SCC. Figure 26, for example, indicates that resistance to cracking of hardened type 410 and type 416 (a free machining grade of type 410 containing high sulfur) in a 0.5 % acetic acid solution containing H₂S can be obtained by keeping the hardness below Rc 24 (i.e. tempering temperature control)¹⁰².

Typical microstructural features of intergranular and transgranular cracking in hardened type 410 stainless steel are shown in Figures 27 and 28. SCC caused by the presence of intergranular carbides (chromium depletion in the grain boundaries) always follows the prior austenite grain boundaries. However, cracking caused by HE may be intergranular or transgranular.

From the above discussion, significant improvement in performance can be obtained by selection of the proper heat treatment. For environments known to cause hydrogen charging, such as those containing H₂S, the steel should be tempered at 1200°F (650°C) and above to keep the hardness below Rc 22. Even this approach may not avoid cracking under severe conditions.

5.2.2 AISI 420

AISI 420 is the high carbon version of AISI 410 and thus can be heat treated to even higher strength levels than the latter and is free of delta ferrite, primarily due to the higher carbon content. AISI 420, however, exhibits poor weldability and loss of toughness at high strength levels. In general, the SSC resistance of AISI 420 is superior to that of AISI 410⁹⁷. The typical chemical composition of AISI 420 is given in table 5. AISI 420 is thus suitable for 13Cr stainless steel oil-country tubular goods (OCTG) from the aspects of ease of heat treatment, strength levels attainable, and resistance to SCC as well as SSC in CO₂ environments containing small amounts of H₂S. Weldability is not a concern for OCTG and the moderate toughness values do not impair applicability for tubulars.

Determining the limits of use of AISI 420 in H₂S-CO₂-Cl⁻ environments is a complex task. The material can become passive, thus greatly reducing the effects of an aggressive environment on the general corrosion which is typical of quenched and tempered carbon steels in the presence of large quantities of CO₂.

A compilation of SSC data on 410, 420, and CA-15 from various sources^{4,103,104} is shown in Figure 29. The aqueous environments used in these studies were saturated with H₂S, thus providing a conservative lower bound. The improvement in the SSC resistance of AISI 420 over AISI 410 or CA-15 may be attributable to microstructural features of the former (fine grained uniform martensitic structure free of delta ferrite).

Data in Figure 29 also provide a measure of confidence in using AISI 420 stainless steel tubular in environments containing low levels of H₂S where the use of AISI 410 for wellhead equipment has been successful. Figure 29 also indicates that the threshold stress for SSC falls off quite rapidly with increase in yield strength in the range 80-110 ksi (0.55 -0.76 MPa). This means that controlling of yield strength and hardness during manufacture must be exercised in order to maximize the SSC resistance. For example, an actual application of type 420 13Cr

steel with C-85 grade in CO₂-Cl⁻ with a very small amount of H₂S has been in successful operation in the Tuscaloosa field for about two years, as reported by Combes et al.⁹⁴. The maximum hardness of Rc 23 has been employed for 420 type 13Cr steel tubular used in the Tuscaloosa field. The environmental conditions are P_{CO₂}, 1.0 to 1.5 ksi; Cl⁻ < 3000 ppm; P_{H₂S}, 0.4 psi; and 180°C at well bottom.

It is possible that corrosion severity in the actual wells is less than in the laboratory simulation test. In addition, AISI 420 stainless steel was found to be substantially more susceptible to SCC than low-alloy steels at comparable strength levels in both field and laboratory environments^{105,106}.

AISI 420 steels can be tempered at higher temperature in comparison with 410 steels to obtain the same strength level. It is mainly due to the higher carbon content of 420 steels. The high tempering temperature of 420 steels is advantageous to make the microstructure favorable to the SCC resistance, that is, more recovered substructure (subgrain, the shape and distribution of carbide particles and the arrangement of dislocations) with a larger amount of coarser and globular carbides.

In addition, the higher SSC resistance of 420 steels compared to that of 410 steels has been related to higher carbon levels. It is attributable partly to finer grain size introduced by higher carbon content⁹⁷.

5.3 α - γ DUPLEX STAINLESS STEEL

Duplex (austenitic/ferritic) stainless steels are a relatively new class of engineering materials used in oil field application. They have been used in wellhead components and, more recently, as high strength tubular goods. They typically have better corrosion resistance than 13%Cr. Since the practical experience of using duplex stainless steels as materials for downhole piping is limited, there is some uncertainty about their performance and many aspects of this material in sour gas production environments are still questionable.

In the past it was generally agreed that duplex stainless steel was quite resistant to SSC in aqueous environments containing H_2S , CO_2 and Cl^- . As a result, duplex stainless steel tube and linepipe were applied for sour service on a moderate scale.

The confidence in this material was based on data produced by manufacturers. However, as time went on, laboratory results showed that SSC of duplex stainless steel might be possible at H_2S levels as low as 0.1 bar or even lower ($T \leq 290^\circ C$)⁸⁴.

Ikeda et al.⁷⁰ summarized SCC susceptibility of 22-25Cr α - γ duplex stainless steel in Figure 30, where essentially two phenomena were pointed out. One is that the temperature region most susceptible to SCC in H_2S - CO_2 - Cl^- environment locates at temperatures between 60 and 100°C, which is consistent in all literature. At this temperature range selective corrosion of the austenitic phase took place⁷². The other is that there is an inconsistency among the published autoclave data, i.e. the criteria for SCC in the high temperature regions over 150°C. Oredsson and Bernhardsson⁸⁵ showed that the lower cracking limit of P_{H_2S} had a tendency to increase with temperature increases, while Mukai et al.⁷² and Prouheze et al.¹⁰⁷ showed that it decreased with temperature increases. Furthermore, the SCC resistance of 22-25%Cr α - γ duplex stainless steels in CO_2 - Cl^- environment was examined by Mukai et al.⁷⁰ and Asphahani¹. They showed that the Cr, Ni, and Cu contents are not the only factors affecting the alloy's resistance to pitting and to SCC. It appears that the percent of the ferrite phase present in a duplex alloy is another important factor to be considered when comparing the performance of these ferritic-austenitic materials. In addition, Mukai et al.⁷² reported that the application criteria of α - γ duplex stainless depended on environmental and metallurgical conditions such as H_2S partial pressure, Cl^- ion concentration, temperature, and cold work.

6. HEAT TREATMENT OF STAINLESS STEELS

The process of heat treatment of stainless steels is used to produce changes in physical properties, mechanical properties and residual stress level, and to achieve maximum corrosion resistance when that property has been adversely affected by previous fabrication or heating processes. Frequently, a combination of satisfactory corrosion resistance and optimum mechanical properties is obtained in the same heat treatment.

6.1 C-Cr-Fe PHASE DIAGRAM

The ternary system carbon-chromium-iron provides a basis for understanding the constitution of these materials. The transition between Fe-Cr ferrite (α)-stabilizing and Fe-C austenite (γ)-stabilizing phases gives rise to complex regions in the ternary systems.

The binary iron-chromium equilibrium diagram, Figure 31, shows that Cr restricts the occurrence of the γ -loop to the extent that above 13%Cr the binary alloys are ferritic over the whole temperature range, while there is a narrow ($\alpha+\gamma$) range between 12% and 13%Cr.

The addition of carbon to the binary alloy extends the γ -loop to higher chromium contents, Figure 32, and also widens the ($\alpha+\gamma$) phase field up to 0.3%C. Above 0.4%C the steel can be made fully austenitic if cooled rapidly from the γ -loop region. The second effect of carbon is to introduce carbides to the structure as indicated in Figure 33¹⁰⁸. These carbide phases have the following formulas and composition limits¹⁰⁹.

M_3C , cementite, containing up to 15 wt% Cr

M_7C_3 , trigonal chromium carbide, containing up to 55 wt% Fe

$M_{23}C_6$, cubic chromium carbide, containing up to 30 wt% Fe

M_3C_2 , orthorhombic chromium carbide, up to 20 wt% Fe.

In austenitic steels, $M_{23}C_6$ is the most significant carbide formed and it can have a substantial influence on corrosion resistance. Figure 32 also shows that the carbide phase $M_{23}C_6$ exists below about 1050°C. However, it goes into solution when the steel is heated to 1100-1200°C and on quenching, a precipitate-free austenite is obtained. However, in reheating (e.g. tempering) in the range 550°-750°C, $M_{23}C_6$ is reprecipitated preferentially at the grain boundaries. While such precipitation can have an adverse effect on mechanical properties, in particular low temperature ductility, the most significant result is the depletion of the regions adjacent to the grain boundaries with respect to chromium. Consequently, the steel is more susceptible to intergranular corrosion.

Considering the addition of Cr to Fe-C alloys, the γ -field is constricted, the eutectoid temperature ($\gamma \rightarrow \alpha + M_3C$) being raised and carbon content of the eutectoid being lowered (Figure 34)¹¹⁰. Thus from a practical standpoint, steels containing 10 to 18% Cr must be heated at temperatures between 900 and 1200°C if full hardening is to be obtained during subsequent quenching, and for maximum hardening by transformation of the γ phase, the carbon content must lie within the limits of the γ region for a given chromium content.

6.2 MARTENSITIC STAINLESS STEELS

Martensitic types are iron-chromium steels with or without small additions of other alloying elements. The martensitic stainless steel must have the proper combination of chromium and carbon (and other elements) so that austenite is present at high temperature, and martensite present upon cooling to 20°C. These steels are stronger than the ferritic and austenitic class, and their utilization relies on the high strength along with corrosion resistance. They are ferritic in the annealed condition, but are martensitic after rapid cooling in air or a liquid medium from above the critical temperature. Steels in this group usually contain no more than 14% Cr except AISI 440, and an amount of carbon sufficient to promote hardening.

Martensitic stainless steels (e.g. grades 410, 416, 420, 440A, 440B and 440C) are similar to other AISI quenched and tempered steels in that they are magnetic and are hardened by austenitizing and tempering. Rapid quenching of austenite to room temperature often results in the formation of martensite, a very hard structure in which the carbon, formerly in solid solution in the austenite, remains in solution in the new phase. Figure 35¹⁰⁸ shows the large effect of carbon content on the hardness of martensite compared with the relatively small effect of carbon on the strength of austenite.

Unlike ferrite or pearlite, martensite forms by a sudden shear process in the austenite lattice, which is not normally accompanied by atomic diffusion. Ideally, the martensite structure is a diffusionless shear transformation, highly crystallographic in character, which leads to a characteristic lath or lenticular microstructure.

The martensite reaction in steels begins at a martensitic start temperature, M_s . Once the M_s is reached further transformation takes place during cooling until the reaction ceases at the M_f temperature. The rate of cooling must be sufficient to suppress the higher temperature diffusion-controlled ferrite and pearlite reactions, as well as other intermediate reactions such as the formation of bainite.

6.3 HEAT TREATMENT OF MARTENSITIC STAINLESS STEEL

The heat treating of martensitic stainless steel is essentially the same as for plain carbon or low-alloy steels, in that maximum strength and hardness depend chiefly on carbon content. The principal metallurgical difference is that the high alloy content of stainless grades causes the transformation to be quite sluggish, and the hardenability to be quite high.

The martensitic stainless steels are more sensitive to heat treating variables (e.g. temperature, soaking time and cooling rate) than are carbon and low-alloy steels. Martensitic stainless steels normally are hardened by being heated above the

transformation range to temperatures of 950°-1250°C (100% austenite) and then cooled in air or oil.

Because of the low thermal conductivity of stainless steels, high thermal gradients and high stresses during rapid heating may cause cracking in some parts. To avoid this problem, preheating is usually recommended in the treatment of martensitic stainless steels. Preheating is usually accomplished at 760° to 790°C, and heating needs to be continued only long enough to assure that all portions of each part have reached the preheating temperature.

The traditional way to high strength in steels is by quenching to form martensite which is subsequently reheated or tempered at an intermediate temperature, increasing the toughness of the steel without too great a loss in strength. Therefore, for the optimum development of strength, a steel must first be fully converted to martensite. To achieve this, the steel must be quenched at a rate sufficiently rapid (from the austenitizing temperature) to avoid the decomposition of austenite during cooling to such products as ferrite, pearlite and bainite.

The austenitizing temperature of martensitic stainless steels is mainly dependent upon the type or the chemical composition of the material, with 100% austenite usually being achieved over a range of temperature. When maximum corrosion resistance and strength are desired, the steel should be austenitized at the high end of the temperature range.

The as-quenched hardness increases with increasing austenitizing temperature to about 980°C, then decreases because of austenite retention and (occasionally) the formation of delta ferrite. The binary iron-chromium equilibrium diagram (Figure 31) shows that above 13% Cr the binary alloys are ferritic over the whole temperature range, while there is a narrow ($\alpha+\gamma$) range between 12% and 13% Cr. The ferrite is normally referred to as delta ferrite because in these steels the phase can have a continuous existence from the melting point to room temperature.

Soaking time of 30 to 60 min. is sometimes recommended for sections 0.5in. thick and under. However, soaking times should be doubled if parts to be hardened have been fully annealed or isothermally annealed¹¹¹.

Quenching of all martensitic stainless steels can be done in either oil or air due to their high hardenability. In stainless steels like types 414, 420, 431 and the 440 grades, carbide precipitation may occur in grain boundary areas if heavy sections are cooled slowly through the temperature range of about 550°-750°C. Although oil quenching is preferred from the ductility and corrosion resistance point of view, air cooling may be required to prevent quench cracking.

The as-quenched martensite is a very strong phase but it is normally very brittle so it is necessary to modify the mechanical properties by heat treatment in the range of 150°-750°C. This process is called **tempering**. Essentially, martensite is a highly supersaturated solid solution of carbon in iron which, during tempering, rejects carbon in the form of a finely divided carbide phase. The end result of tempering is a fine dispersion of carbides in an iron matrix which often has little structural similarity to the original as-quenched martensite¹¹².

In chromium steels, two chromium carbides are very often encountered: Cr_7C_3 (trigonal) and $Cr_{23}C_6$ (complex cubic). The normal carbide sequence during tempering is Matrix \rightarrow $(FeCr)_3C \rightarrow Cr_7C_3 \rightarrow Cr_{23}C_6$. The Cr_7C_3 does not normally form until the chromium content of the steel exceeds 1% at a carbon level of about 0.2%. Steels up to 9% Cr do not show secondary hardening peaks in tempering curves (Figure 36)¹⁰⁸. However, at higher chromium contents, these curves do exhibit peaks which are associated with the precipitation of Cr_7C_3 . In addition, $Cr_{23}C_6$ nucleates at about the same time but at different sites, particularly former austenite grain boundaries and at ferrite lath boundaries. $Cr_{23}C_6$ grows at the expense of the Cr_7C_3 which disappears from the microstructure, at the stage when the steel has completely over-aged. The effect of tempering temperatures on tensile properties and hardness of type 420 martensitic stainless steel is shown in Figure 37¹¹¹.

7. SCC AND SSC TEST METHODS

There are several different test methods used to detect SSC and HIC . Solutions vary in concentration, pH, temperature, and dissolved components to simulate operating environments.

The various known SCC and/or SSC test methods can be classified under three major testing methods:

- (1) constant strain test methods,
- (2) constant load test methods, and
- (3) the slow strain rate test method.

7.1 CONSTANT STRAIN AND CONSTANT LOAD TEST METHODS

These are traditional methods of determining SCC resistance of an alloy. They could be conducted by exposing stressed, smooth specimens in the environment of interest. Such specimens could be exposed under, near or beyond their yield strengths.

Examples of constant strain specimens are plastically deformed U-bends, C-rings, and beams supported in restraining jigs. The major advantage of constant strain specimens is that they are compact and relatively inexpensive. A disadvantage of constant strain tests is that stress levels are not known accurately and are difficult to reproduce from specimen to specimen. Further, stress relaxation due to crack growth may slow or even stop crack propagation. Where fracture of the specimen does not occur, metallographic analysis may be required to determine if the cracks have formed.

Constant load tests employ either tensile or bend specimens. They require more complex apparatus than constant strain tests, but they have the advantage that

the stress level is well defined and easily measured. Loads may be applied by weights, levers, springs, or hydraulically. An advantage of constant load tests compared to constant strain tests is that crack propagation decreases the cross-sectional area and increases the net section stress. Consequently, such tests are more likely to lead to early and total failure than are constant strain tests.

Both types of specimens are normally exposed in the environment of interest for a predetermined period. The susceptibility to SCC of an alloy which cracks within the test period selected may be expressed quantitatively by time to failure.

A method which has frequently been used to speed up the generation of SCC susceptibility data is to increase the severity of tests by altering the composition of the environment, raising the temperature, or introducing a notch or a precrack. Such methods have the disadvantage of no longer simulating actual service conditions, and while notched or precracked specimens allow study of the crack propagation kinetics and crack arrest conditions very well, they have the disadvantage of eliminating the initiation stage which is rate-controlling in many systems.

7.2 SLOW STRAIN RATE TEST (SSRT)

The slow strain rate test is a form of simple tensile test in which a smooth specimen is pulled in tension in the environment of interest at a slow strain rate until failure occurs. By using this method, many of the disadvantages of the traditional forms of SCC susceptibility testing are eliminated. The major advantage of the test is its ability to produce rapid, positive indications of SCC susceptibility. Stress corrosion crack growth markedly decreases the ductility of the specimen and results in the formation of secondary cracks near the main fracture. If the environment is not aggressive or is benign, fracture occurs with normal ductility. Results are direct and unambiguous. The test requires a few days at most, depending upon the ductility of the alloy and the strain rate.

Conceptually, the SSRT achieves a balance between the rates of mechanical processes which promote ductile failure and the rates of corrosion processes which promote stress corrosion crack propagation and brittle fracture.

The choice of the suitable strain rate used, therefore, is the most important factor governing the outcome of a test. If the rate is too high, ductile failure will occur before the necessary corrosion reactions can have any effect. If the environment is one that produces filming of the metal surface, too slow a strain rate may permit film repair to keep pace with the rate at which bare metal is formed so that the cracking reaction is not sustained. In most of the engineering alloys, SCC will occur at strain rates between 10^{-5} to 10^{-7} s^{-1} .

SCC susceptibility may be classified by comparing time to failure, reduction in area, elongation or plastic strain to fracture (approximately proportional to the area under the load versus time curve). Additional information may be gained by recording load versus time curves from which mechanical properties such as yield stress, ultimate tensile stress, and fracture stress may be determined and compared.

In cases where susceptibility is doubtful because of only slight changes in ductility, time to failure, etc., it is useful to examine the specimen surface with a low-power microscope to determine if small cracks are present. SCC may be confirmed with a scanning electron microscope (SEM). The SEM readily reveals changes in fracture mode accompanying SCC, i.e. quasicleavage or intergranular facets are observed in contrast to the dimple mode observed in the absence of SCC.

8. Material and Solutions

8.1 Material

The test material was martensitic stainless steel (AISI 420). Five strips (1 in, 2.5 cm, wide, 0.25 in, 0.6 cm, thick and 132 in, 335 cm, long) of 420 type martensitic stainless steel along with a list of composition and mechanical properties were supplied by Fry Steel Company in the annealed condition. The material is a medium carbon grade of 12.57%Cr stainless steel with high hardenability. Although the chemistry was supplied by the steel producer, the steel was analyzed chemically in our laboratory by using the Hitachi S-2700 Scanning Electron Microscope with a link eXL Energy Dispersive X-Ray Analysis System (EDX). This system is able to detect as low as 0.3% of the specific alloying element where an error of $\pm 5.0\%$ is expected. The chemical composition of the as-received steel is listed in table 6. The hardness was measured, too.

8.2 Test Solutions

Modified standard NACE solutions¹¹³ were used: 5% sodium chloride, 0.5% acetic acid, in de-ionized water, saturated with N₂ or CO₂ or mixtures of H₂S-CO₂. The high-purity compressed gas mixtures were supplied by Linde Union Carbide; the mixing was done by partial pressure. The 100% CO₂ gas was industrial grade and the N₂ gas was extra dry grade. The test conditions which were used in this work are given in table 7. The pH of the test solutions was 2.5-3.0. In addition, solutions of 10%NaOH and saturated FeCl₃ in water were used to absorb any extra H₂S gas coming out of the recirculation system.

9. Experimental Procedures

9.1 Microstructure of the Steel

9.1.1 Specimen Preparation

Small specimens, 6.45 cm^2 (1 in^2), were cut from the supplied material for the purpose of microscopic examination. The specimens were ground with 200, 400 and 600 grit SiC paper in order to get fresh, clean surfaces and to avoid any contamination during the heat treatment processes. The specimens were then washed with soap, rinsed with water, and dried.

9.1.2 Specimen Heat Treating

In order to increase the strength of the test material, and according to the carbon and the chromium contents of the steel, a 1150°C austenitizing temperature was chosen from the C-Cr phase diagram, see Figure 32. This temperature is the lowest to obtain 100% austenite and to avoid the grain growth process.

The 6.45 cm^2 (1 in^2) annealed specimens were austenitized at 1150°C for two hours and then oil quenched. The oil quenching is recommended by the ASM handbook¹¹¹ to achieve the maximum ductility. Quench cracking was observed in the specimens after oil quenching; the reason is believed to be the oil quenching medium which results in a very rapid cooling rate and high thermal gradient. To avoid such problem, the oil quenching medium was replaced by a slower cooling rate medium which was air cooling. New specimens were prepared, austenitized at 1150°C for two hours, air cooled and then tempered for one hour. The applied tempering temperatures were 550°C , 650°C , 750°C , 800°C and 850°C . The specimens were then wet ground with 100, 200, 400 and 600 grit SiC paper, washed and dried with ethyl alcohol and a hot air blower.

9.1.3 Hardness Measurements

Hardness measurements were taken with Rockwell Hardness Tester Model 4TT BB. The Rockwell C scale was used to measure the hardness of as-received,

as air quenched and as quenched and tempered specimens by using the 150 kg load and the diamond Brale.

9.1.4 Examination with the Microscope

To observe the microstructure of the martensitic stainless steel in the different heat treatment conditions, two different etchants were used:

Etchant No. 1, for general structure: 5g FeCl₃, 15mL HCl, 60mL methanol.

Etchant No. 2, for carbide resolution: 10g ammonium persulfate, 100mL water (electrolytic etching).

The steps of specimen preparation and etching were as follows:

- a. The specimen was wet ground with 600 grit SiC paper, and dried with ethyl alcohol and a hot air blower.
- b. The specimen was then rough polished with 6 micron diamond paste and Buehler Metadi Fluid on nylon, washed with soap, rinsed with water and dried.
- c. The specimen was final polished with 0.05 micron gamma-alumina and water on cloth, washed with soap, rinsed with water and dried.
- d. The first set of specimens was etched with etchant no. 1 (immersion time 10-15s), rinsed with ethyl alcohol, and dried.
- e. The second set of specimens was electrolytically etched with etchant no. 2 in a 6V cell for 30-60s.

The different microstructures were observed under the metallurgical light microscope. Magnifications of 180x, 400x and 600x were used and photomicrographs were taken.

9.1.5 X-ray Diffraction

The constituents of the microstructures which were quenched and tempered at 800°C and 850°C were analyzed in our laboratory by the X-ray Diffraction (XRD) technique. A Philips X-ray system with Cu tube was used, with a PW 1380 horizontal goniometer equipped with an AMR (Amray) 3-202 graphite monochromator.

9.2 Slow Strain Rate Tests (SSRT)

9.2.1 Specimen Preparation

Since the slow strain rate test was used for determining SSC susceptibility in a slow strain tensile test in a specific medium, a tensile specimen was used.

The tensile specimen was machined from the as-received, full-annealed steel strips where the longitudinal direction of the specimen was the rolling direction. Figure 38 shows the dimensions of the specimen used. These specimen dimensions were chosen for their suitability to perform such kind of tests. The specimens were machined by the Technical Services workshop at the University of Alberta.

9.2.2 Specimen Heat Treating

The tensile specimens were austenitized at 1150°C for two hours and air cooled, then tempered for one hour. The tempering temperatures were 550°C, 650°C, 750°C and 850°C.

A K-type (chromel-alumel) thermocouple was used to control the temperature of the furnace. In addition, each tensile specimen was wrapped with 316 stainless steel sheet prior to heat treating it. The reason for that was to minimize as much as possible the oxidation of the tensile specimen surfaces during the heat treatment stages.

Before running the SSRT test, the tensile specimen was carefully wet ground with 600 grit SiC paper in the reduced section. The hardness of each specimen was measured at different spots but not at the reduced section of the specimen.

9.2.3 Equipment

The Material Test System (MTS, model 810) was used as the tensile testing machine.

9.2.3.1 The Material Test System

The model 810 MTS with a 25 tonne (27.6 ton) capacity load frame and load cell, 20.7 MPa hydraulic supply and two 100 kN hydraulic grips were used, see Figure 39.

The system consists of a fixed stiff frame, a carriage, a drive mechanism and a load cell recorder. The recorder was replaced with a data acquisition system (IBM computer) as shown in Figure 40.

The MTS was able to handle the required slow strain rate. The commonly used, engineering strain rate of $2 \times 10^{-6} \text{ s}^{-1}$ was selected; this strain rate has become more or less standard for ferrous alloys.

The stroke control was set with an MTS 442 Controller and the MTS 410 Digital Function Generator. Simple ramp and dual slope functions were set on the function generator. Instantaneous measurements of the stroke (crosshead movement) and the load were given by the MTS 430 Digital Indicator.

The maximum load was set at 10,000 lb (44.5 kN) for some tests and 25,000 lb (111.2 kN) for others dependent on the expected strength of the specimen. The time interval for recording the data (by data acquisition system) was

five minutes in some tests and 15 minutes in others. In addition, the load versus time curve was displayed on the computer screen throughout the test.

All the slow strain tests performed with the MTS were continued until the failure of the specimen. Time to failure, total elongation, maximum stress and area under the curve were determined from the resulting curves.

9.2.3.2 Testing Cell

The cell consisted of the tensile specimen, inlet and outlet for the test solution and pH electrode to measure any change in the pH along the test period. A plastic container was used to hold the specimen in the test solution, see Figure 41. Figure 42 shows the tensile specimen with the attached nylon sleeves. These nylon sleeves were required to allow the specimen to slide smoothly and freely through the top and the bottom opening of the plastic container during straining of the specimen. Silicone rubber adhesive sealant was used to seal the tiny gaps between the nylon sleeves and the tensile specimen. The silicone was allowed to set overnight before assembling the cell.

9.2.3.3 Recirculation System

The recirculation system consisted of an external flask, peristaltic pump and the corrosion cell (the plastic container) as shown in Figure 43. Two litres of test solution were used; the solution was pumped through Tygon tubing at 6mL/s flow rate from the external flask to the plastic container which surrounded the test specimen.

For each test, new solutions were prepared and the section of Tygon tubing which was under cyclic pinching during pumping was replaced. Because of high H₂S concentration and cyclic pressure, the Tygon tubing may become hard; consequently cracking of the tubing may occur.

9.2.4 Test Procedure

The test procedure for slow strain testing was as follows:

1. After heat treating the tensile specimen, the reduced section was wet ground by hand with 600 grit SiC paper in order to remove the thin oxide layer which was formed during the heat treatment process.
2. Only the reduced section of the tensile specimen was in direct contact with the test solution, while the rest was protected with Teflon tape. The nylon sleeves were attached to the specimen by silicone rubber adhesive; which was allowed to dry for eight to ten hours.
3. The reduced section of the tensile specimen was then washed with soap, rinsed with water, dried and degreased with ethyl alcohol.
4. The tensile specimen was fastened to the plastic container along with all the attachments and then the test solution was added to the external flask. When H₂S gas was in use, the experiment was designed to trap and get rid of the extra H₂S gas which exhausted from the external flask. The gas was passed through saturated FeCl₃ in water solution and 10% NaOH solution in turn.
5. Nitrogen was bubbled at a rate of 0.5 cm³/s through the external flask for 30 minutes before testing began, to remove the oxygen from the test apparatus and test solution. The nitrogen gas was bubbled into the completely sealed system and during nitrogen bubbling, the plastic test cell with the attached specimen was completely immersed in water to detect any gas leaking.
6. The test cell was fixed in the hydraulic grips of the MTS machine. The acquisition system was then loaded with the needed information, e.g. time interval for output data recording, sample name and test description.

7. The test solution was then saturated with the gas or gas mixture which was used for that particular test. The gas bubbling was for one hour at a rate of $0.5 \text{ cm}^3/\text{s}$ and in order to keep the saturation level, continuous gas bubbling ($0.2 \text{ cm}^3/\text{s}$) was kept throughout the test period.

8. The solution circulation was started and after 5-10 minutes, the slow strain rate test was started with extension rate of $2 \times 10^{-6} \text{ s}^{-1}$. All the SSRT tests were performed at room temperature (22°C).

9. When the test specimen failed; it was removed from the assembly, rinsed with distilled water and dried.

9.2.5 Visual and Microscopic Examination

The fracture surfaces of the specimens were examined visually and by light microscope at low magnification (7x). The main features examined were the mode of fracture, scale formation and the existence of secondary cracks.

All the fracture surfaces were examined with the scanning electron microscope (SEM). Magnifications of 50x, 100x, 300x, 1500x and 2500x were used to observe the cracking mode. Photomicrographs of the cracking modes were taken.

10. Results and Discussion

10.1 Microstructure and Hardness

The microstructure of the as-received material was examined by using the FeCl_3 etchant, for general structure. The as-received material was in the annealed condition and its hardness range was 10-13 Rockwell C (Rc). The microstructure of this material is shown in Figure 44. The structure is large particles of primary carbide and spheroidized particles of secondary carbide in a ferrite matrix. The carbide particles are randomly distributed and some carbides have precipitated at the ferrite grain boundaries.

Since the martensite transformation can take place at even a low cooling rate in 13% Cr steels, the microstructure of the tested material after air cooling from 1150°C consists of martensite and carbide as shown in Figure 45. After air cooling, the resulting microstructure reflects the structural composition at the austenitizing temperature.

The martensite is in the form of needles which are aligned in specific directions, parallel to each other, within each prior austenite grain. The distribution of the carbides (the dark areas) is not uniform. The hardness range of this martensitic structure was 54-56 Rc which is relatively high and close to the maximum hardenability value (54.5 Rc) which was given by the material supplier.

The general structures of the tested steels after tempering at 550°C, 650°C and 750°C are shown in Figures 46, 47 and 48 respectively. The microstructures of these steels are quite similar; they consist of tempered martensite, carbides and very small areas of retained austenite. The most important significant difference between these structures is the distribution of the carbide particles within the martensite matrix. The carbide particle distribution in the steels which were tempered at 550°C, 650°C and 750°C is shown in Figures 49, 50 and 51 respectively as black spots. The structures were revealed by etchant no. 2 (electrolytic etching). It is clear that

the distribution of carbides is affected by tempering temperature. In the steel tempered at 550°C, the spherical coarse carbide particles were mainly precipitated at the grain boundaries of the prior austenite structure.

As the tempering temperature increased from 550°C to 650°C and then to 750°C, more carbon precipitated out of the solution and the distribution of the fine carbide particles became more uniform, especially in the structure which was tempered at 750°C. Such substructures and differences seem to relate to the susceptibility of the steel to sulfide stress corrosion cracking and also might play an important role in the definition of the fracture mode.

The hardness ranges for all tested specimens at different conditions and tempering temperatures are given in table 8. The hardness value is remarkably affected by the tempering temperature, where the hardness decreased as the tempering temperature was raised from 550°C to 800°C.

The general microstructure of the steel which was tempered at 800°C is shown in Figure 52. This microstructure is quite different compared to the general structure of the steel which was tempered at lower temperatures. The constituents of this microstructure were analyzed by the x-ray diffraction technique. The structure consists of tempered martensite and carbides in a ferrite matrix. The carbide distribution in the structure (electrolytically etched) is shown in Figure 53. According to the equilibrium phase diagram, Figure 32, by tempering at 800°C, the steel is very close to the $\alpha + \gamma + \text{carbide}$ region and the possibility of γ phase formation is small. However, if the γ phase had a chance to form, it would transform to martensite while cooling. In addition, more carbides were precipitated in the structure, due to the fact that as the tempering temperature of the quenched steel (unstable structure) was increased, the tendency of the carbon to diffuse out of the solid solution and precipitate as chromium carbides should increase. Also, carbon is an austenite stabilizer and its solubility in the ferrite phase is very small.

All the gradual changes in the microstructure and the phase transformations which took place at different tempering temperatures were controlled by diffusion kinetics, or the diffusion process. The carbon diffusion rate was increased gradually as the tempering temperature of the steel was increased from 550°C to 800°C. At 800°C tempering, the diffusion rate of carbon was the highest, resulting in coarser carbide precipitates and well-defined carbide-free ferrite grains. Consequently, the hardness was dropped as a result of ferrite phase formation. The hardness of the microstructures was dropped from Rc 52 to Rc 21 as the tempering temperature was raised from 550°C to 800°C.

The SSC resistance of the steel quenched and tempered at 800°C was not studied, because of the resulting low hardness and the strength of the steel. The high strength is an essential property for the steel to be used in deep oil wells.

A set of specimens was quenched and tempered at 850°C for one hour. By looking at the phase diagram, one can see that 850°C is well above the bottom boundary of the $\alpha + \gamma + \text{carbide}$ zone, i.e. where the carbon starts to diffuse out of the martensite phase and form carbides; consequently the resulting ferrite phase transformed to austenite. After air cooling, the resulted microstructure was carbides, retained austenite and untempered martensite.

The actual hardness value of the martensitic structure might be lower than the measured one (45-48 Rc), but carbide precipitation makes the hardness value go up. This (fresh) martensite contains less carbon compared to the martensite which was formed by quenching the steel from 1150°C. This difference in the carbon content results in different hardness values. The approximate carbon content in each martensitic structure can be estimated from Figure 54 by using the hardness values. For the steel which was tempered at 850°C, the carbon content in the martensite is about 0.2% where in the steel quenched from 1150°C, the %C in the martensite is about 0.3%.

Figure 55 shows the general structure of the steel which was tempered at 850°C. It consists of martensite, carbides and retained austenite; these constituents were confirmed by using the x-ray technique. Figure 56 shows the distribution of the coarse carbides in the same steel (electrolytically etched) and the retained austenite which was completely transformed to martensite.

10.2 Stress-Time Curves

The slow strain rate tests of the specimens which were tempered at different tempering temperatures were performed in different environments at 22°C. Table 8 lists all the specimens with their corresponding tempering temperatures, hardness, test environment, time-to-failure, elongation and the maximum stress.

The stress-time reference curve for each set of specimens, tempered at specific temperature, was derived in air at 22°C. The remaining specimens of each set were tested in the following test solutions at 22°C in sequence: N₂, 90%H₂S/10%CO₂, 50%H₂S/50%CO₂, 10%H₂S/90%CO₂ and CO₂. All the test solutions contained 5% NaCl and 0.5% acetic acid. The tests were performed in the above given order, so that the effect of increasing the %CO₂ gas could be studied easily.

10.2.1 Steel Quenched and Tempered at 550°C

This steel, when tempered at 550°C, became progressively embrittled in an intergranular way (temper embrittlement). The stress-time reference curve (in air) for this specimen is shown in Figure 57. The specimen failed in a brittle manner with no necking taking place in the fracture region and without any reduction in area at the fracture surface. In spite of using slow strain rate ($2 \times 10^{-6} \text{ s}^{-1}$), the time-to-failure of this specimen was quite short (2.75h). In other test solutions, especially in H₂S environments, the time-to-failure will be definitely much shorter than 2.75h, which is not long enough for the SSC of the specimen to take place. As a result, testing of those specimens which were tempered at 550°C was rejected.

10.2.2 Steel Quenched and Tempered at 650°C

The slow strain rate test in air of the specimen quenched and tempered at 650°C was performed at 22°C. The stress-time curve of this test (reference curve) is shown in Figure 58. The specimen showed some ductility with little necking taking place in the fracture region. The time-to-failure was 21.75h and the maximum sustained stress was 1132.4MPa. The elongation is directly dependent on time, since the strain rate was set by the cross-head displacement rate of the MTS. The total elongation was 15.66%.

The SSRT test was run in the nitrogen saturated solution (50g^l-¹ NaCl, 0.5% acetic acid, bubbled N₂) at 22°C. The resulting stress-time curve is shown in Figure 59. The specimen showed little ductility compared to the reference specimen, and the time-to-failure dropped to less than half (8.9h). This earlier failure was believed to be caused by the existence of chloride ions and the solution acidity may prevent the passivation of the specimen surfaces and reduce the incubation period required for crack nucleation and propagation.

Some localized corrosion was observed on the specimen surfaces which might act as crack initiation points. Also, the low pH solution and the chloride ions accelerate the corrosion process at the crack tip which maintained active by breaking the passive film. This specimen failed at lower maximum stress (1005.5MPa) and less total elongation (6.36%) compared to the reference specimen.

Test 4 was performed in 90%H₂S/10%CO₂ solution. The specimen failed rapidly by deep SSC cracks, accompanied by brittleness; see Figure 60 for stress-time curve. Secondary cracks perpendicular to the applied stress were seen along the reduced section as shown in Figure 61. In addition, homogeneous black scale (FeS) was observed on the specimen gage length. The time-to-failure was 2.75h with a maximum stress of 539MPa.

Test 5 was done in 50% H_2S /50% CO_2 and test 6 in 10% H_2S /90% CO_2 . The stress-time curves of tests 5 and 6 are shown in Figures 62 and 63 respectively. Generally, these results indicate that dilution of H_2S with CO_2 up to 10% H_2S brought very little improvements compared with the test run on 90% H_2S /10% CO_2 . The time-to-failure and total elongation of tests 4 and 5 were exactly the same, whereas in test 6 they were slightly higher. The dilution of H_2S with CO_2 increased the maximum sustained stress as shown in table 8. In all H_2S test solutions, secondary cracks and black scales were observed.

The result of test 7 which was run in 100% CO_2 test solution was much better than the tests with H_2S . The time-to-failure and total elongation of test 7 were lower than that in N_2 environment and almost double that in H_2S environment. According to Figure 64, the specimen exhibited little or no ductility and the maximum stress was close to that in test 3 (N_2). The gage length was partly covered with $FeCO_3$ deposit.

It is evident from the above observations that chloride and acidity play an important role in favouring the initiation of localized and general corrosion, at least at 22°C, in agreement with previously published data¹¹⁴.

10.2.3 Steel Quenched and Tempered at 750°C

Specimens quenched and tempered at 750°C were tested under the conditions which are given in table 8. The reference stress-time curve (in air) is shown in Figure 65. The time-to-failure of this specimen was the longest among all the tested specimens (33.5h). The specimen showed a reasonable amount of ductility with little necking at the fracture region and little reduction in area at the fracture surface. The maximum stress was 851MPa.

The elongation to failure dropped from 24% in air (test 8) to 14% in N_2 (test 9). The stress-time curve for test 9 is shown in Figure 66. By comparison, the specimen of test 8 (in air) showed a larger amount of plastic deformation before

failure. Once again, the drop in the total elongation value of test 9 was due to the presence of Cl ions and low pH value of the solution. They reduced the incubation time for crack nucleation and propagation.

All the specimens tested in H₂S/CO₂ environments failed rapidly by deep SSC cracks. The failure of these specimens (tests 10, 11 and 12) was accompanied by severe loss of ductility, see Figures 67, 68 and 69 for stress-time curves of the specimens tested in 90%H₂S/10%CO₂, 50%H₂S/50%CO₂ and 10%H₂S/90%CO₂ respectively. All these specimens failed in a brittle manner; the time-to-failure was relatively short (3.25h-4.5h) compared with test 8 in air or test 9 in N₂. Secondary cracks parallel to the fracture surfaces were observed close to the fracture regions. In addition, the similarity in the results of 10%H₂S/90%CO₂ solution and the 90%H₂S/10%CO₂, which was concluded earlier is revealed again. Also, the tendency of CO₂ to form protective film on the specimen surfaces was disturbed due to the presence of chloride ions along with formation of FeS deposit. The little increase in the maximum stress as the percentage of the H₂S decreased, can be explained by assuming that in 10%H₂S/90%CO₂, the amount of hydrogen atoms which entered the steel was less compared to that in 90%H₂S/10%CO₂. In other words, the degree of embrittlement is proportional to the concentration of hydrogen atoms in the steel.

The addition of H₂S has two opposite effects. The first effect is that H₂S accelerates the corrosion rate through the cathodic reaction and the other effect that H₂S decreases the corrosion rate through the deposition of FeS. It can be assumed that the concentration of Fe²⁺ on the specimen surface could not reach the critical Fe²⁺ concentration required for FeCO₃ deposition because of a formation of FeS. Also, H₂S makes the corrosion potential noble so that the passivation film of this steel was easily destroyed.

Test 13 was performed in 100%CO₂; the stress-time curve is shown in Figure 70. The curve shows that for a short time, the specimen behaved plastically before failure. The time-to-failure and total elongation are relatively smaller in value

than those in test 9 (N₂). 420 martensitic stainless steel has been known for its resistance to CO₂ corrosion⁸¹.

From the results of test 13, it is evident that martensitic stainless steel type 420 is very susceptible to SSC cracking in environments containing H₂S. Also, chloride ions play an important role in the stability of the protective films.

10.2.4 Steel Quenched and Tempered at 850°C

The last set of specimens tested by the SSRT technique was tempered at 850°C. The results of the tests which were performed in solutions containing H₂S, see table 8, indicated that this tempering temperature results in the structure (martensite) most susceptible to SSC cracking among all tested specimens.

The reference stress-time curve in air is shown in Figure 71. The most significant feature of this curve is the maximum sustained stress (1638MPa), which is the highest among all the tested specimens. The high strength of this specimen was due to the (fresh) martensite structure which replaced the tempered martensite in the previous specimens.

The stress-time curve of test 15, in N₂, is shown in Figure 72. The specimen failed in a brittle manner after 7.9h. By comparison, the time-to-failure in air was 20h.

In H₂S solutions diluted with 10, 50 and 90%CO₂, the time-to-failure dropped dramatically. The stress-time curves are shown in Figures 73, 74 and 75 respectively. There is not much difference in the behaviour of the steel in these three different test solutions. Again, dilution of the H₂S with CO₂ up to 10%H₂S brought very little improvements compared with test 16 run in 90%H₂S/10%CO₂.

The results of test 19 run in 100%CO₂ are shown in Figure 76. The specimen failed in a brittle manner, the time-to-failure was 3.4h and the maximum

stress was 628.7MPa. By comparison, the specimen which was tested in 10% H_2S /90% CO_2 showed shorter time-to-failure but, in general, the difference is not remarkable.

Tests 14-19 proved that the untempered martensitic structure is very susceptible to SSC cracking in H_2S environments as well as SCC in 100% CO_2 . By comparison, the SSC resistance of tempered martensitic structure was much higher.

10.3 Fracture Appearance

All the fracture surfaces of the tested specimens were observed under the SEM including the tests which were performed in air for comparison purposes.

10.3.1 Steel Quenched and Tempered at 550°C

Figure 77 is an SEM fractograph of specimen 1, tempered at 550°C and tested in air, which shows a typical brittle (cleavage) fracture with quasicleavage fracture in some areas. The fracture surfaces were flat and the mode of cracking was typically intergranular as shown in the fractograph. The intergranular cracking can be related to the precipitation of the carbides at the grain boundaries. The grain boundaries became harder than the rest of the structure which made them a favorable path for the crack to propagate. Martensitic stainless steels are subject to temper embrittlement when they are tempered at this temperature after quenching.

10.3.2 Steel Quenched and Tempered at 650°C

Specimen 2, tempered at 650°C and tested in air, showed two different types of fracture. The first type is shown in Figure 78 which is a typical brittle fracture, and the mode of cracking is intergranular. In other small areas, the specimen showed ductile fracture due to microvoid coalescence as shown in Figure 79.

The fracture features of specimen 3, tested in NACE solution with N_2 , were similar to that of specimen 2, tested in air. Figure 80 shows the brittle fracture of this specimen along with small areas where quasicleavage fracture took place. Some rust along with a few pits was observed on the reduced section of the specimen. The fracture surfaces of specimens 4, 5 and 6, tested in H_2S/CO_2 solutions, showed the same fracture features. The fracture is brittle and the mode of cracking is intergranular. The fracture surfaces were flat with no sign of any ductility. Figures 81, 82 and 83 show the fractographs of these three specimens in the above order. The reduced sections of the specimens were covered with black deposit (FeS). Figure 84 shows the SEM fractograph of specimen 7 which was tested in 100% CO_2 solution. Once again, the fracture was brittle. The fractograph shows typical intergranular secondary cracks. The reduced section of the specimen was partly covered with grey deposit ($FeCO_3$).

10.3.3 Steel Quenched and Tempered at 750°C

Figure 85 is the SEM fractograph of specimen 8, tested in air. The fractograph shows a mixture of two fracture types, ductile fracture and brittle fracture. The ductile fracture which occurs due to microvoid coalescence and the quasicleavage fracture are shown in Figure 86 with higher magnification. The intergranular cracking (IGC) mode was also revealed in this specimen. The fracture surfaces were not flat. Very similar fracture features were observed in specimen 9, tested in solution saturated with N_2 , see Figure 87. A few pits were also observed on the specimen surfaces.

The fractograph of specimens 10 and 11, tested in 90% $H_2S/10\%CO_2$ and 50% $H_2S/50\%CO_2$, are shown in Figures 88 and 89 respectively. In both specimens, the fracture type was typically brittle with flat fracture surfaces and intergranular cracking. Specimen 12 which was tested in 10% $H_2S/90\%CO_2$ solution, showed quasicleavage fracture type in some areas. Its SEM fractograph is shown in Figure 90. All the specimens which were tested in H_2S -containing solutions showed a black deposit on their reduced sections. Generally, the above

results and observations indicate that the degree of embrittlement slightly depends on the concentration of H_2S .

The fracture surfaces of specimen 13, tested in 100% CO_2 , was also studied visually and with the SEM. Grey deposit ($FeCO_3$) was observed on the reduced section of the specimen. The fractograph of this specimen is shown in Figure 91. The fracture was mainly brittle but in some areas, quasicleavage fracture was also seen.

10.3.4 Steel Quenched and Tempered at 850°C

The SEM fractograph of specimen 14, tested in air, is shown in Figure 92. In comparison with specimens 2 and 8 which were tempered at 650°C and 750°C respectively and tested in air, the predominant fracture type was quasicleavage with brittle fracture in some areas. This different type of fracture features is related to the microstructure of this specimen. The fracture surfaces were flat and the IGC mode was revealed in the brittle fracture areas. The same fracture features were observed in specimen 15, tested in solution with N_2 , see Figure 93.

Specimen 16 was tested in solution with 90% H_2S /10% CO_2 and the SEM fractograph is shown in Figure 94. This fractograph was taken at lower magnification in order to show both types of fracture, the brittle and the quasicleavage. The central area showed both types of fracture where the surrounding areas were mainly quasicleavage.

Figures 95, 96 and 97 show the SEM fractographs of specimens 17, 18 and 19, which were tested in solution with 50% H_2S /50% CO_2 , 10% H_2S /90% CO_2 and 100% CO_2 respectively. The fracture features are exactly the same as those in specimen 16. Figure 98 shows the brittle fracture and the quasicleavage fracture (next to each other) with higher magnification.

10.4 Evaluation of Slow Strain Rate Test Results

10.4.1 Indication of SSC Susceptibility

Visual examination and the fractography were used to verify the presence or absence of SSC after each test. The unambiguous evidence indicating SSC susceptibility included secondary cracks along the gage length oriented perpendicular to applied stress, loss of ductility and crack propagation by brittle mode (IGC).

Among the tests which were performed in air, ductile fracture was observed in specimen 8 which was tempered at 750°C and to a lesser extent in specimen 2 which was tempered at 650°C. The loss of ductility was clearly observed in the specimens tempered at 750°C and/or 650°C when they were tested in solutions containing H₂S and/or CO₂.

The other two criteria, secondary cracks and brittle fracture mode, were observed in all the tested specimens except those which were tested in air (specimens tempered at 550°C and 850°C, tested in air, showed brittle fracture).

10.4.2 Measurement of SSC Severity

Measures of SSC severity in this work are based upon time-to-failure and stress versus time (or elongation) behaviour.

a. Time-to-Failure (TTF)

The SSC severity is expressed as the ratio of TTF when SSC was observed versus TTF for the specimen tested in air. The TTF ratios, for all tested specimens, are given in table 9. A ratio of 1 indicates no SSC while ratios less than 1 indicate SSC susceptibility. As the TTF ratios decrease, the SSC severity increases.

Table 9 shows that as the concentration of the H₂S in the gas mixture increased, the SSC severity increased (smaller ratios), disregarding the tempering temperature. Regarding the effect of the tempering temperature on the SSC severity, table 9 also shows that specimens tempered at 850°C showed the highest SSC severity compared to the specimens tempered at 750°C or 650°C. The SSC severity of the specimens tempered at 750°C and 650°C is very similar in solutions containing H₂S. However, the tempering temperature of 750°C gives a higher TTF ratio than that for 650°C in 100%CO₂ solution.

b. Stress versus Time Behaviour

The SSRT test results are represented by the stress versus time curves. Figure 99 shows the stress versus time behaviour of the specimens tempered at 650°C and tested in air and in solutions with N₂, H₂S/CO₂ and CO₂. The same relationships are plotted in Figure 100 for specimens tempered at 750°C and in Figure 101 for specimens tempered at 850°C.

Specimen elongation is related directly to time because a constant cross-head extension was imposed throughout the test. Typically, SSC severity is expressed as the ratio of a parameter from the SSC curve to a parameter of the air curve. As before, a ratio of 1 indicates no susceptibility and lower ratios indicate increasing SSC severity. Several parameters were used for comparison, i.e. maximum stress (MPa), total elongation (%El) and area under the curve (A), see table 9.

10.4.3 Chloride Stress Corrosion Cracking

From the SSRT results, Figures 99, 100 and 101, and disregarding the tempering temperature, one can see that testing the 420 steel in 5% NaCl + 0.5% acetic acid solution saturated with N₂, remarkably reduces the time-to-failure in comparison with the reference time-to-failure (in air). It is evident from these observations that, at least at room temperature, chlorides and acidity are the two

factors which are favouring the start of localized corrosion. Consequently, the incubation time for crack initiation and propagation was reduced.

Considering the effect of tempering temperature on the resistance of the 420 steel to chloride stress corrosion cracking, the steel which was tempered at 650°C and 850°C showed a high degree of susceptibility compared to the steel which was tempered at 750°C. The ratios of the area under the curve, see table 9, show such difference in the degree of susceptibility. For the steel tempered at 650°C and 850°C, the ratios of the area under the curve were 0.282 and 0.232 respectively, where for the steel tempered at 750°C the ratio was 0.537 which indicates better resistance to cracking in solutions containing chloride ions. This enhancement in the resistance can be related to the microstructure and the strength of the steel. However, from the microstructure point of view, tempering at 750°C results in a structure with a large amount of randomly distributed chromium carbide precipitates compared to that of the steel tempered at lower temperatures. Hence, there were local depletions of chromium in the vicinity of the precipitate, the corrosion resistance suffered especially if the carbide precipitates were restricted to the grain boundary, see Figure 49, where the steel (tempered at 550°C) would be more susceptible to localized attack. The chromium depleted zones (small in area) represent the anode of the corrosion cell while the rest of the matrix (large in area) represents the cathode.

From the microstructure of the steel tempered at 650°C, and due to the non-uniform distribution of the coarse carbides, it can be expected that this steel may suffer from general corrosion as well as from pitting corrosion. Figure 99 shows a decrease in the value of the applied stress compared to the corresponding part of the reference curve (in air), in the steel tempered at 650°C and tested in NaCl solution saturated with N₂. This observation might be referred to the occurrence of general corrosion.

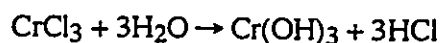
For the steel tempered at 850°C, the untempered martensite and retained austenite structure is very hard and high in strength. In addition, the carbide

distribution is not uniform. All these factors make the steel more susceptible to pitting corrosion and cracking in chloride-containing solutions.

The most significant difference between the steel tempered at 650°C and 750°C was the amount of the recovered ductility, which is related to the amount of carbide precipitates. As the tempering temperature increased (from 650°C to 750°C), the amount of precipitates increased which result in a structure with higher ductility. It seems that the amount of recovered ductility is the main factor which determines the degree of the steel susceptibility to cracking in chloride-containing solutions.

In fact, the enhancement in the cracking resistance of the steel tempered at 750°C cannot be referred to the microstructure alone or to the strength. The strength of the steel is a result of its microstructure, where the amount of carbide precipitates increased, i.e. as more carbon comes out of the solution, the strength of the steel decreases. In other words, as the tempering temperature increased (maximum 750°C), the amount of carbide precipitate increased, consequently, the strength dropped and the stress corrosion cracking resistance improved.

The factors of local breakdown of passivity and local acidification are very important, too. In the presence of chloride ions the passive film on stainless steel tends to break down. The local formation of hydrochloric acid is possible through this reaction:



If the concentration of HCl acid is high, it is difficult for the stainless steel to re-form a protective passive film, and a corrosion pit may form at which the crack may initiate.

10.4.4 Sulfide Stress Corrosion Cracking in H₂S/CO₂ Solutions

Disregarding the tempering temperature effect and the H₂S concentration, all the specimens which were tested in H₂S/CO₂ solutions experienced a severe SSC cracking and they failed after quite a short time. All the fractures took place in brittle manner, i.e. for the steel tempered at 750°C, and to some extent the steel tempered at 650°C, the ductility was entirely lost. This loss in ductility in the presence of H₂S, and the failure of the specimen after a short time, indicates that the fracture mechanism in those specimens was hydrogen assisted cracking (HAC). In addition, at specific tempering temperatures, the time-to-failure of the specimens which were tested in different H₂S concentrations was close to each other (not much difference) and also the cracking modes and the fracture appearance were almost the same. The intergranular cracking in H₂S environments does not exhibit sufficient ductility to permit the anodic dissolution of the plastically deformed metal at the advanced crack tip, and it seems reasonable to relate the failure to HAC. The results of metallographic studies showed that the density of carbide particles was quite high, due to high carbon content, especially in steels tempered at higher temperatures. The interfaces of incoherent carbides and inclusions have been documented as strong trap sites for hydrogen¹¹⁵. The accumulation of hydrogen at these interfaces might reduce the stress required for interface decohesion¹¹⁶. In addition, high stress concentration can develop easily at the interfaces of the carbide particles due to the elastic-plastic incompatibility. The combination of hydrogen and high stress concentration can enhance the decohesion of the interfaces and consequently the cracking initiates at the these interfaces.

In high strength steel with a microstructure similar to that of the steel tempered at 550°C, Figure 49, where the carbide particles along the prior austenite grain boundaries are more closely spaced and less spheroidized, the elastic-plastic incompatibility stress concentration is probably higher than that of the steel tempered at 650°C and 750°C. As the stress concentration becomes higher, the

critical amount of hydrogen required to initiate the crack becomes lower. This was indicated by the short time-to-failure for steel tempered at 650°C compared to that of steel tempered at 750°C. The crack propagation could occur more easily at the decohered carbide/matrix interfaces along the prior austenite grain boundaries.

Furthermore, the fine carbide particles which were observed in the steel tempered at 750°C, Figure 51, are related to the better SSC resistance of this steel compared to that tempered at 550°C and 650°C. This observation can be explained by the postulate that in a fine carbide structure, the area of the carbide/matrix interfaces per unit volume is quite high, which demands a longer time to attain the critical amount of hydrogen required for cracking, i.e. the SSC resistance increases.

Slightly longer time-to-failure was observed while testing in the solution saturated with 10% H_2S /90% CO_2 gas mixture, in comparison with those which were tested in solutions with higher H_2S concentration. This small difference in behaviour can be explained from the H_2S poisoning effect and the CO_2 catalytic poisoning point of view. In order to cause cracking, a hydrogen molecule has to dissociate into atoms. However, in hydrogen sulfide-containing solutions, the absorption of atomic hydrogen into the metal is enhanced by the poisoning effect of sulfur-containing species²⁰. In other words, the presence of H_2S in the solution prevents the combination of hydrogen atoms from forming hydrogen molecules which cannot diffuse into the steel or cause cracking. In gaseous environment, it was concluded that the dissociation of molecular hydrogen on the metal surface is the first step in the process of hydrogen embrittlement¹¹⁷. Similarly, it can be assumed that in aqueous environments the adsorption of hydrogen atoms on the metal surface is the first step in the process of hydrogen embrittlement. If this step can be controlled then the embrittlement phenomenon itself can be controlled. If, however, the adsorption site is poisoned, i.e. occupied by a foreign atom or molecule, like CO_2 , the hydrogen adsorption is prevented and the cracking process stops. The concept of competitive adsorption is well known. The more strongly adsorbed molecule will dominate the surface coverage. As proved in gaseous environment¹¹⁸, it is reasonable to assume that, in the H_2S/CO_2 mixtures, H_2S was

more strongly adsorbed. If the amount of CO_2 in the solution was increased, the displacement of H_2S on the surface by CO_2 would be higher. In addition, as the concentration of CO_2 is increased, the poisoning effect of H_2S become less effective. Consequently, the concentration of hydrogen atoms on the steel surface became lower and the time taken to reach the sufficient concentration of hydrogen atoms to cause cracking was increased, i.e. time-to-failure was increased.

According to the time-to-failure results, total elongation and the ratios of the area under the curve, tempering temperature and/or strength had very small effect on the degree of susceptibility to SSC in solutions saturated with 10-90% H_2S . The pH of the test solutions, saturated with different $\text{H}_2\text{S}/\text{CO}_2$ concentrations, did not show any significant change throughout the test. It is evident that the addition of up to 90% CO_2 to the H_2S -containing solutions does not affect the acidity of the solution.

Black deposits (FeS) were formed on the surfaces of the specimens while testing them in H_2S -containing solutions. The absence of the FeCO_3 deposit in those specimens which were tested in high H_2S environments, can be explained through the competitive film formation between FeCO_3 and FeS , and only if we assume that the concentration of Fe^{+2} ions on the surface could not attain the critical concentration required for FeCO_3 deposition, due to FeS formation. Furthermore, the free energy (ΔG) for FeCO_3 film formation is almost double that of FeS film formation at 22°C ¹¹⁹.

10.4.5 Stress Corrosion Cracking in CO_2 Environment

SSC susceptibility of 420 steels in solutions saturated with 100% CO_2 was strongly affected by tempering temperature and the strength, see tables 8 and 9.

The ratios of the area under the curve for the steels tempered at 650°C and 850°C were 0.18 and 0.049 respectively, where for the steel tempered at 750°C , the ratio was 0.329. The superior SCC resistance of the steel tempered at 750°C in CO_2

environment can be related to the microstructure, carbide dispersion and strength. The tempered martensite and uniform carbide distribution with lower strength result in better CO₂ SCC resistance.

The formation of siderite film on the specimens' surfaces was not homogeneous and/or not complete, the completion of protective FeCO₃ film being delayed by the adsorption of chloride ions on the corrosion surface. The resulting unprotected areas represented the anodic areas where the pitting corrosion took place and consequently, the cracks were initiated from those pits. The local breakdown of passivity and local acidification mechanism is also possible. The 420 steel may show better SCC resistance in CO₂ environment if the concentration of chloride ions is lower.

Due to the absence of the H₂S poisoning effect, the available hydrogen atoms have a chance to combine and form hydrogen molecules, which are unable to enter the steel and cause the embrittlement. Also, the hydrogen embrittlement mechanism was reduced by the lack of poisoning effect and therefore CO₂ is probably assisting the SCC by the dissolution mechanism.

The complete loss of ductility in the steel tempered at 650°C and the quasicleavage fracture together with the brittle fracture in the steel tempered at 750°C could be related to the occurring of SCC, which is the brittle fracture of the specimens in the corrosive environment.

11. Conclusions

From the presented results and analyses, it is apparent that the sulfide stress corrosion (SSC) cracking and/or stress corrosion cracking (SCC) behaviour of AISI 420 martensitic stainless steel, in chloride-containing solutions saturated with N_2 , with H_2S/CO_2 and with CO_2 environments at $22^\circ C$, is extremely complex and not easily understood. Considerable additional experimental and analytical work must be conducted to completely explain the observed SSC and/or SCC behaviour. However, the following conclusions have been drawn from this study.

1. The sulfide stress corrosion (SSC) cracking and/or stress corrosion cracking (SCC) susceptibility of the martensitic stainless steel, type 420, in environments containing H_2S , CO_2 and Cl ions is strongly affected by tempering temperature. Tempering at $750^\circ C$ produces the most favourable microstructure for SSC resistance, that is, a well-recovered substructure with fine carbides.
2. The precipitation of the closely spaced carbide particles along the prior austenite grain boundaries plays an important role in favouring the intergranular cracking of the (0.38%C) 420 steel. The relatively high density of carbide particles along the grain boundaries makes the grain boundaries harder and more brittle compared to the rest of the microstructure. Consequently, these grain boundaries become a favorable path for cracking.
3. Regardless of the tempering temperature, the SSC susceptibility of the 420 steels in H_2S -containing solutions is very high. 10% H_2S is enough to cause considerable embrittlement. Above 10% H_2S , the degree of susceptibility only slightly increases with H_2S concentration.

4. The dilution of H₂S-containing solution with CO₂ slightly lowers the aggressiveness of the environment. Although it does not affect the acidity of the NACE solution, increasing the concentration of CO₂ in the H₂S/CO₂ gas mixture results in reducing the severity of the H₂S poisoning effect and as a result, the concentration of the hydrogen atoms which are available for entry into the structure to enhance the embrittlement mechanism. This effect is related to the lowering of the H₂S concentration in the solution and probably to the competitive adsorption of CO₂ on the steel surface.
5. In H₂S-free solutions, the effect of CO₂ seems to be the increasing of the corrosion rate. The local destroying of the FeCO₃ film due to the existence of a relatively high concentration of chloride ions in CO₂-saturated solutions plays an essential role in favouring the start of localized corrosion. In these environments, the controlling cracking mechanism is most likely to be the anodic dissolution mechanism.

Table 1. A Short History of Investigation on CO₂ Corrosion⁶⁷

| | 1950's | Since 1973 |
|--------------------------|--|---|
| Summary of Investigation | 1. Accumulation of field experience 1 Water ratio 2 CO ₂ > 0.4 atm 2. Prevention method 1 Cr steel (Valve etc.) 2 Inhibitor 3 Homogeneity of microstructure | 1. CO ₂ corrosion mechanism 2. Effect of factor 3. Prevention method 9Cr-1Mo, 13Cr, Duplex S. S. |
| Background | 1. Increasing CO ₂ gas wells 2. Corrosion at welded portion of line pipe 3. Ringworm corrosion at upset portion of tubing | 1. Exploiting high temperature CO ₂ gas reservoirs 2. Exploiting offshore gas wells (Maintenance free) |

Table 2. SCC of 13Cr Steel Test Conditions⁸⁷

| | Temperature (°C) | NaCl (wt%) | gas composition(atm) | | | Solubility of gas (calculated) | | pH ³⁾ | Testing Period |
|-------------------|------------------|------------|-----------------------------|-----------------------------|----------------------------|--------------------------------|------------------------|------------------|----------------|
| | | | P _{CO₂} | P _{H₂S} | P _{N₂} | CO ₂ (ppm) | H ₂ S (ppm) | | |
| I | 80 | 3.5 | 0 | 0 | 1.0air | 0.4 | 0 | 6.0 | 720h (30day) |
| II | 80 | 3.5 | 1.0 | 0 | 0 | 550 | 0 | 5.0 | |
| III | 25 | 3.5 | 0.7 | 0.007 | Bal. | 880 | 21 | 5.2 | |
| IV | 25 | 3.5 | 0.7 | 0.07 | Bal. | 880 | 210 | 4.9 | |
| V | 25 | 3.5 | 0.7 | 0.3 | 0 | 880 | 904 | 4.7 | |
| VI | 25 | 3.5 | 0 | 1.0 | 0 | 0 | 3000 ²⁾ | 5.0 | |
| VII ¹⁾ | 25 | 5.0 | 0 | 1.0 | 0 | 0 | 3000 ²⁾ | 3.9 | |

Table 3. The Results of SCC Tests in CO₂/H₂S Environments⁸⁷

| | Composition (wt%) | Tempering Temperature (C) | Tensile Strength | | SCC Test Results | | |
|------------------|---------------------|---------------------------|--------------------------|--------------------------|---|-------------------------------------|-----------------------------------|
| | | | YS (kg/mm ²) | TS (kg/mm ²) | Condition III P _{CO₂} : 0.7 atm P _{H₂S} : 0.007 atm | Condition IV 0.7 atm 0.07 atm | Condition V 0.7 atm 0.3 atm |
| C-type | 0.19C-13Cr | 640 | 73 | 90 | O (0.8) | X (0.6) | X (2.1) |
| | | 720 | 60 | 78 | O (1.3) | X (1.4) | X (2.3) |
| | 0.15C-13Cr | 630 | 70 | 88 | O (0.8) | X (1.0) | X (5.3) |
| | | 720 | 60 | 75 | O (2.6) | O (1.6) | X (2.4) |
| 0.15C-13Cr-0.06N | 630 | 75 | 93 | O (1.1) | X (1.7) | X (2.0) | |
| | 720 | 60 | 78 | O (1.5) | O (1.6) | O (2.6) | |
| 0.10C-13Cr-0.06N | 600 | 70 | 90 | O (3.4) | O (2.4) | X (2.6) | |
| | 680 | 58 | 76 | O (1.6) | O (1.7) | O (2.4) | |
| Ni-type | 0.066C-13Cr-2.5Ni | 580 | 70 | 78 | X (0.5) | X (0.6) | X (0.9) |
| | | 650 | 60 | 70 | O (0.3) | O (0.4) | X (1.0) |
| | 0.05C-13Cr-4Ni-1Mo | 600 | 68 | 82 | X (0.2) | X (0.4) | X (0.7) |
| | | 650 | 62 | 84 | X (0.2) | X (0.3) | X (0.8) |
| | 0.003C-13Cr-2Ni-1Mo | 600 | 72 | 78 | O (0.2) | O (0.3) | O (0.9) |
| | | 630 | 65 | 78 | O (0.2) | O (0.2) | O (0.8) |
| | 0.003C-12Cr-5Ni | 580 | 69 | 73 | O (0.4) | O (2.7) | X (0.9) |
| | | 630 | 62 | 74 | O (0.3) | O (0.6) | X (0.7) |
| | 0.004C-13Cr-6Ni | 580 | 72 | 78 | O (0.4) | O (0.4) | X (0.8) |
| | | 630 | 72 | 79 | O (0.3) | O (0.4) | O (0.8) |
| Low alloy steel | KS80 | 640 | 67 | 79 | O (12) | O (15) | O (7.4) |
| | K090SE | 670 | 63 | 72 | O (6.0) | O (6.5) | O (4.5) |
| | KS95 | 600 | 73 | 85 | O (17) | O (16) | O (7.2) |

Note: () = corrosion rate (mpy).
O = crack-free.

Table 4. Typical High-Alloy Materials Being Considered for Corrosive Oilfield Service⁸⁹

| Type | Materials | Source | Composition, wt-% | | | | | | | | | |
|------------------|------------------------------|--------------------------|-------------------|------|------|-----|---------|----------|-----|-----|--------------------|-------------------------|
| | | | Fe | Ni | Cr | Mo | Nb + Ta | Ti | Al | Cu | Others | |
| Stainless steels | Martensitic | 12-13%Cr | ... | Bal. | ... | 12 | ... | ... | ... | ... | ... | ... |
| | | CA6NM | ... | Bal. | 4 | 12 | 0.70 | ... | ... | ... | ... | ... |
| | Precipitation hardened | 17-4 PH (martensitic) | 1 | Bal. | 4 | 17 | ... | ... | ... | ... | 4 | ... |
| | | Custom 450 (martensitic) | 2 | Bal. | 6 | 15 | 0.75 | ... | ... | ... | 1.5 | ... |
| | Austenitic | A-286 (austenitic) | ... | Bal. | 26 | 15 | 1-3 | ... | 2.0 | 0.2 | ... | 0.015B |
| | | 20Cb-3 | 2 | Bal. | 33 | 20 | 2-5 | 1.0 max. | ... | ... | ... | ... |
| | | 904 L | 3 | Bal. | 25 | 20 | 4-5 | ... | ... | ... | 1.5 | ... |
| | | AL 6X | 4 | Bal. | 24 | 20 | 6.0 | ... | ... | ... | ... | ... |
| | Duplex (austenitic-ferritic) | Sanicro 28 | 5 | Bal. | 31 | 27 | 3-5 | ... | ... | ... | 1.0 | ... |
| | | AF-22, SAF-2205 | 6,5 | Bal. | 5-5 | 22 | 3 | ... | ... | ... | ... | 0.14N |
| Nickel alloys | Jrenus 50 | ... | Bal. | 7 | 21 | 2-5 | ... | ... | ... | 1.5 | ... | |
| | Ferralium | 7 | Bal. | 5-5 | 26 | 3 | ... | ... | ... | 3 | 0.1N min. | |
| | DP-3 | 8 | Bal. | 6 | 25 | 1-5 | ... | ... | ... | ... | 0.1N min. | |
| Cold reduced | Hastelloy C-276 | 7 | 6 | Bal. | 15 | 16 | ... | ... | ... | ... | 2.5Co max. 4.0W | |
| | | Hastelloy G | 7 | 20 | Bal. | 22 | 6 | 2 | ... | ... | 2.0 | 2.5Co max. 1.0W max. |
| | Inconel 625 | 9 | 25 | Bal. | 21 | 9 | 3.5 | 0.2 | 0.2 | ... | ... | |
| | | Incoloy 825 | 9 | 30 | 42 | 22 | 3 | ... | 0.9 | ... | 2.25 | ... |
| | | Incoloy 800 | 9 | 45 | 32 | 21 | ... | ... | 0.4 | 0.4 | 0.38 | ... |
| | Precipitation hardened | Inconel 718 | 9 | 19 | Bal. | 19 | 3 | 5.0 | 0.9 | 0.5 | 0.15 | ... |
| | | Pyromet 31 | 2 | 15 | Bal. | 23 | 2 | 0.85 | 2.3 | ... | 1.3 | 0.095B |

Table 5. Chemical Composition of Selected Alloy Steels⁹¹

| Material | C | Mn | Si | Cr | Ni | P | S | Mo |
|----------|--------------|--------------|--------------|-----------|------|-------|--------------|------|
| 9Cr-1Mo | 0.12 | 0.41 | 0.49 | 8.50 | 0.11 | 0.022 | 0.002 | 0.95 |
| AISI 410 | 0.15 max. | 1.00 max. | 1.00 max. | 11.5-13.5 | -- | -- | 0.03 max. | -- |
| AISI 420 | 0.15 min. | 1.00 | 1.00 | 12.0-14.0 | -- | -- | 0.03 | |

Table 6. The Chemical Composition of Steel Used (wt%)

| C | Mn | P | S | Si | Ni | Cr | Mo | Cu | Al | Sn |
|------|------|-------|-------|------|------|-------|------|-------|-------|-------|
| 0.38 | 0.43 | 0.022 | 0.003 | 0.41 | 0.17 | 12.57 | 0.19 | 0.078 | 0.015 | 0.009 |

Table 7. Test Conditions

| | Temperature (°C) | NaCl (wt%) | Acetic Acid (wt%) | PCO ₂ | PH ₂ S | PN ₂ |
|-----|------------------|------------|-------------------|------------------|-------------------|-----------------|
| I | 22 | 0 | 0 | 0 | 0 | 1.0air |
| II | 22 | 5.0 | 0.5 | 0 | 0 | 1.0 |
| III | 22 | 5.0 | 0.5 | 0.1 | 0.9 | 0 |
| IV | 22 | 5.0 | 0.5 | 0.5 | 0.5 | 0 |
| V | 22 | 5.0 | 0.5 | 0.9 | 0.1 | 0 |

Table 8. Slow Strain Rate Test Results

| Specimen and/or Test No. | Tempering Temperature (°C) | Hardness Range (Rc) | Test Environment* | Time-to-Failure Hours | Time-to-Failure Minutes | Elongation % | Max. Stress (MPa) |
|--------------------------|----------------------------|---------------------|--|-----------------------|-------------------------|--------------|-------------------|
| 1 | 550 | 50-52 | air | 2 | 30 | 1.80 | 498 |
| 2 | 650 | 36-40 | air | 21 | 45 | 15.66 | 1130 |
| 3 | 650 | 36-40 | N ₂ | 8 | 54 | 6.36 | 1000 |
| 4 | 650 | 36-40 | 90%H ₂ S/10%CO ₂ | 2 | 45 | 1.98 | 539 |
| 5 | 650 | 36-40 | 50%H ₂ S/50%CO ₂ | 2 | 45 | 1.98 | 549 |
| 6 | 650 | 36-40 | 10%H ₂ S/90%CO ₂ | 3 | 19 | 2.40 | 657 |
| 7 | 650 | 36-40 | CO ₂ | 6 | 23 | 4.50 | 956 |
| 8 | 750 | 23-27 | air | 33 | 30 | 24.12 | 851 |
| 9 | 750 | 23-27 | N ₂ | 19 | 40 | 14.04 | 838 |
| 10 | 750 | 23-27 | 90%H ₂ S/10%CO ₂ | 3 | 15 | 2.34 | 551 |
| 11 | 750 | 23-27 | 50%H ₂ S/50%CO ₂ | 3 | 45 | 2.70 | 581 |
| 12 | 750 | 23-27 | 10%H ₂ S/90%CO ₂ | 4 | 32 | 3.24 | 608 |
| 13 | 750 | 23-27 | CO ₂ | 13 | 11 | 9.42 | 820 |
| 14 | 850 | 45-48 | air | 20 | 05 | 14.34 | 1640 |
| 15 | 850 | 45-48 | N ₂ | 7 | 55 | 5.64 | 1220 |
| 16 | 850 | 45-48 | 90%H ₂ S/10%CO ₂ | 1 | 40 | 1.20 | 340 |
| 17 | 850 | 45-48 | 50%H ₂ S/50%CO ₂ | 1 | 36 | 1.14 | 327 |
| 18 | 850 | 45-48 | 10%H ₂ S/90%CO ₂ | 2 | 11 | 1.56 | 475 |
| 19 | 850 | 45-48 | CO ₂ | 3 | 22 | 2.40 | 629 |

* N₂, H₂S/CO₂ and CO₂ gases were saturated in (5% NaCl + 0.5% acetic acid).

Table 9. Severity of the Slow Strain Rate Tests

| Specimen No. | Tempering Temperature (°C) | (%) Test Environment* | TTF(env.)/ TTF(air) | %El(env.)/ %El(air) | Area Under the Curve (A) A(env.)/A(air) |
|--------------|----------------------------|--|------------------------|------------------------|--|
| 1 | 550 | air | 1 | 1 | 1 |
| 2 | 650 | air | 1 | 1 | 1 |
| 3 | 650 | N ₂ | 0.409 | 0.406 | 0.282 |
| 4 | 650 | 90%H ₂ S/10%CO ₂ | 0.126 | 0.126 | 0.041 |
| 5 | 650 | 50%H ₂ S/50%CO ₂ | 0.126 | 0.126 | 0.041 |
| 6 | 650 | 10%H ₂ S/90%CO ₂ | 0.152 | 0.153 | 0.054 |
| 7 | 650 | CO ₂ | 0.293 | 0.291 | 0.18 |
| 8 | 750 | air | 1 | 1 | 1 |
| 9 | 750 | N ₂ | 0.587 | 0.582 | 0.537 |
| 10 | 750 | 90%H ₂ S/10%CO ₂ | 0.097 | 0.097 | 0.048 |
| 11 | 750 | 50%H ₂ S/50%CO ₂ | 0.112 | 0.112 | 0.056 |
| 12 | 750 | 10%H ₂ S/90%CO ₂ | 0.135 | 0.134 | 0.071 |
| 13 | 750 | CO ₂ | 0.394 | 0.391 | 0.329 |
| 14 | 850 | air | 1 | 1 | 1 |
| 15 | 850 | N ₂ | 0.394 | 0.393 | 0.232 |
| 16 | 850 | 90%H ₂ S/10%CO ₂ | 0.083 | 0.084 | 0.014 |
| 17 | 850 | 50%H ₂ S/50%CO ₂ | 0.0797 | 0.079 | 0.013 |
| 18 | 850 | 10%H ₂ S/90%CO ₂ | 0.109 | 0.109 | 0.025 |
| 19 | 850 | CO ₂ | 0.168 | 0.167 | 0.049 |

* N₂, H₂S/CO₂ and CO₂ gases were saturated in (5%NaCl + 0.5%acetic acid).

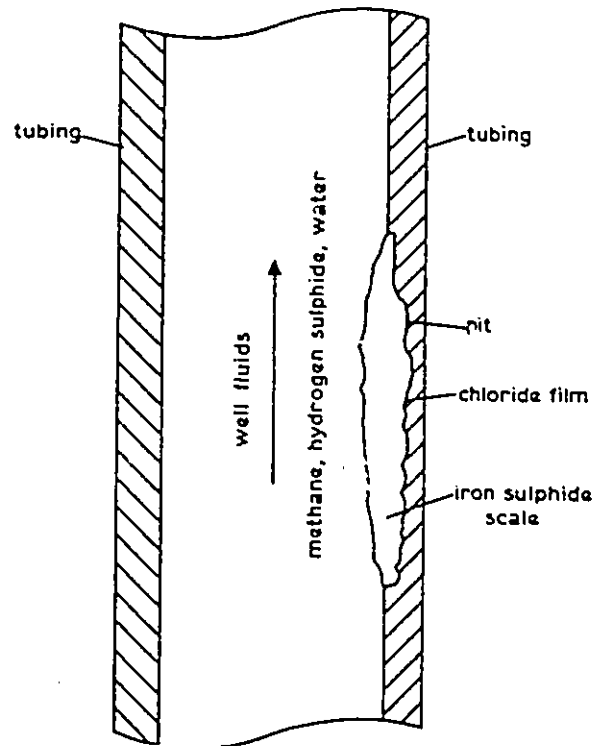


Figure 1. Mechanism of Pitting Corrosion in a Sour Gas System⁶

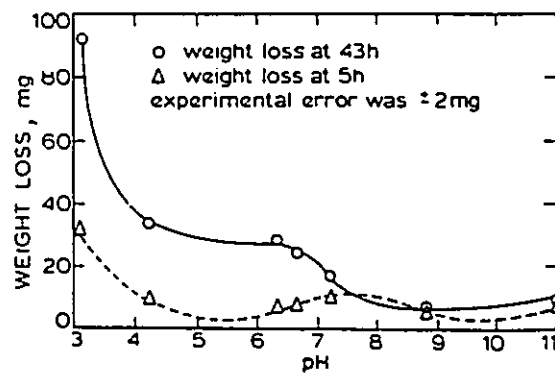


Figure 2. Weight-Loss Corrosion of Low-Alloy Steel versus pH in Solution of Water and H₂S/CO₂ Gas Mixture¹²⁰

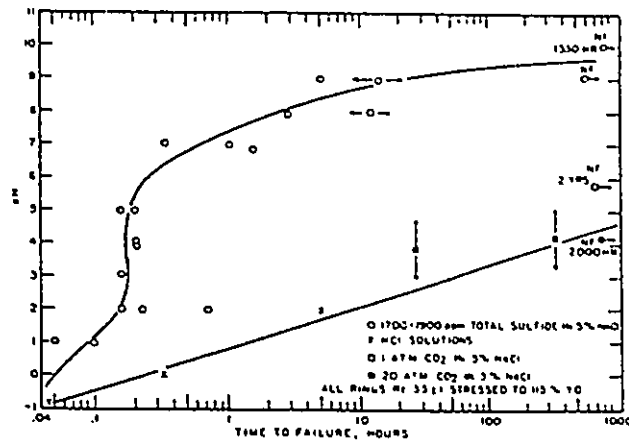


Figure 3. Failures Times as a Function of pH, with and without H_2S ³⁰

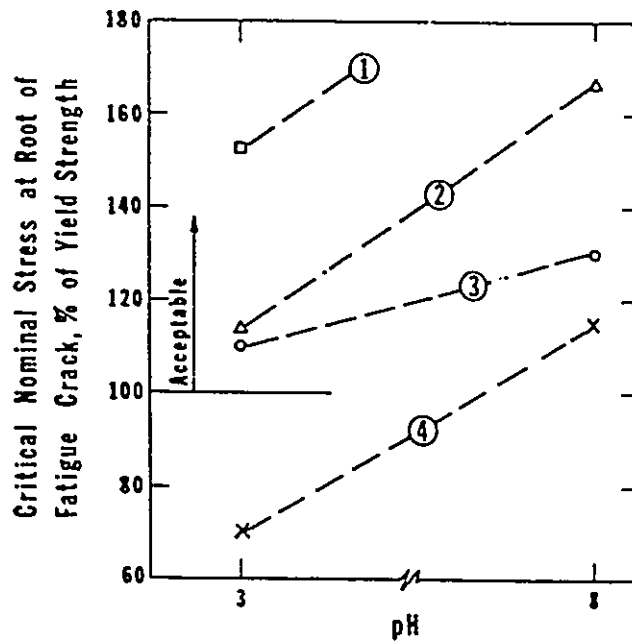


Figure 4. Effect of H_2S and pH on Sulfide Stress Cracking of P-110 Casing. (1) 25 ppm H_2S , (2) 150 ppm H_2S , (3) 300 ppm H_2S , (4) 2800 ppm H_2S ³¹

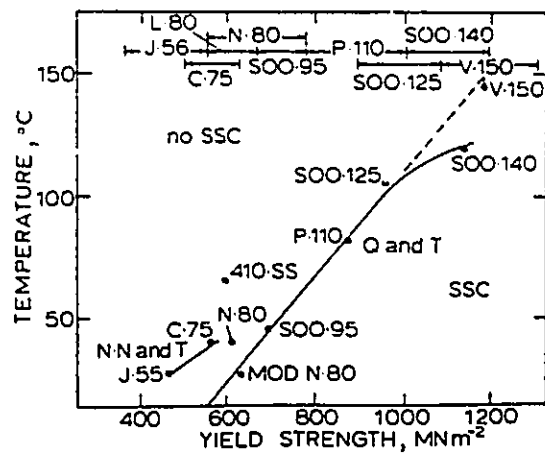


Figure 5. Temperature for SSC Resistance Behavior versus Material Yield Strength for API Casing Steels³⁴

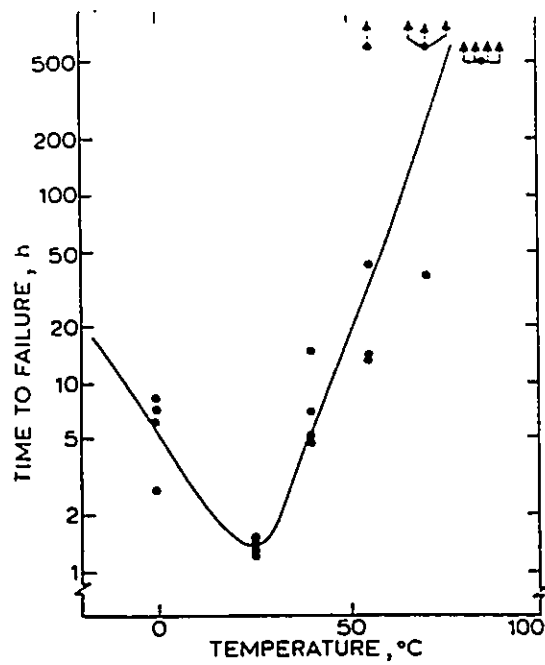


Figure 6. Time-to-Failure for Sulfide Stress Cracking versus Temperature for a HSLA (C-Mn) Steel³⁶

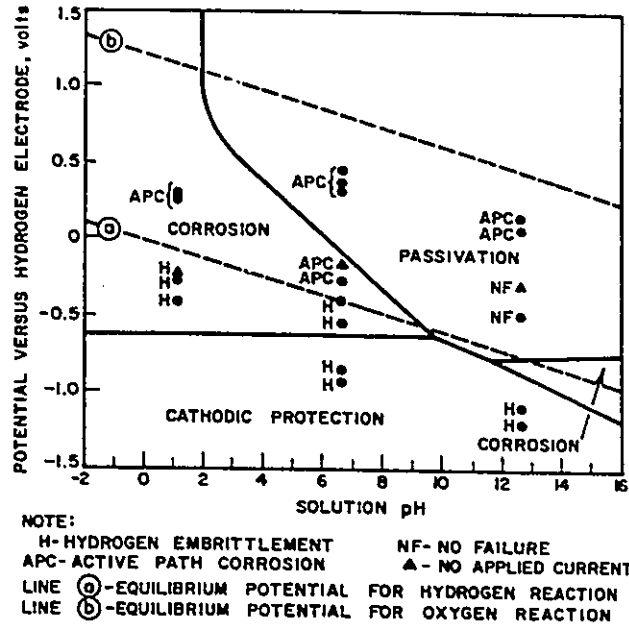


Figure 7. Equilibrium Potential-pH Diagram for iron in water with superimposed Stress Corrosion Results on 12 Mo-V Stainless in 3% NaCl Solution³⁸

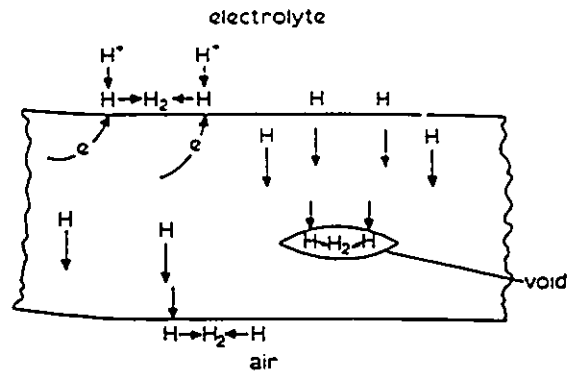


Figure 8. Formation of Hydrogen Blister in Steel⁴⁶

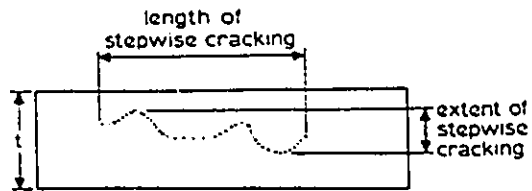


Figure 9. A Schematic of Stepwise Cracking in Line-Pipe Steel¹²¹

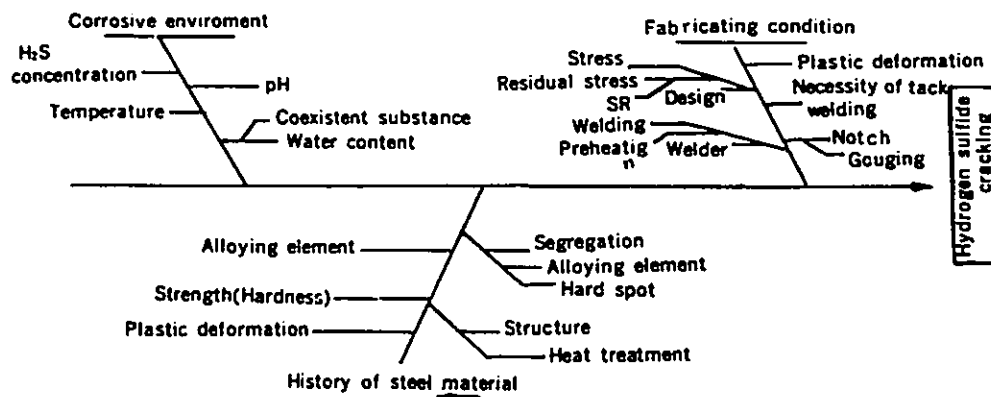


Figure 10. A Schematic Diagram of Factors Affecting Hydrogen Sulfide Induced Cracking¹²²

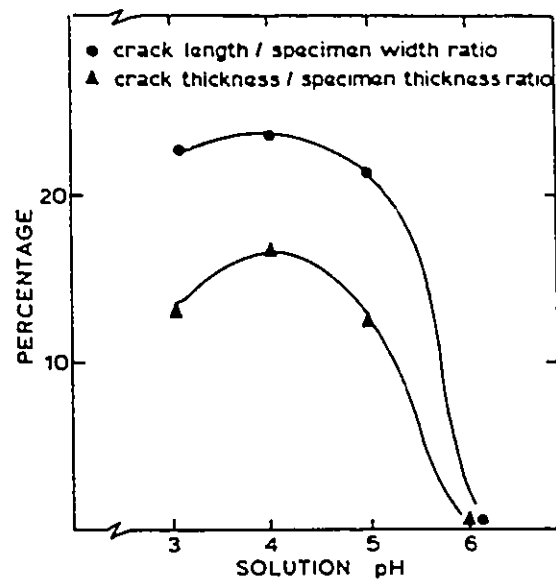
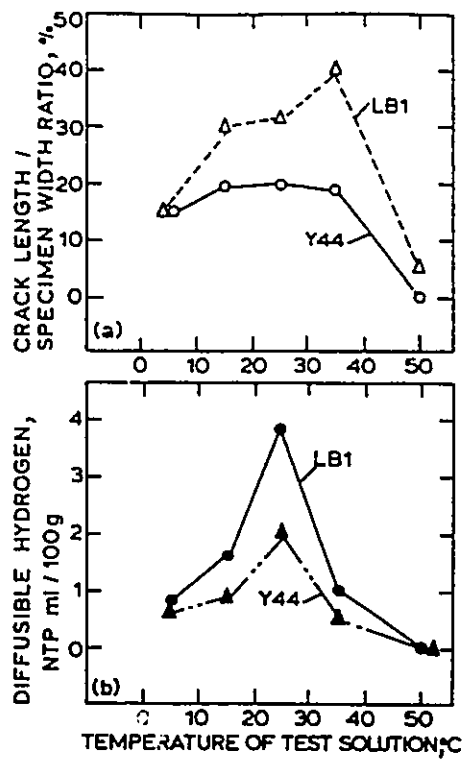


Figure 11. Effect of pH Value on Stepwise-Cracking Behavior for API Line-pipe Steel⁶¹



a susceptibility to HIC; b diffusible hydrogen

Figure 12. Effect of Temperature on Stepwise-Cracking Behavior for API Line-Pipe Steels with Various Modifications¹⁰

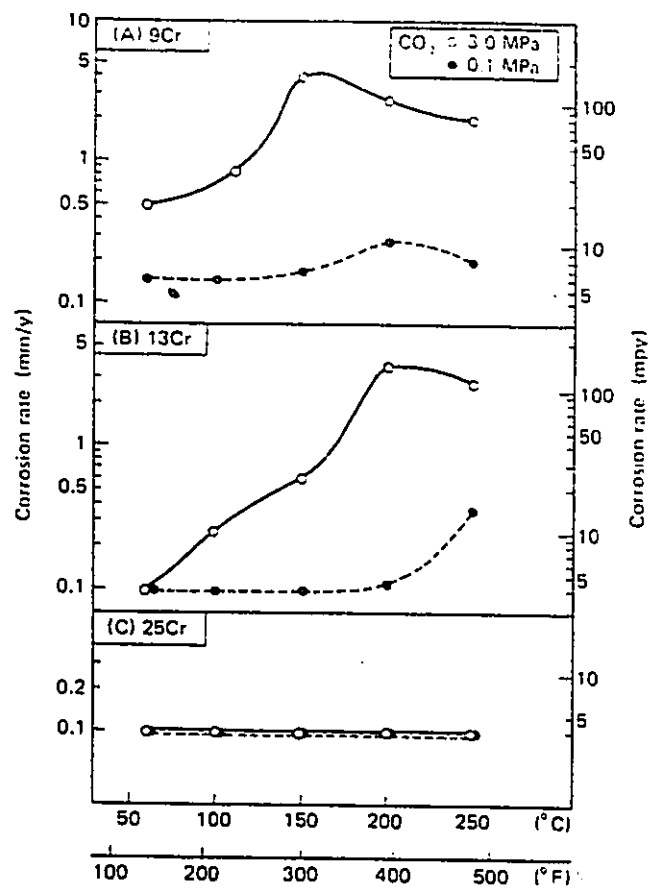


Figure 13. Effect of CO₂ Partial Pressure and Temperature on Corrosion Rate of Cr Steel⁷²

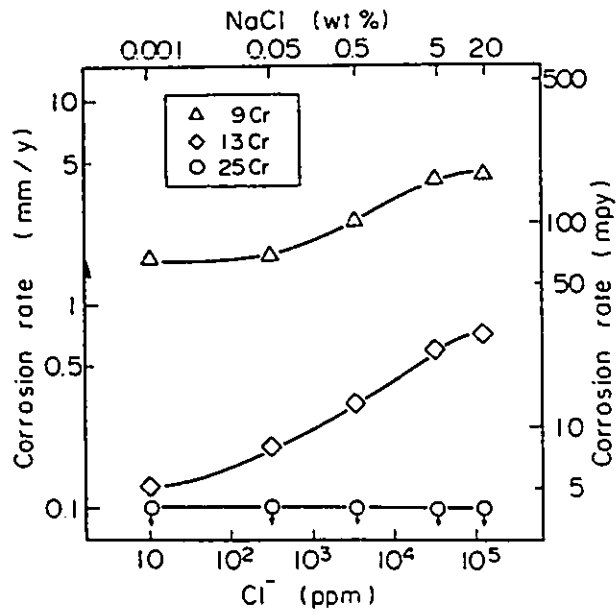


Figure 14. Effect of Cl^- Ion Concentration on the Corrosion Rate of Cr Steel at 150°C ⁷⁰

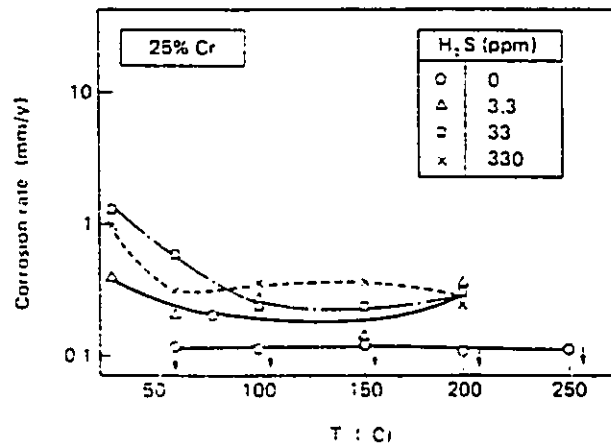


Figure 15. Effect of Temperature and a Small Amount of H_2S on Corrosion Rate (Cr Steel)⁷⁷

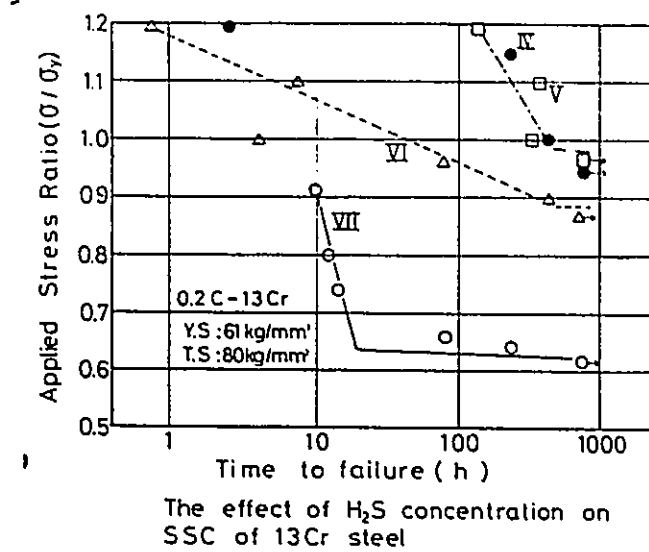


Figure 16. Stress - Time to Failure Curves of a 0.2%C - 13%Cr Steel Under Conditions iv, v, vi and vii Shown in Table (2)⁸⁷

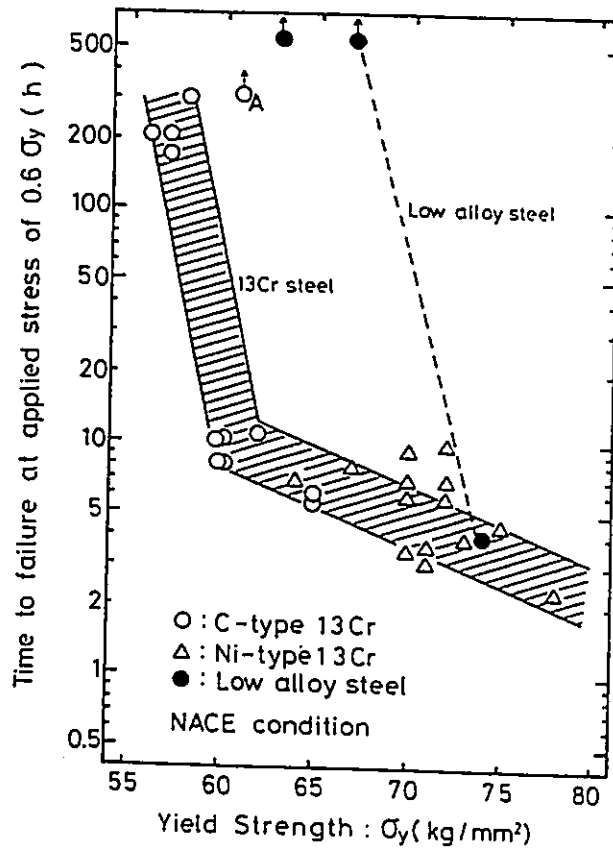


Figure 17. Effect of Yield Strength on SCC Susceptibility of 13Cr Steels¹⁰⁵

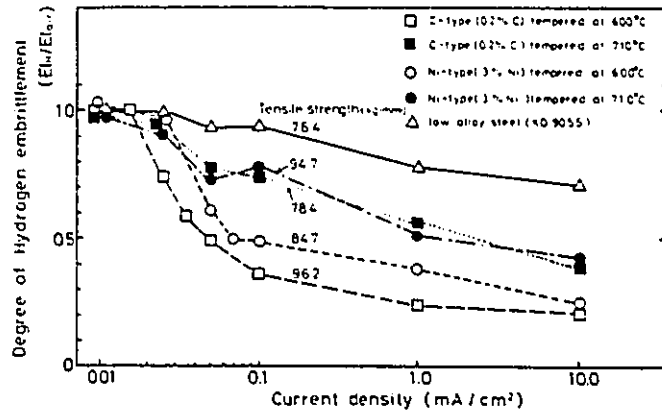


Figure 18. Effect of Current Density for Hydrogen Charging on Degree of Hydrogen Embrittlement, (E_H/E_{air}), Measured by SSRT Testing⁸⁷

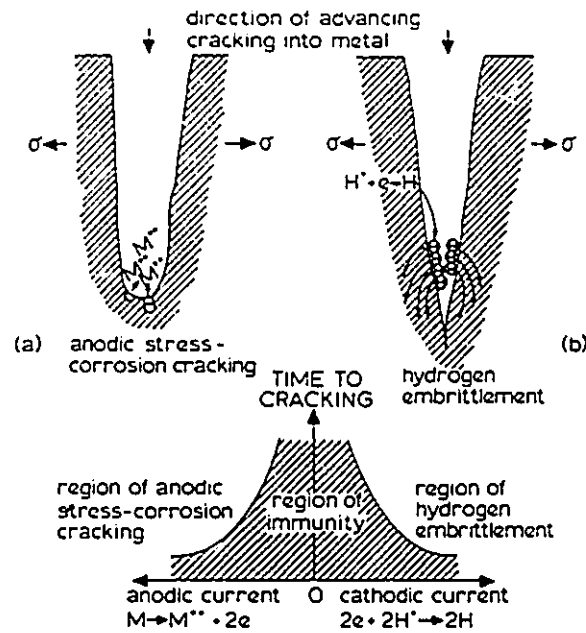


Figure 19. Comparison of (a) Anodic Stress Corrosion Cracking and (b) Hydrogen-Embrittlement Cracking⁴⁶

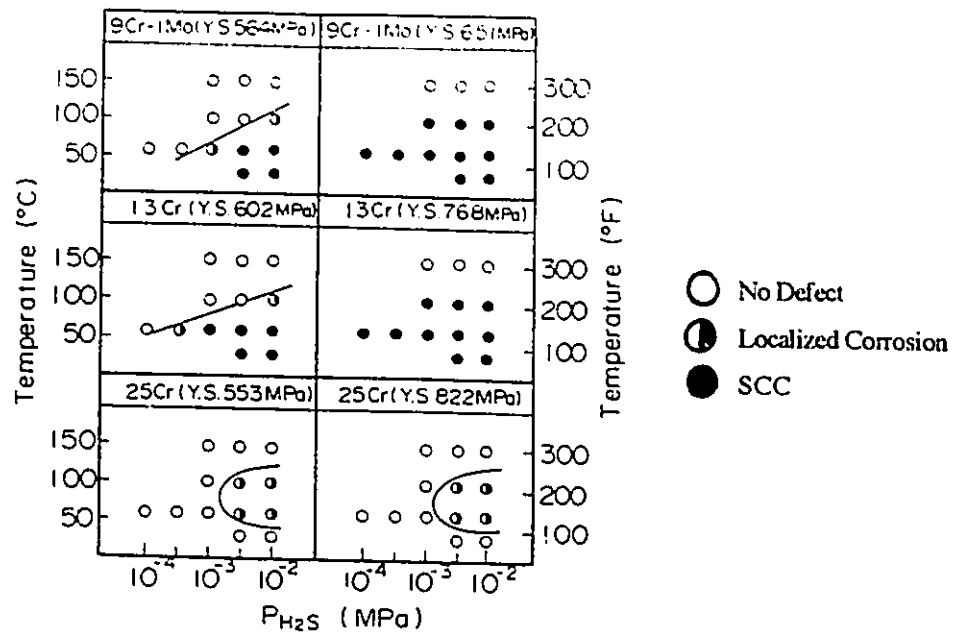


Figure 20. Effect of H_2S Partial Pressure and Temperature on Susceptibility to SSC^{70} , (5% NaCl; 3.0MPa CO_2+H_2S at 25°C, test duration, 336h; flow velocity, 2.5m/s; stress, $1\sigma_y$ with notch).

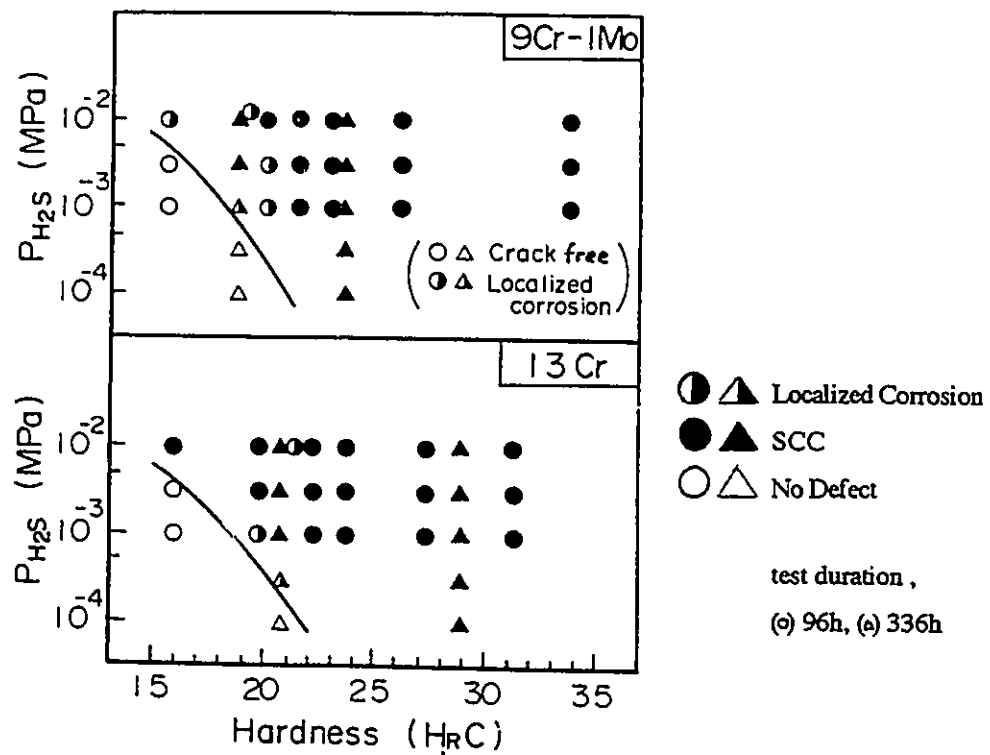


Figure 21. Effect of H₂S Partial Pressure and Strength of 9Cr-1Mo and 13Cr Steels on Susceptibility to SSC⁷⁰ (5% NaCl; 3.0MPa CO₂+H₂S at 25°C; test temperature, 60°C; flow velocity, 2.5m/s; stress, 1oy with notch)

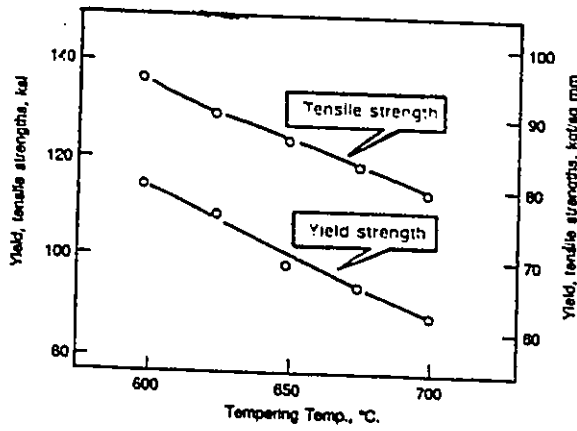


Figure 22. The Relationship Between Tempering Temperature and Tensile Properties¹²³

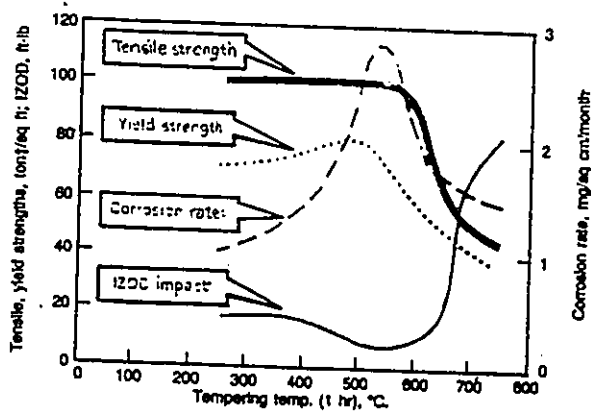
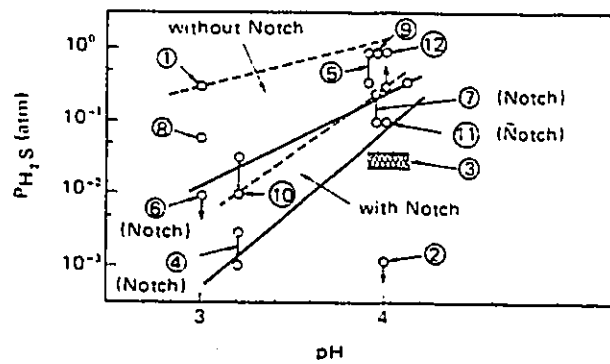


Figure 23. The Relationship Between Tempering Temperature, Yield Strength, Tensile Strength and Impact Resistance¹²³



| No. | Environment | | | Y.S (MPa) | Stress |
|-----|--|--------------------------------------|---------------|--------------------|-------------------|
| | Gas | Solution | Temp. (°C) | | |
| 1 | 1 atm N ₂ | 5%NaCl + 0.5%CH ₃ COOH | 25 | 610 | C ring |
| 2 | 1 atm (CO ₂ +CH ₄) | 0.1%NaCl | 90 | 259,268 (H= 30) | Tensile |
| 3 | Actual Field | | | | |
| 4 | 30 atm CO ₂ | 5%NaCl | 60 | 602 | Bend (Notch) |
| 5 | 1 atm CO ₂ | 3.5%NaCl | 25 | 598 | Tensile |
| 6 | 1 atm N ₂ | 5%NaCl + 0.5%CH ₃ COOH | 25 | 610 | C ring (Notch) |
| 7 | 1 atm CO ₂ | 5%NaCl | 25 | 610 | C ring (Notch) |
| 8 | 1 atm N ₂ | 5%NaCl + 0.5%CH ₃ COOH | 25 | 586/620 | Tensile |
| 9 | - | 5%NaCl (pH 4) | 25 | 586/620 | Tensile |
| 10 | 30 atm CO ₂ | 5%NaCl | 60 | 602 | C ring |
| 11 | 1 atm CO ₂ | 5%NaCl | 25 | 624 | Bend (Notch) |
| 12 | - | 5%NaCl | 25 | 602 | Tensile |

Figure 24. Effect of H₂S Partial Pressure and pH on SSC susceptibility of L-80 Grade 13Cr Steel⁹⁹

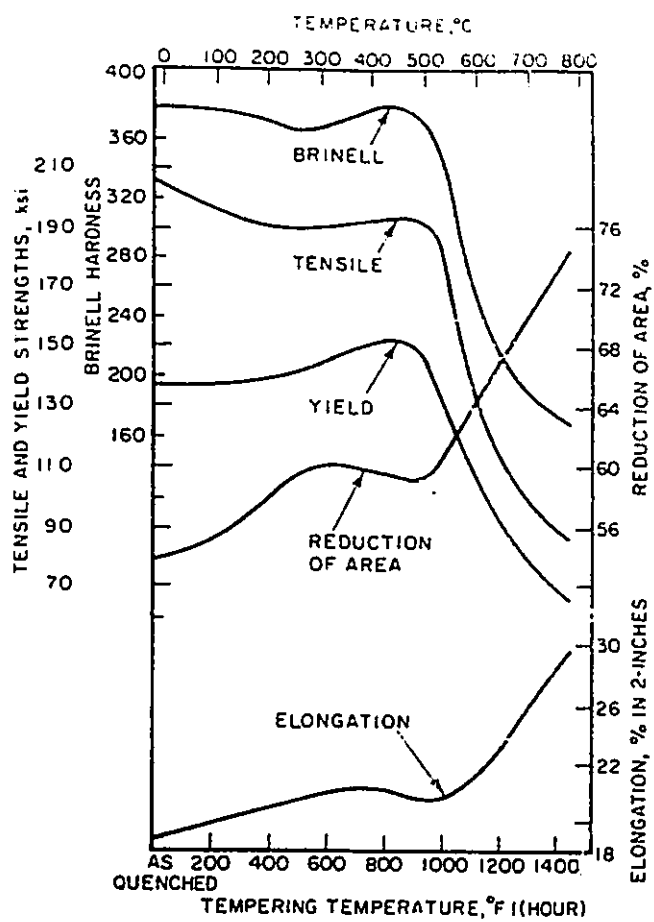


Figure 25. Effect of Tempering Temperature on the Mechanical Properties of Type 410 Stainless Steel⁹⁵

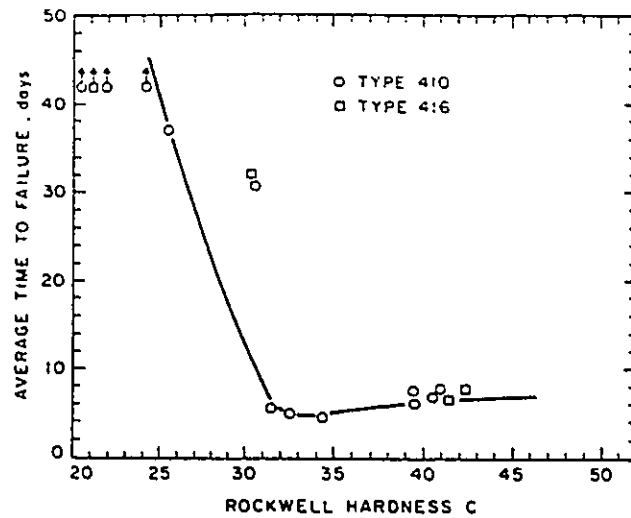


Figure 26. Effect of Rockwell Hardness on Time-to-Failure of Type 410 and 416 Stainless Steels¹⁰²



Figure 27. Intergranular Cracking of Type 410 Stainless Steel⁹⁵

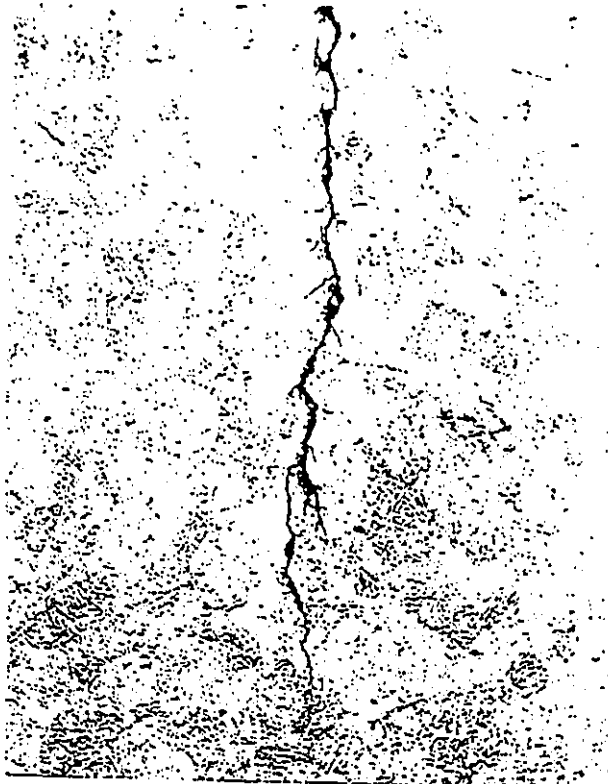


Figure 28. Transgranular Cracking of Type 410 Stainless Steel⁹⁵

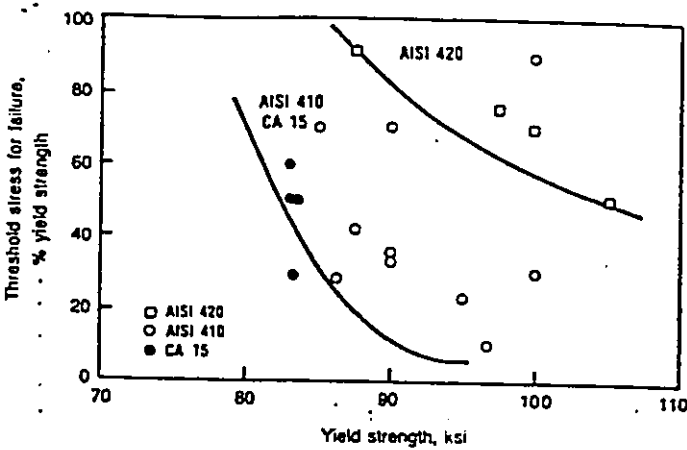
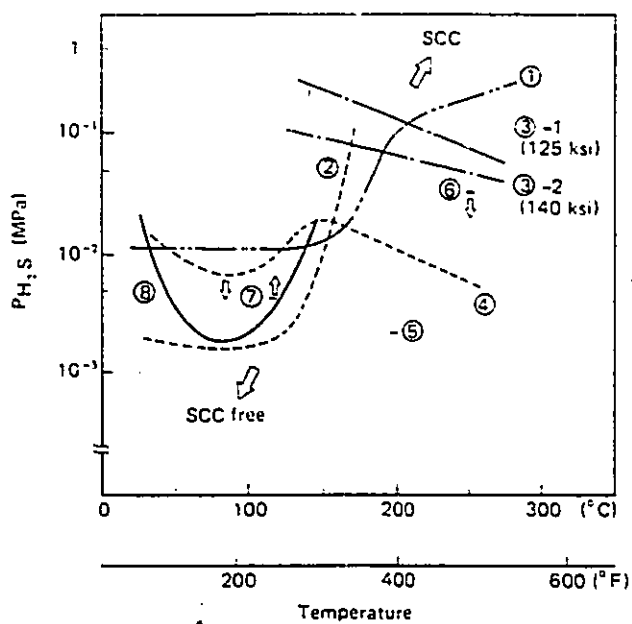


Figure 29. SSC and Three Martensitic Stainless Steels¹⁰³



| No. | Environment | | Stress | Material |
|-----|-----------------------|--------------------|--------------|----------|
| | Gas (P_{CO_2}) | Solution (NaCl) | | |
| 1 | 7 MPa | 5-15% | Tensile | 22 Cr |
| 2 | 2.5 | 20 | SSRT | 22 Cr |
| 3 | 5.0 | 10 | U bend | 22 Cr |
| 4 | 1.0 | 20 | Bend (Notch) | 25 Cr |
| 5 | 2.0 | 25 | SSRT | 22 Cr |
| 6 | 1.0 | 20 | Bend | 25 Cr |
| 7 | 12.2 | 11 | U bend | 22 Cr |
| 8 | 3.0 | 5 | Bend (Notch) | 25 Cr |

Figure 30. Effect of H_2S Partial Pressure and Temperature on Susceptibility to SSC of 22-25%Cr α - γ Duplex Stainless Steel⁷⁰

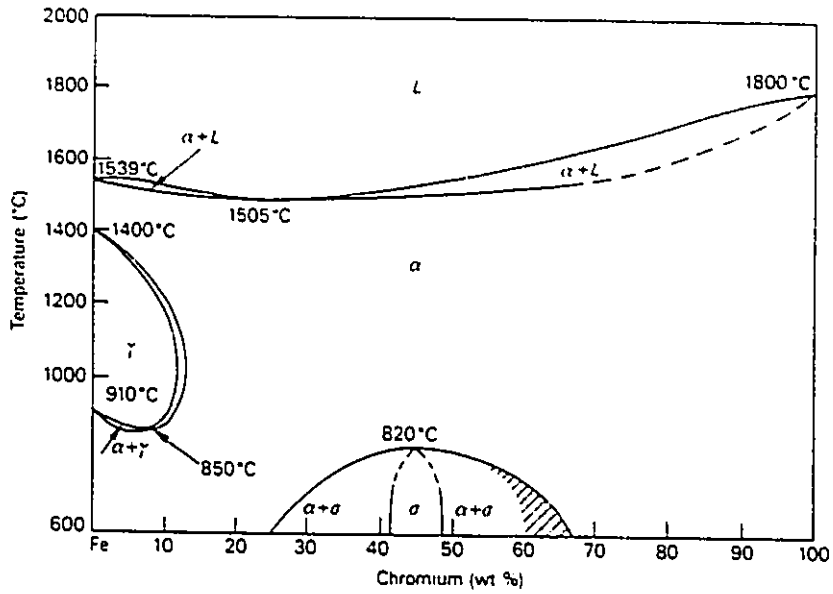


Figure 31. The Iron-Chromium Equilibrium Diagram¹⁰⁸

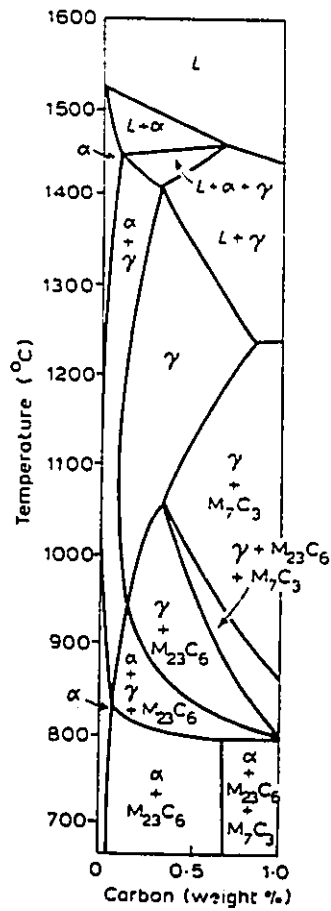


Figure 32. Vertical Section at 13% Chromium¹¹⁰

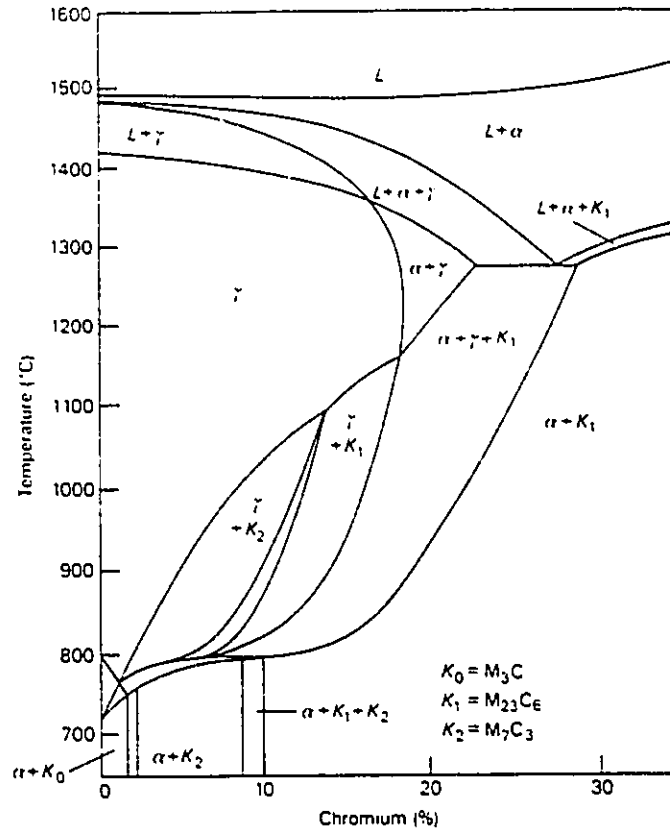


Figure 33. Effect of Carbon on the Fe-Cr Diagram (0.4%C)¹¹⁰

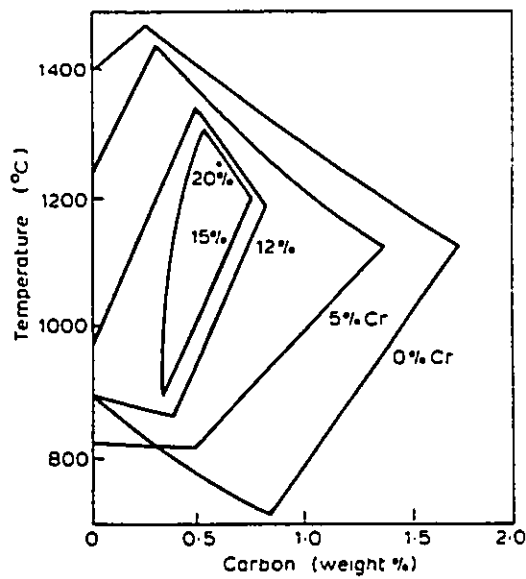


Figure 34. Effect of Chromium Additions on the Temperature and Carbon Content of the $\gamma \leftrightarrow \alpha + M_3C$ Eutectoid¹¹⁰

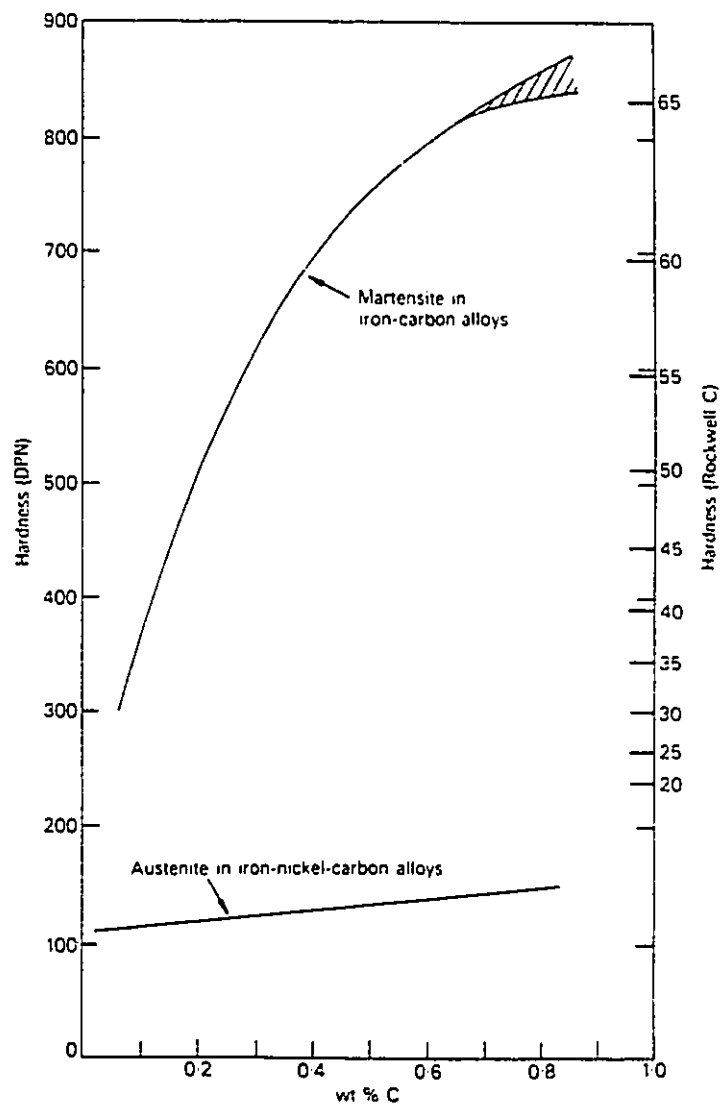


Figure 35. The Effect of Carbon on the Hardness of Martensite and Austenite¹⁰⁸

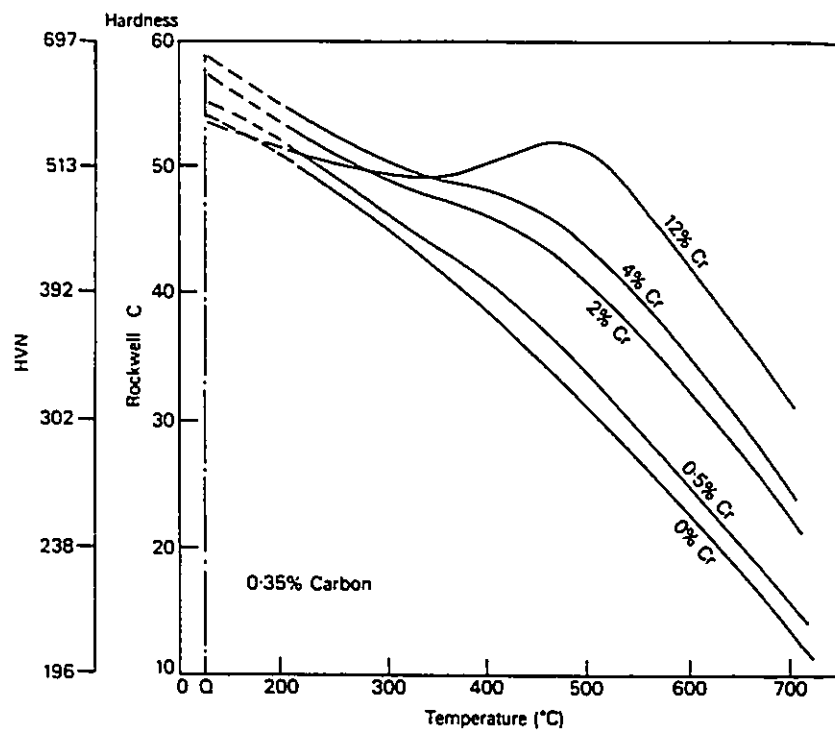


Figure 36. The Effect of Chromium on the Tempering of a 0.35C Steel¹⁰⁸

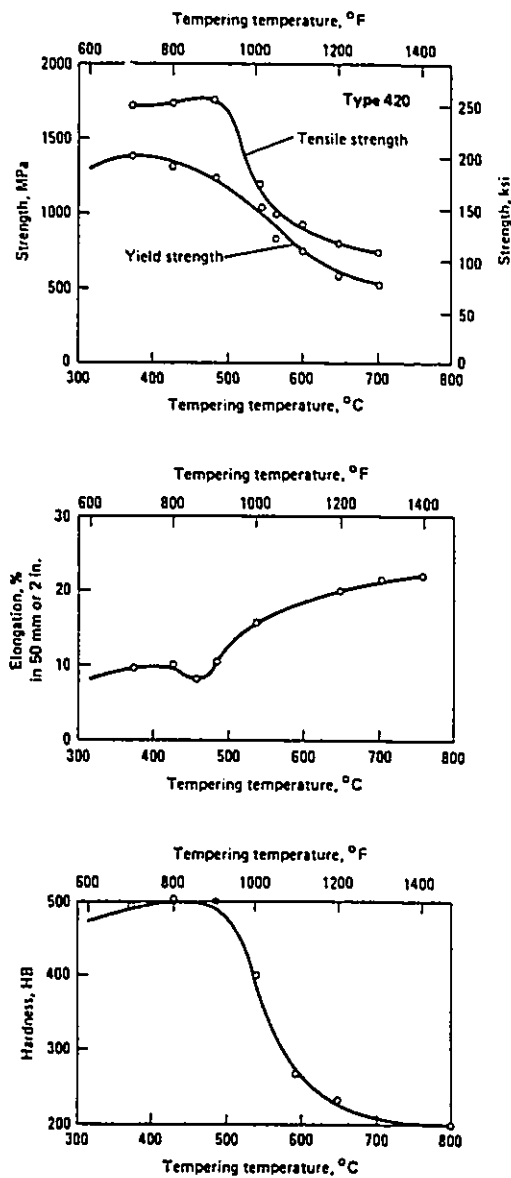


Figure 37. Effect of Tempering Temperature on Tensile Properties and Hardness of Type 420 Martensitic Stainless Steels¹¹¹

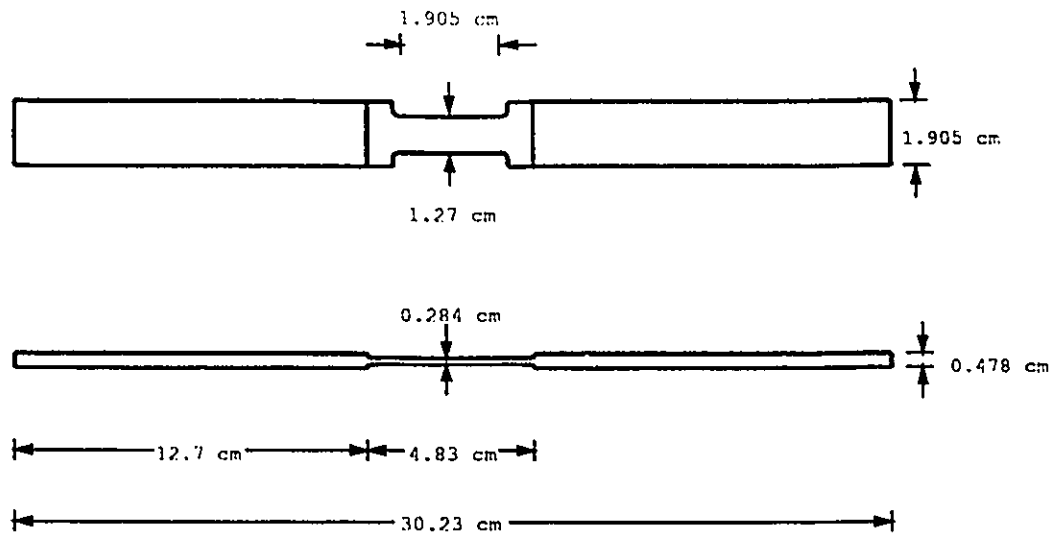


Figure 38. Tensile Test Specimen



Figure 39. Material Test System

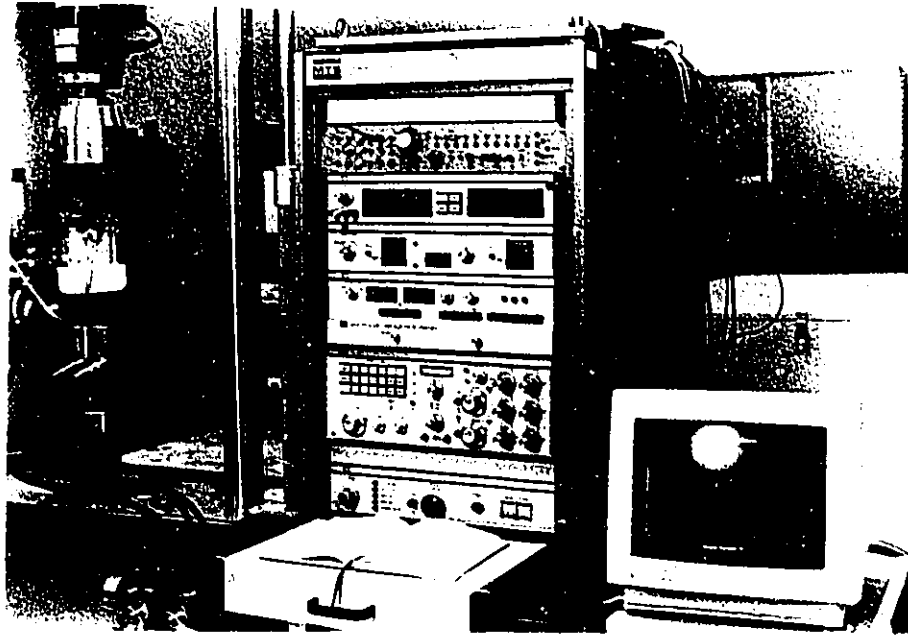


Figure 40. Data Acquisition System

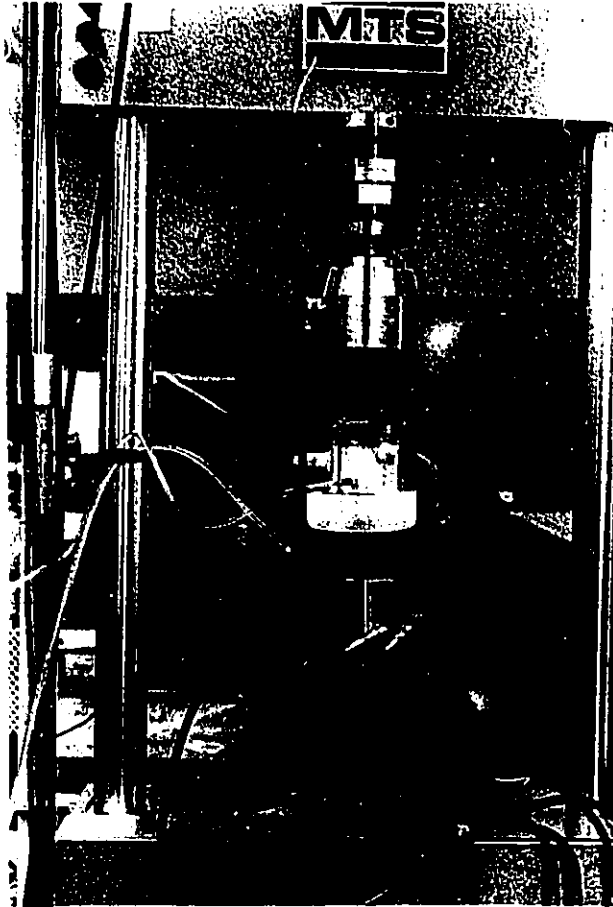


Figure 41. Test Cell



Figure 42. Attached Nylon Sleeves

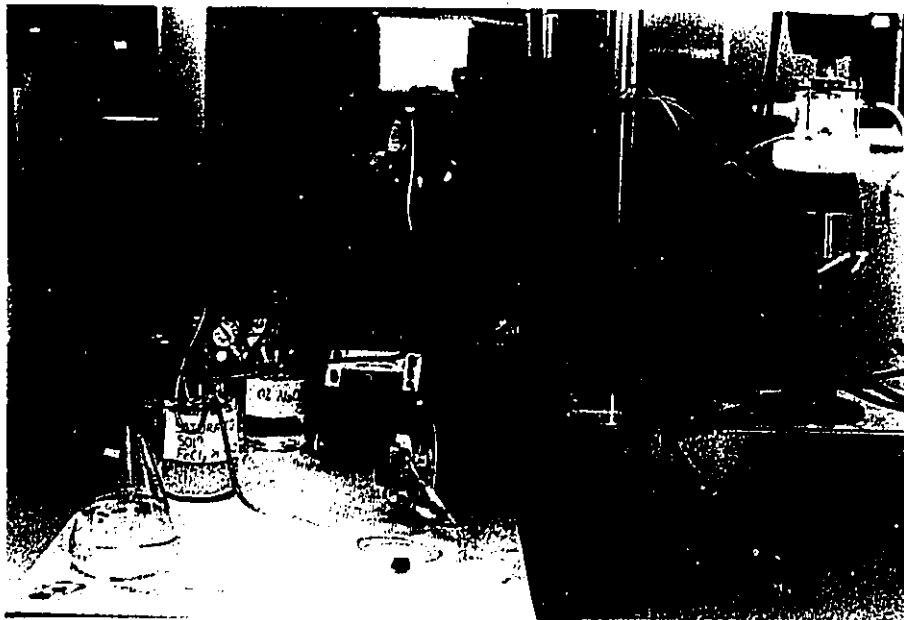


Figure 43. Recirculation System



Figure 44. The Microstructure of As-Received Material, FeCl_3 Etchant , 600x



Figure 45. The Microstructure of the 420 Steel after Air Cooling from 1150°C , FeCl_3 Etchant, 180x



Figure 46. The Microstructure of 420 Steel Tempered at 550°C,
FeCl₃ Etchant, 180x



Figure 47. The Microstructure of 420 Steel Tempered at 650°C,
FeCl₃ Etchant, 180x

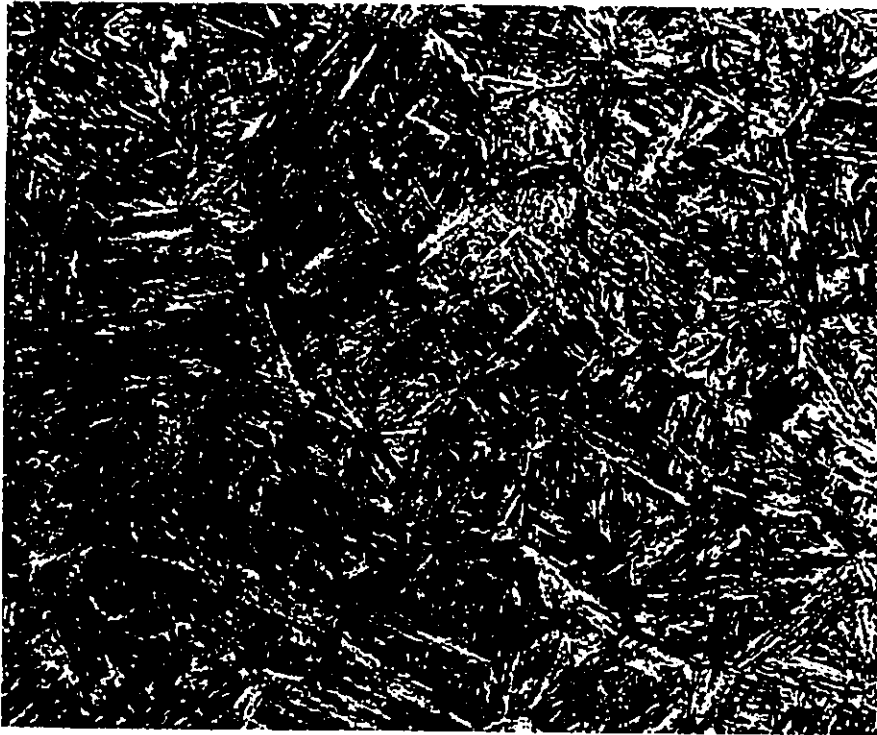


Figure 48. The Microstructure of 420 Steel Tempered at 750°C,
FeCl₃ Etchant, 180x

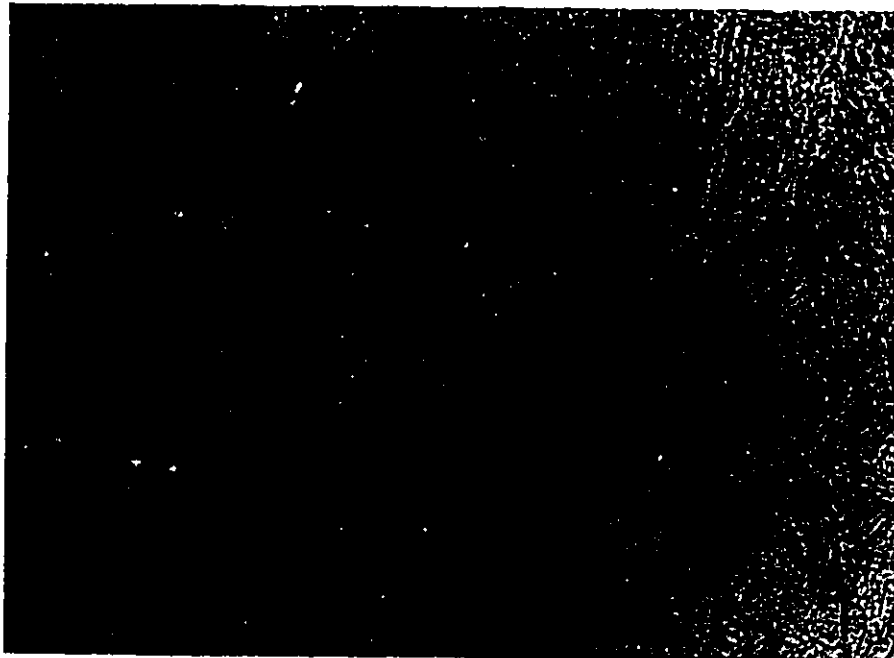


Figure 49. Carbide Distribution in 420 Steel Tempered at 550°C,
Electrolytic Etchant, 400x

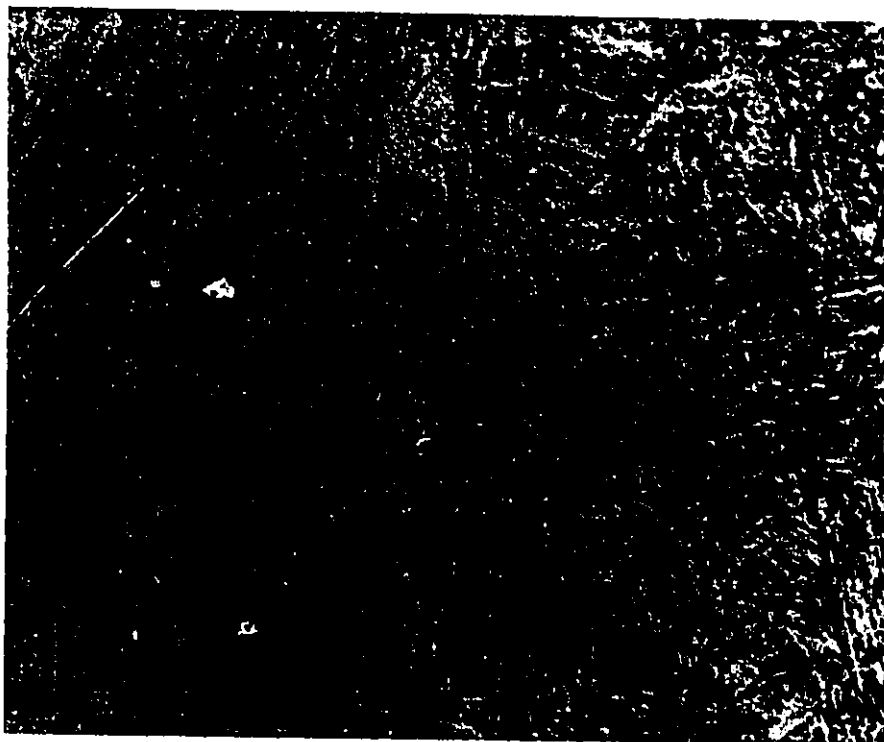


Figure 50. Carbide Distribution in 420 Steel Tempered at 650°C,
Electrolytic Etchant, 400x

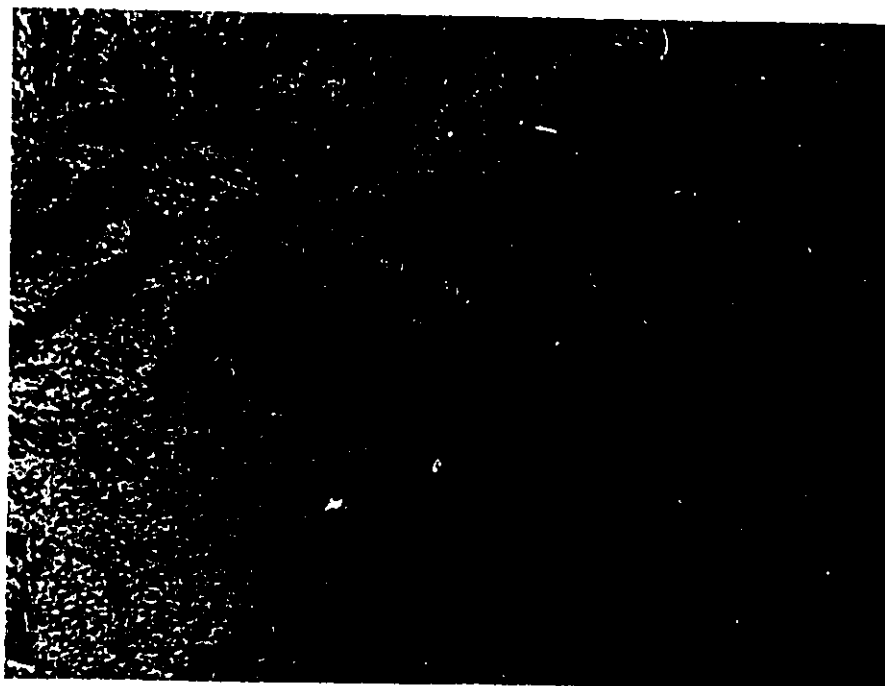


Figure 51. Carbide Distribution in 420 Steel Tempered at 750°C,
Electrolytic Etchant, 400x



Figure 52. The Microstructure of 420 Steel Tempered at 800°C,
FeCl₃ Etchant, 180x

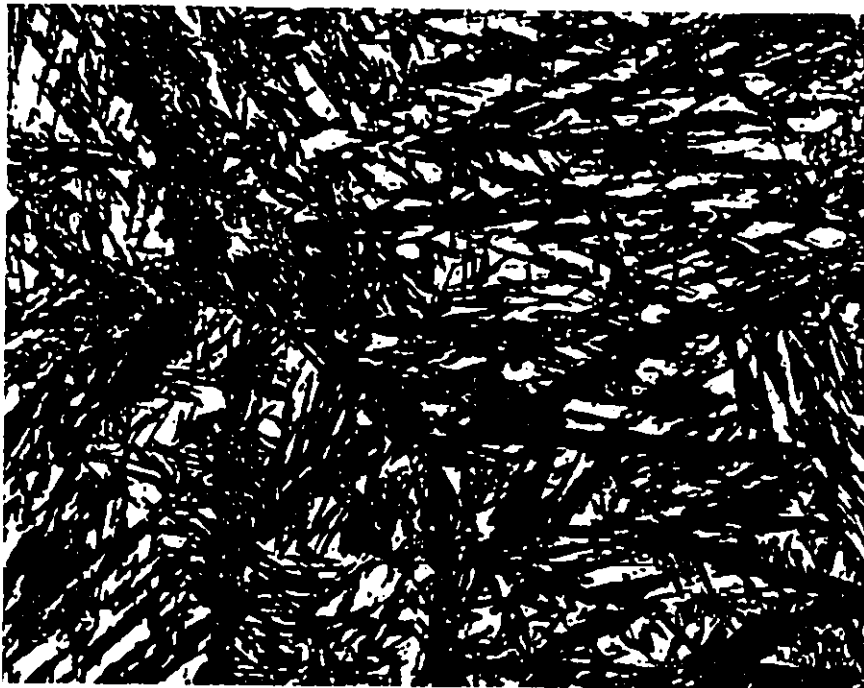


Figure 53. Carbide Distribution in 420 Steel Tempered at 800°C,
Electrolytic Etchant, 400x

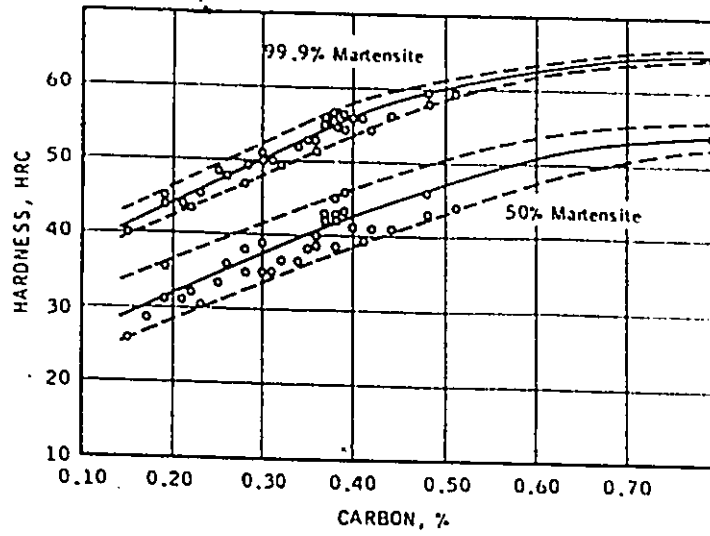


Figure 54. Martensite Hardness versus Carbon Content¹⁰⁵

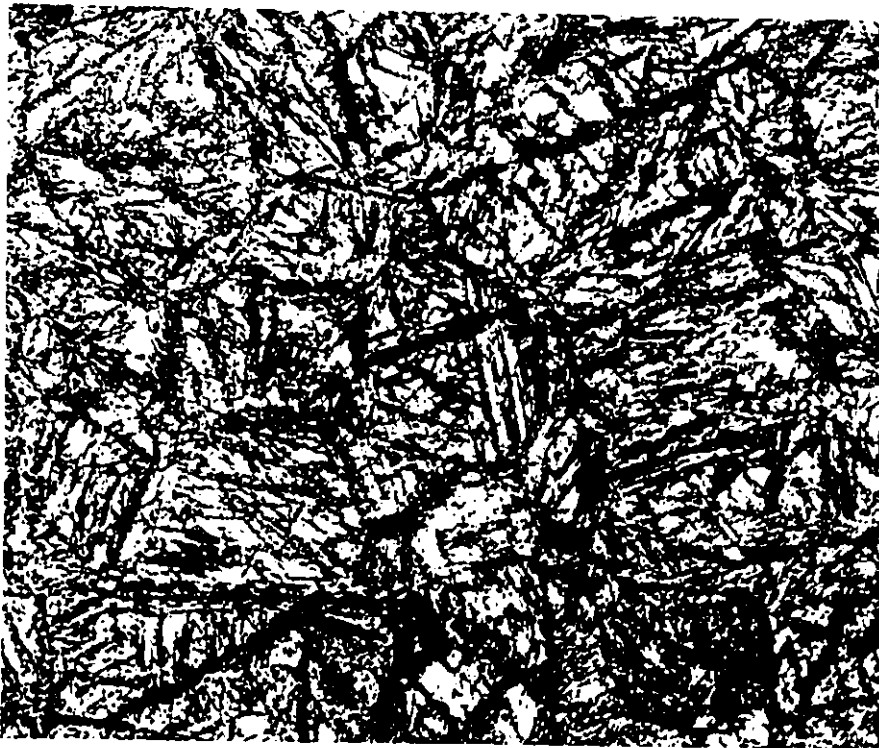


Figure 55. The Microstructure of 420 Steel Tempered at 850°C,
FeCl₃ Etchant, 180x

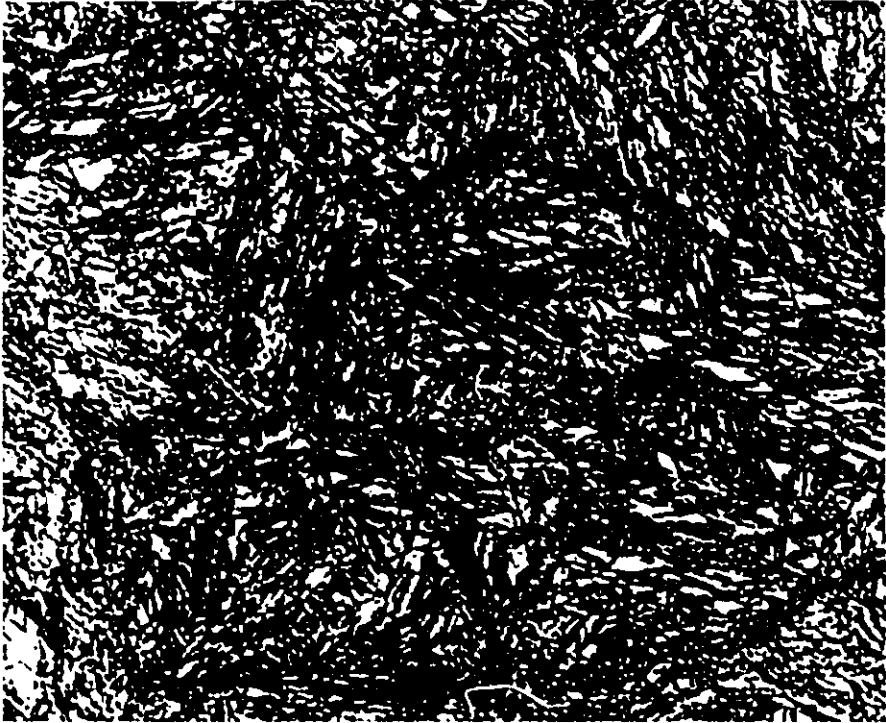


Figure 56. Carbide Distribution in 420 Steel Tempered at 850°C, Electrolytic Etchant, 400x

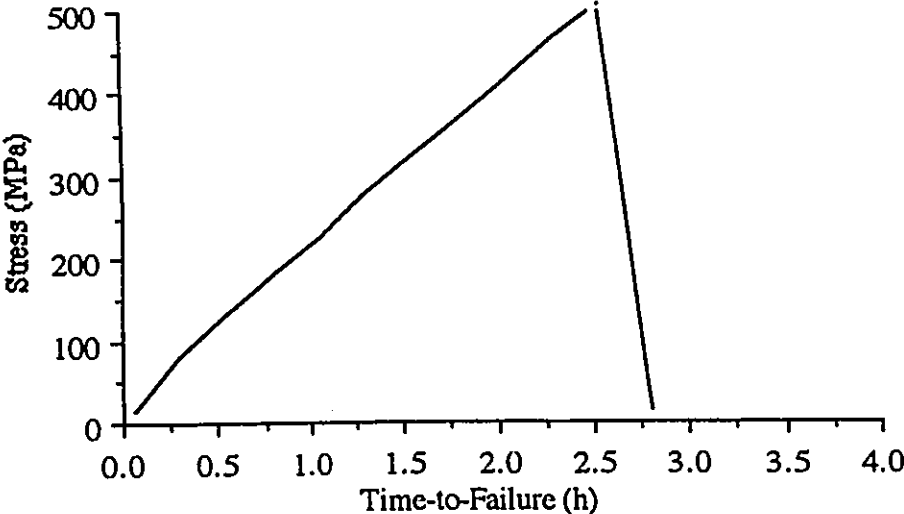


Figure 57. Stress versus Time Curve for Specimen 1 SSRT

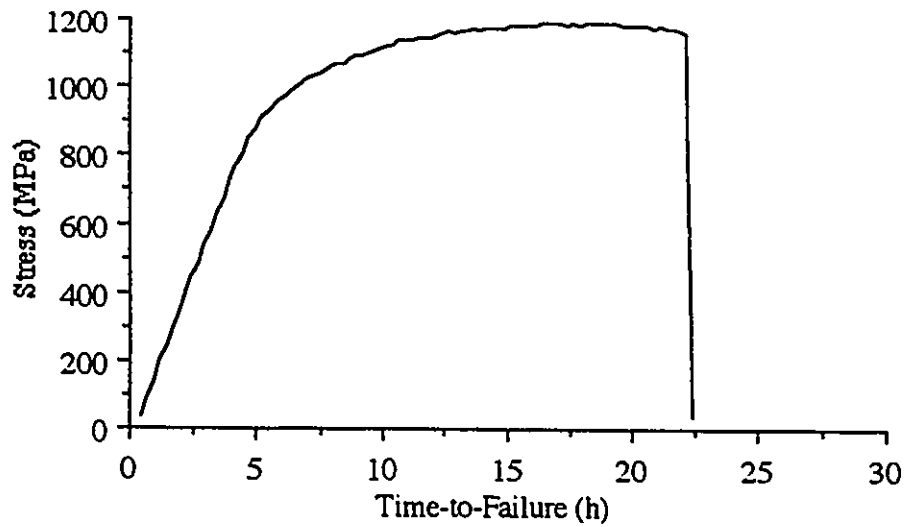


Figure 58. Stress versus Time Curve for Specimen 2 SSRT

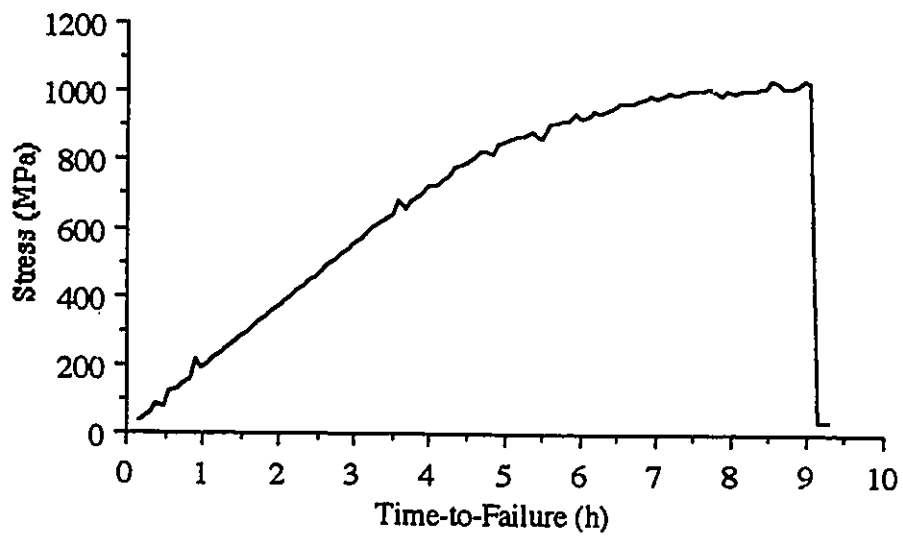


Figure 59. Stress versus Time Curve for Specimen 3 SSRT

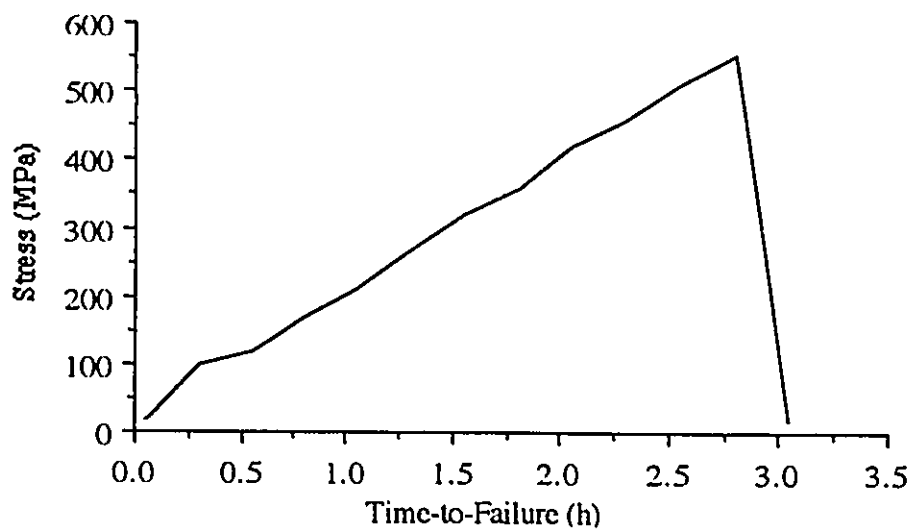


Figure 60. Stress versus Time Curve for Specimen 4 SSRT



Figure 61. Secondary Cracks in the Reduced Section of Specimen Failed with SSC, 7x

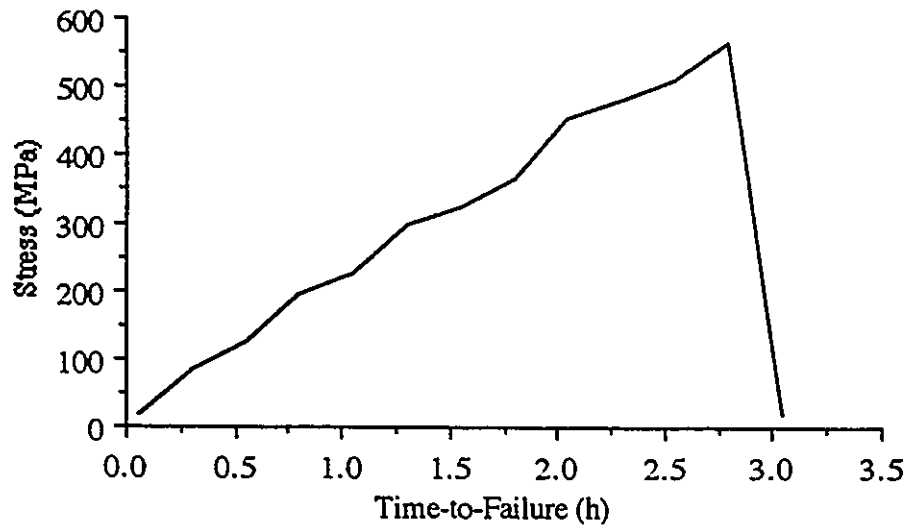


Figure 62. Stress versus Time Curve for Specimen 5 SSRT

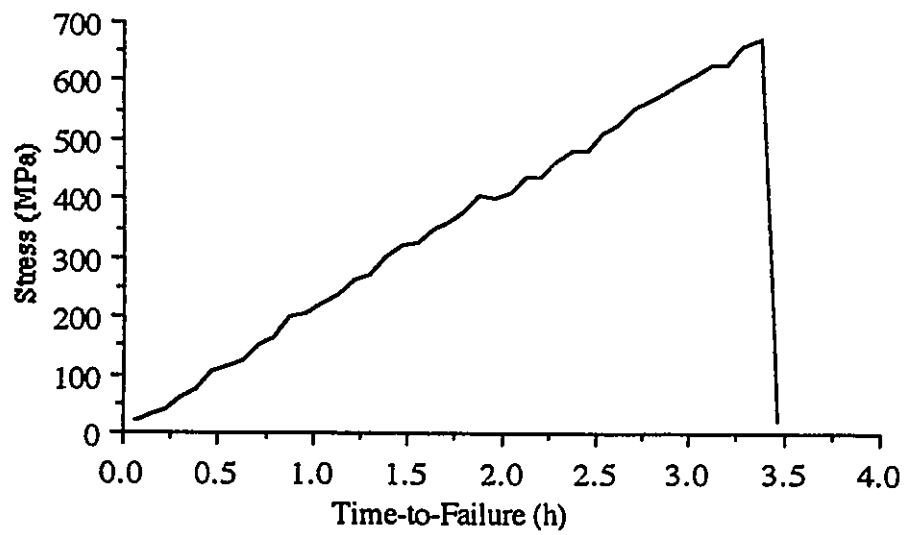


Figure 63. Stress versus Time Curve for Specimen 6 SSRT



Figure 64. Stress versus Time Curve for Specimen 7 SSRT

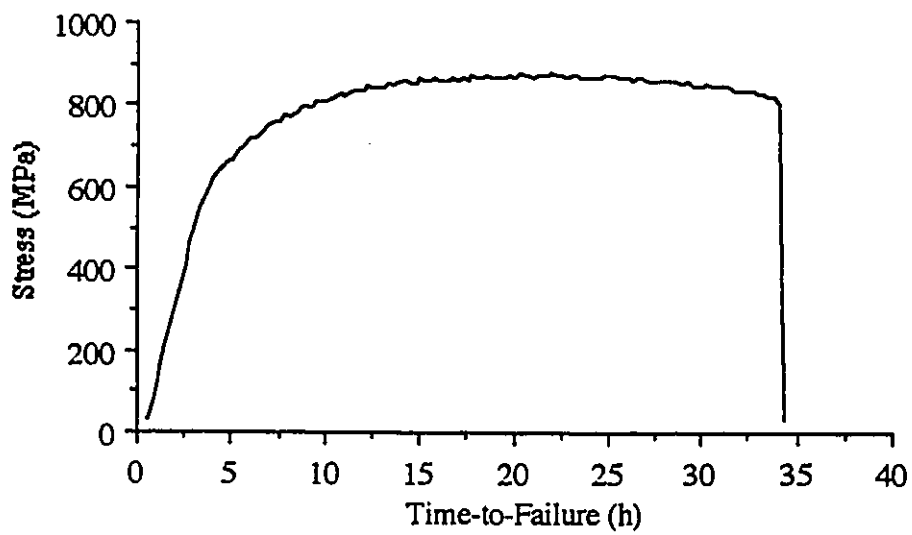


Figure 65. Stress versus Time Curve for Specimen 8 SSRT

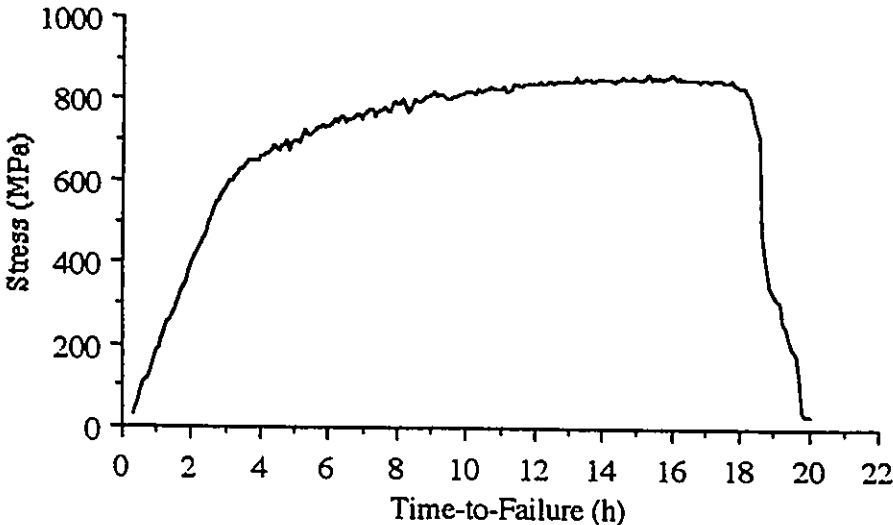


Figure 66. Stress versus Time Curve for Specimen 9 SSRT

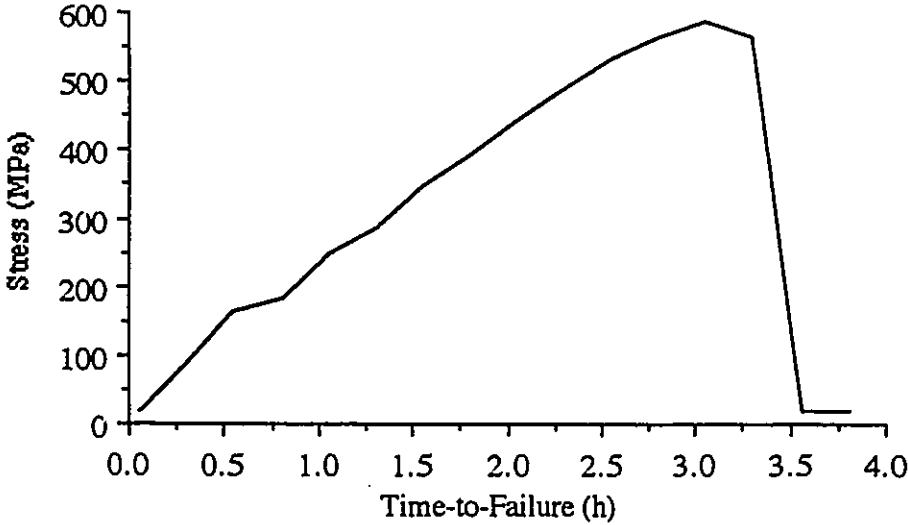


Figure 67. Stress versus Time Curve for Specimen 10 SSRT

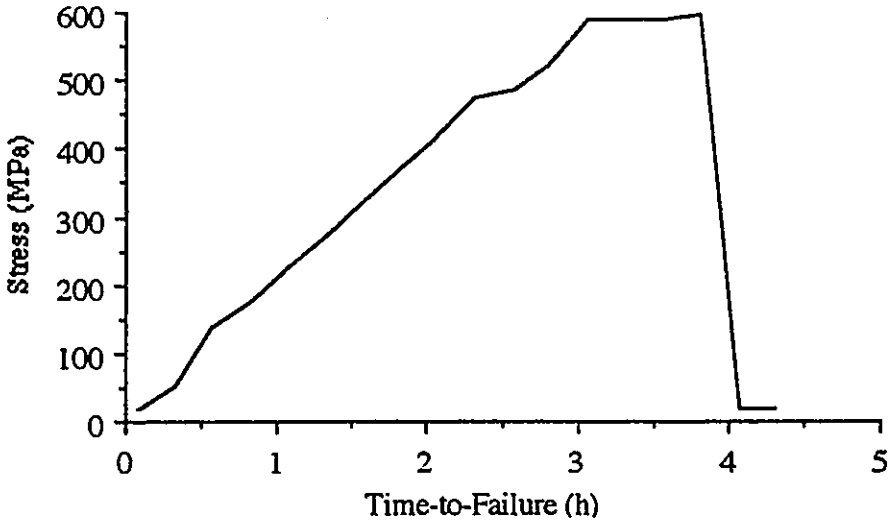


Figure 68. Stress versus Time Curve for Specimen 11SSRT

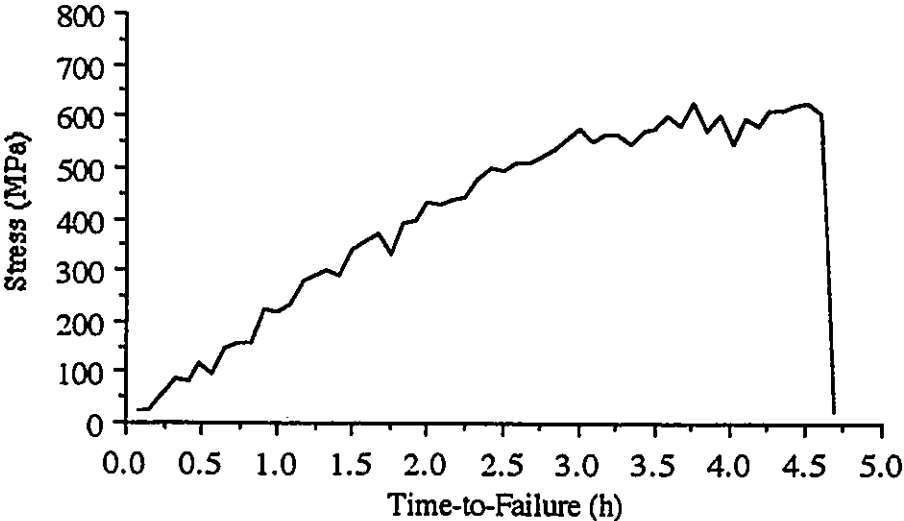


Figure 69. Stress versus Time Curve for Specimen 12 SSRT

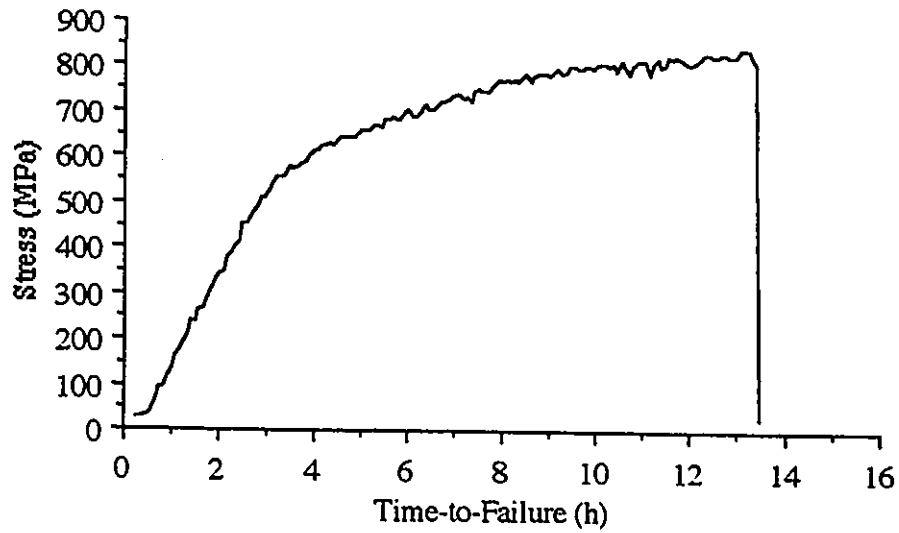


Figure 70. Stress versus Time Curve for Specimen 13 SSRT

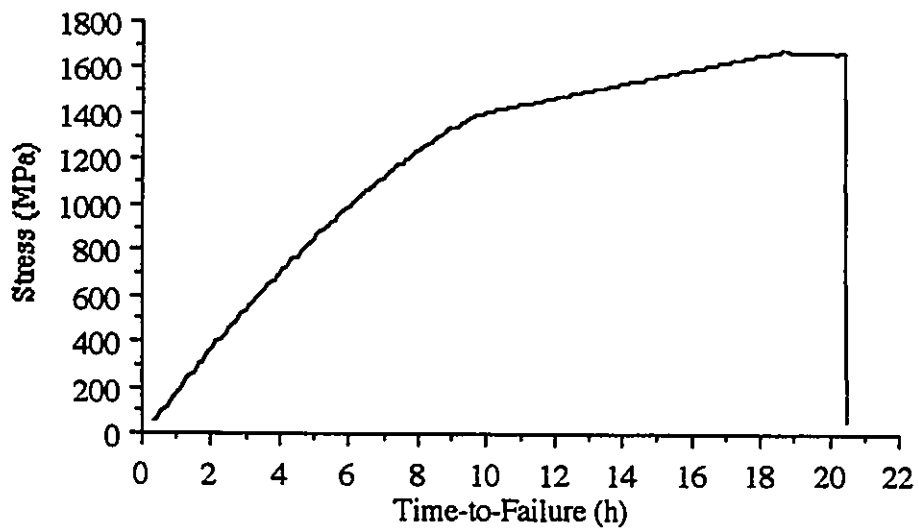


Figure 71. Stress versus Time Curve for Specimen 14 SSRT

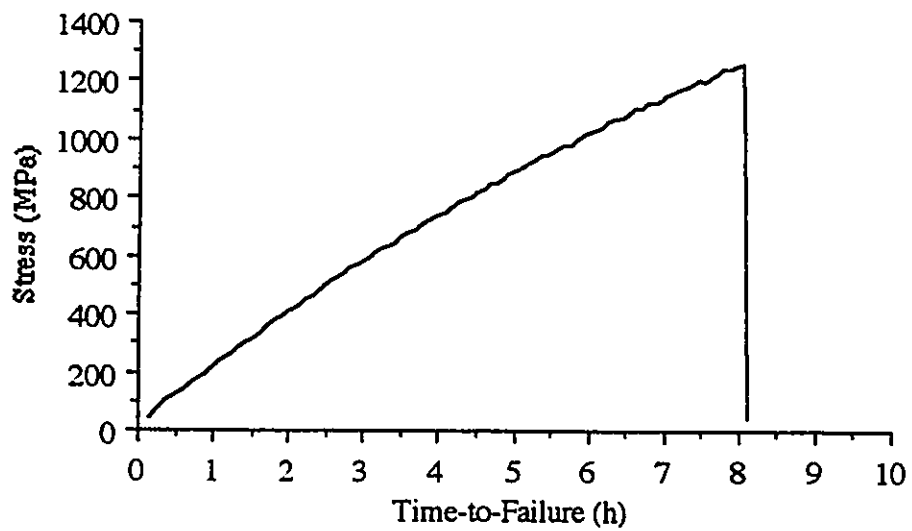


Figure 72. Stress versus Time Curve for Specimen 15 SSRT

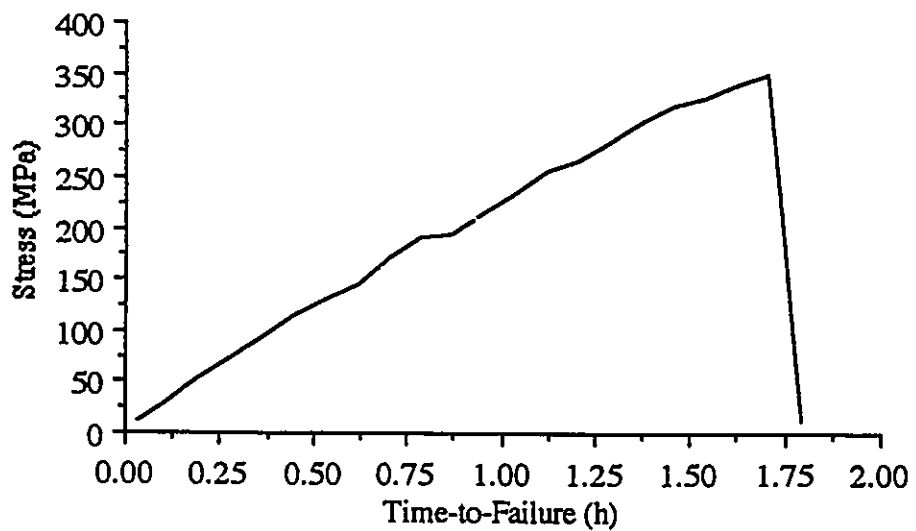


Figure 73. Stress versus Time Curve for Specimen 16 SSRT

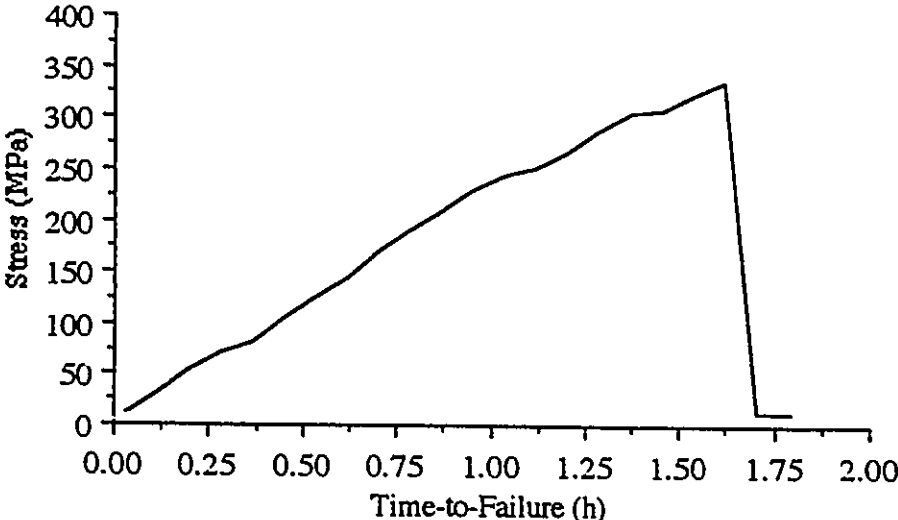


Figure 74. Stress versus Time Curve for Specimen 17 SSRT

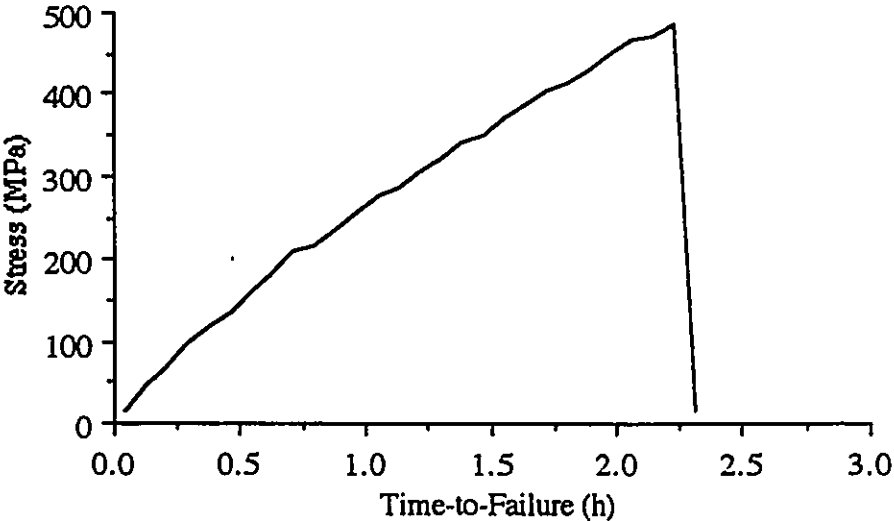


Figure 75. Stress versus Time Curve for Specimen 18 SSRT

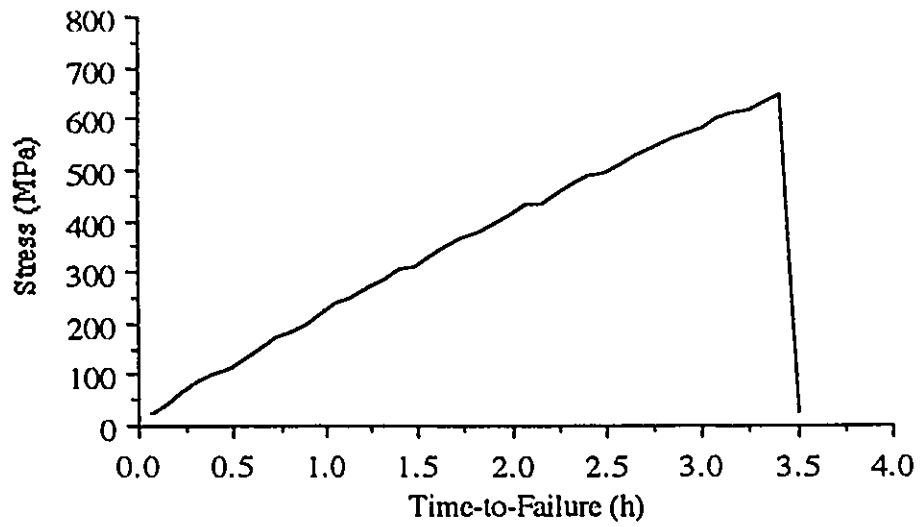


Figure 76. Stress versus Time Curve for Specimen 19 SSRT



Figure 77. SEM Fractograph of Specimen 1

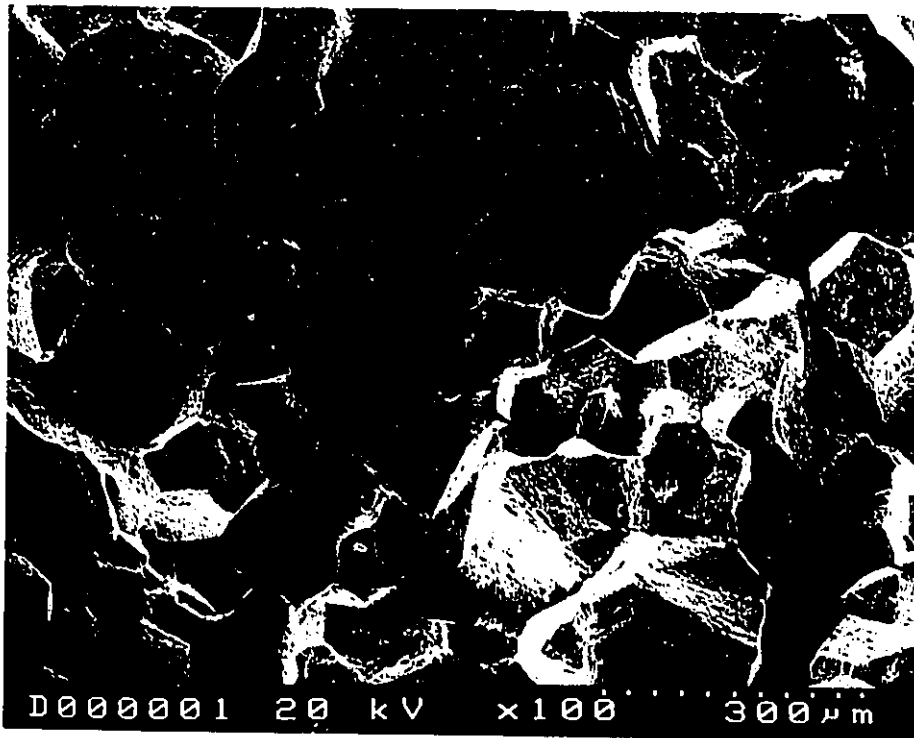


Figure 78. SEM Fractograph of Specimen 2 (Brittle Fracture Zone)

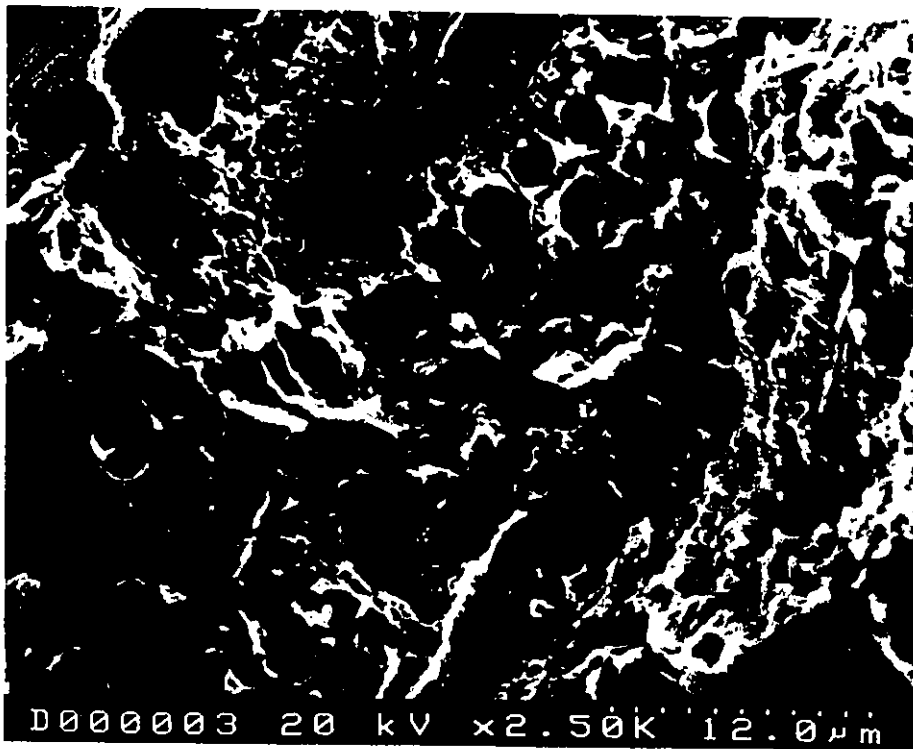


Figure 79. SEM Fractograph of Specimen 2 (Ductile Fracture Zone)



Figure 80. SEM Fractograph of Specimen 3

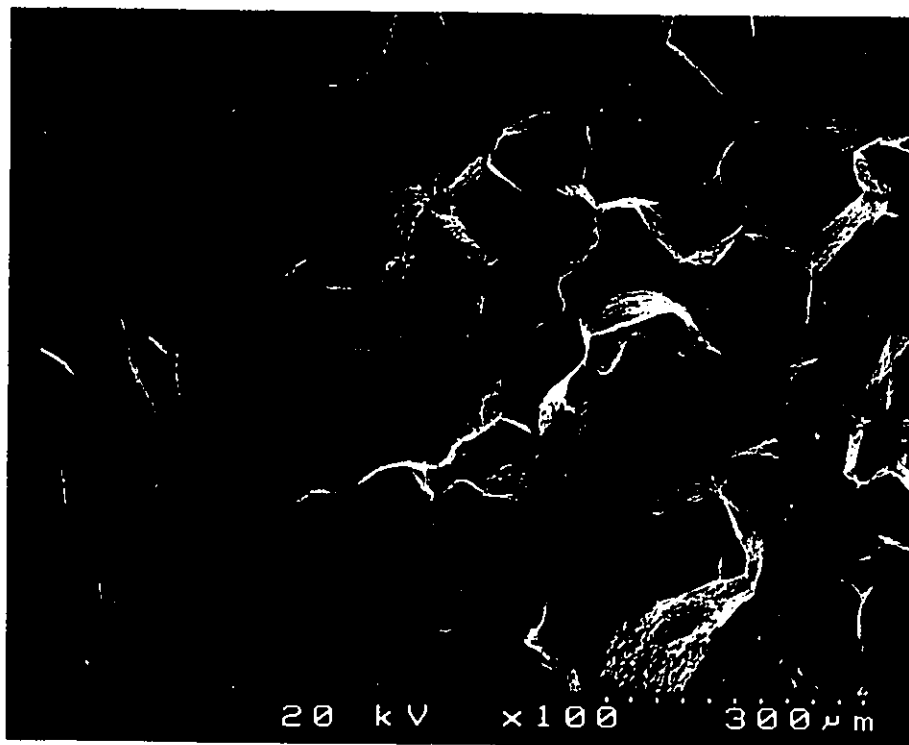


Figure 81. SEM Fractograph of Specimen 4



Figure 82. SEM Fractograph of Specimen 5

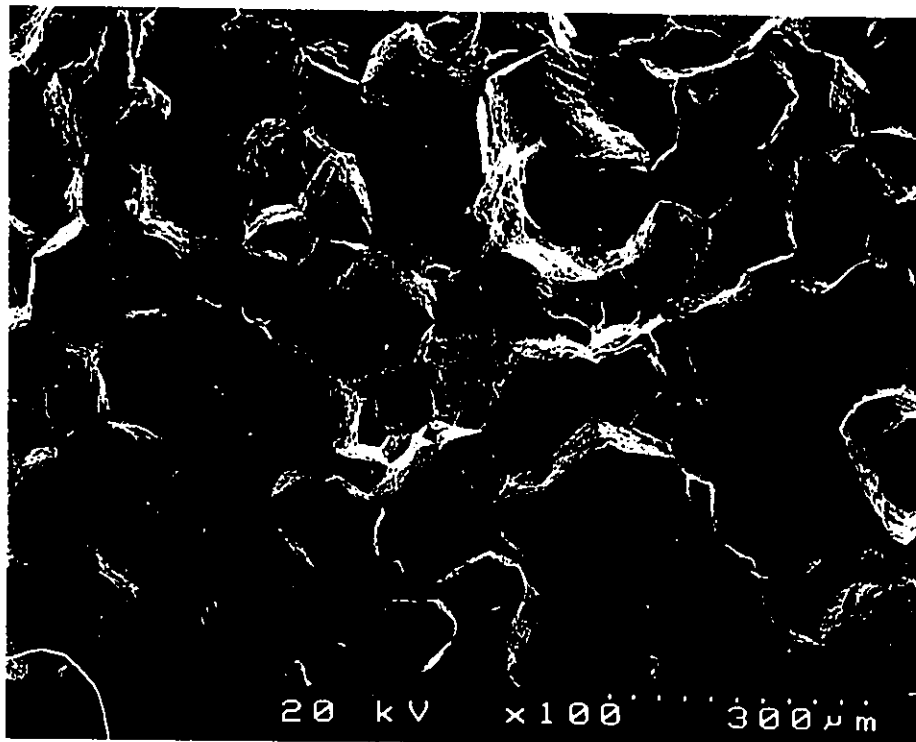


Figure 83. SEM Fractograph of Specimen 6



Figure 84. SEM Fractograph of Specimen 7



Figure 85. SEM Fractograph of Specimen 8

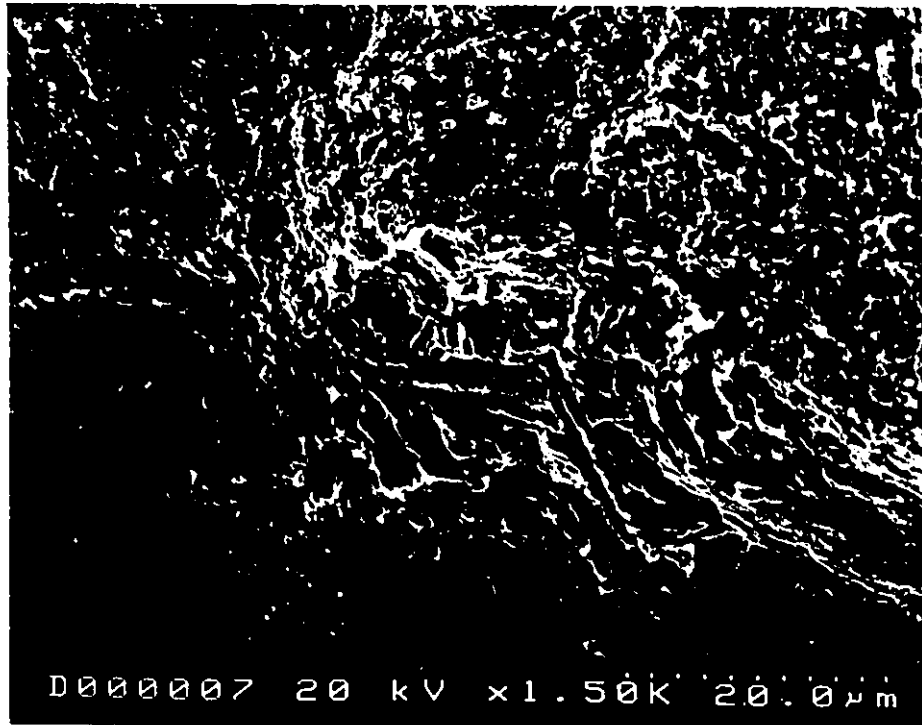


Figure 86. SEM Fractograph of Specimen 9

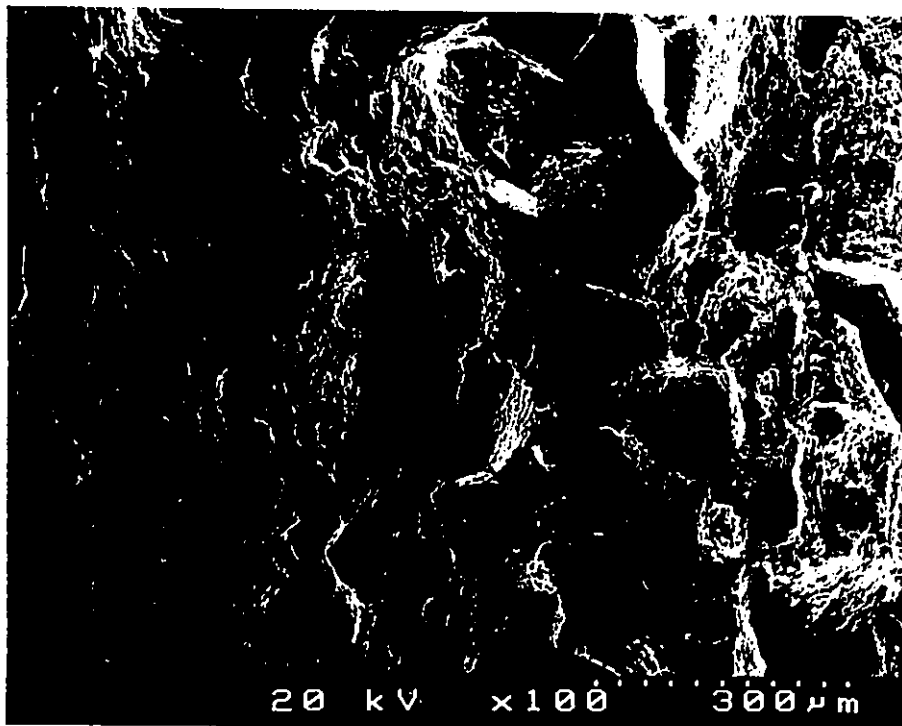


Figure 87. SEM Fractograph of Specimen 9

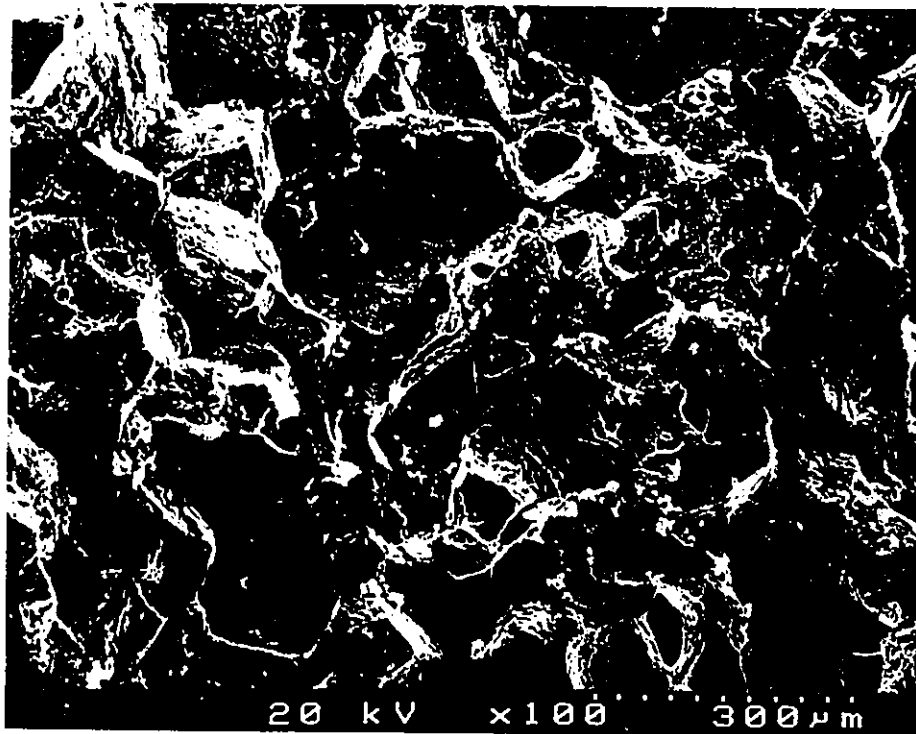


Figure 88. SEM Fractograph of Specimen 10

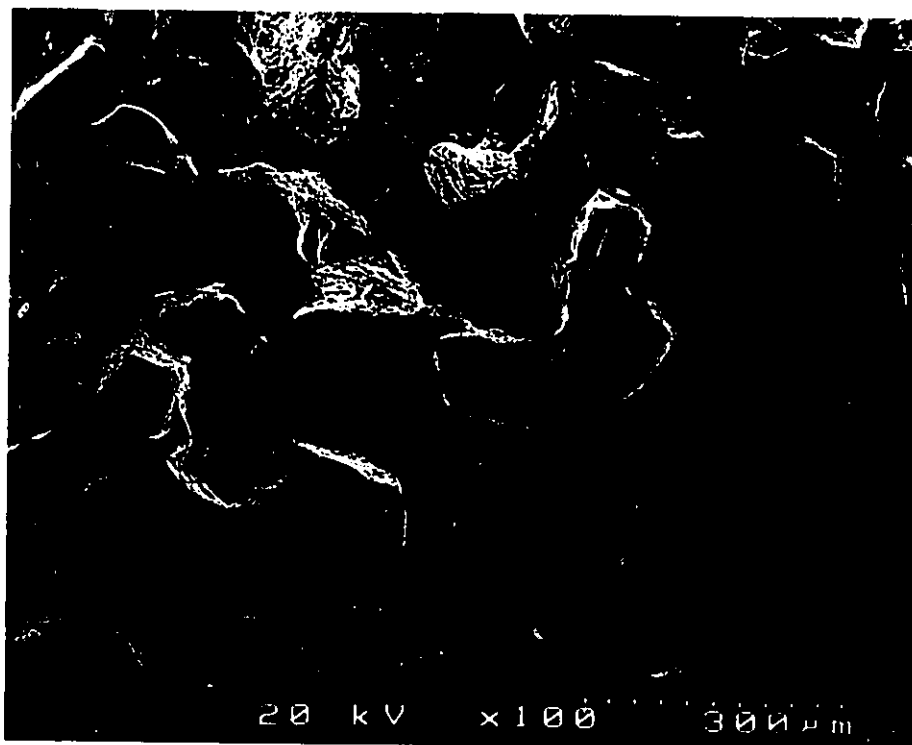


Figure 89. SEM Fractograph of Specimen 11

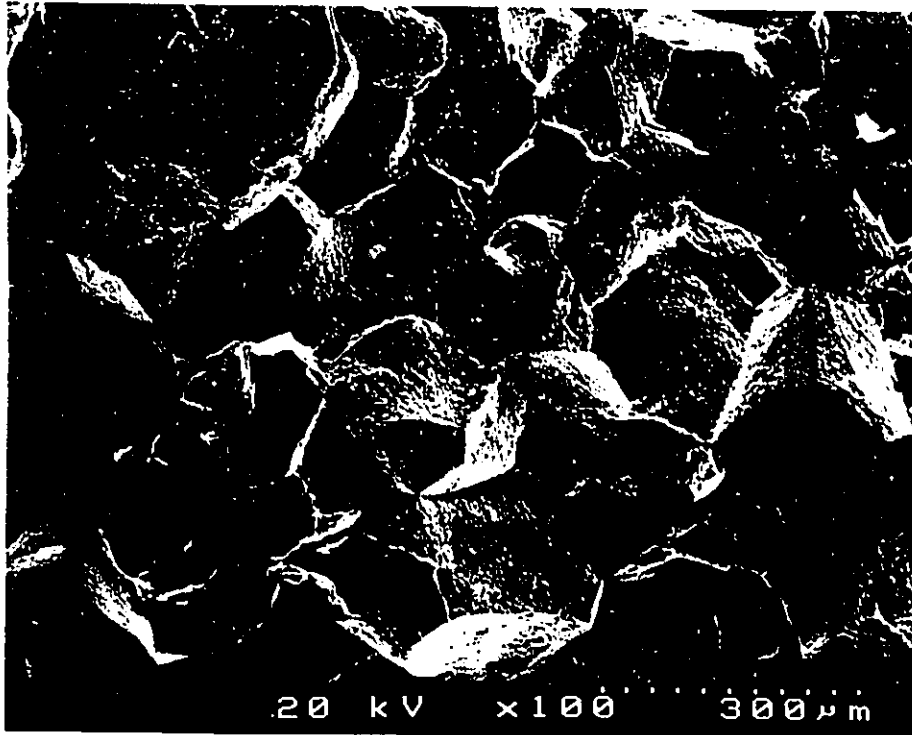


Figure 90. SEM Fractograph of Specimen 12

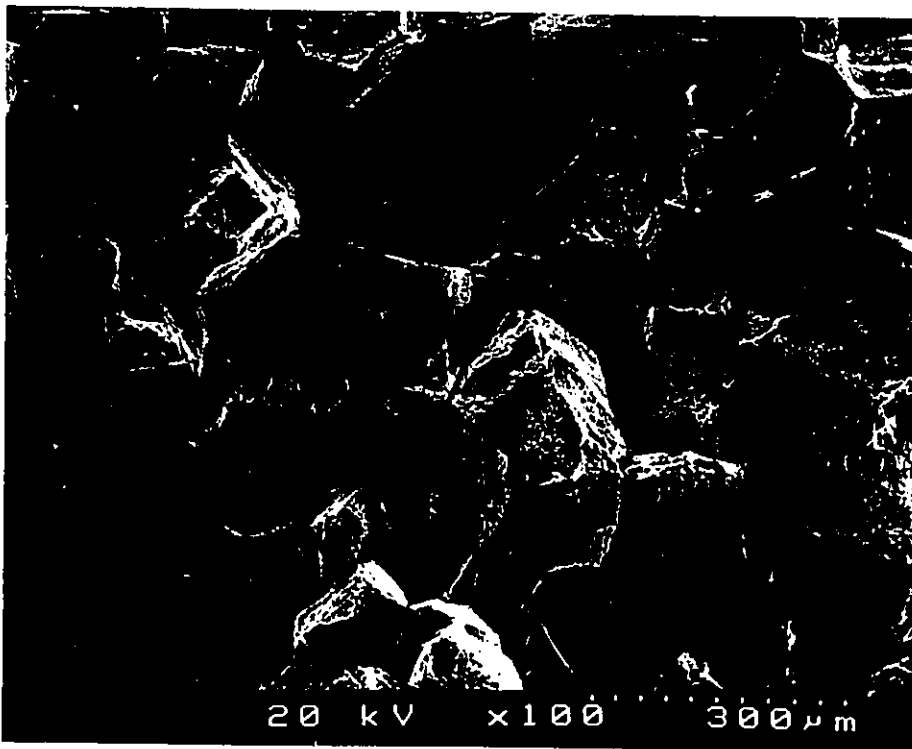


Figure 91. SEM Fractograph of Specimen 13

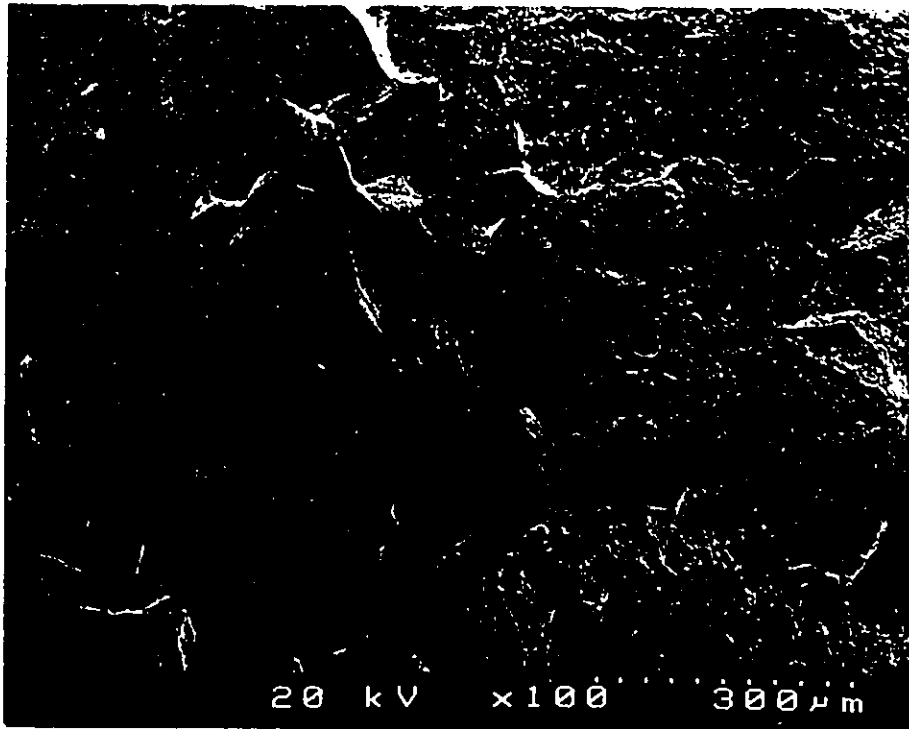


Figure 92. SEM Fractograph of Specimen 14

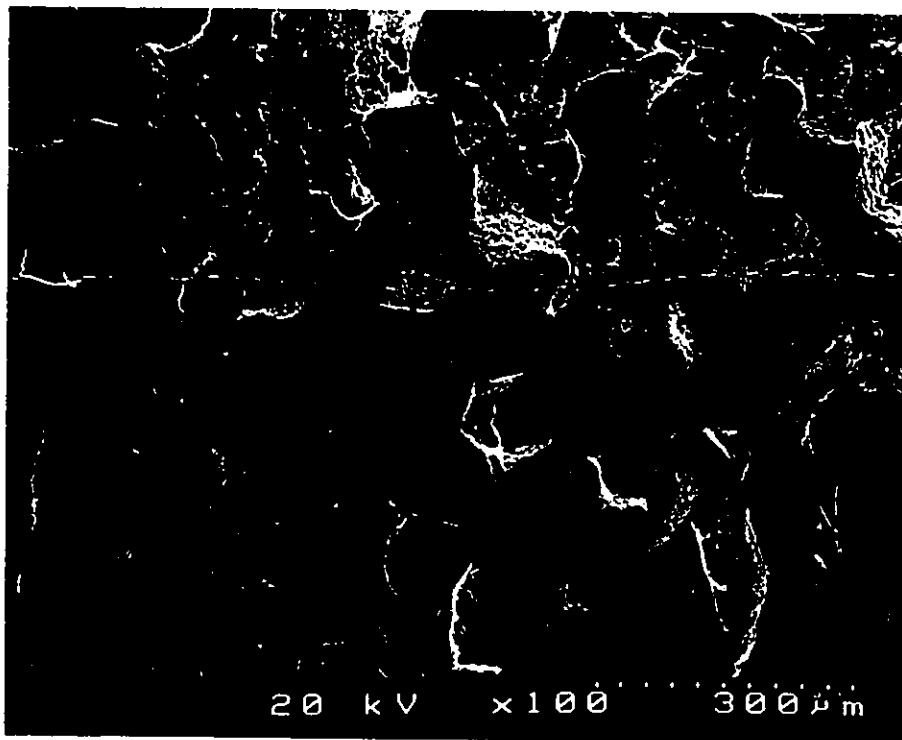


Figure 93. SEM Fractograph of Specimen 15

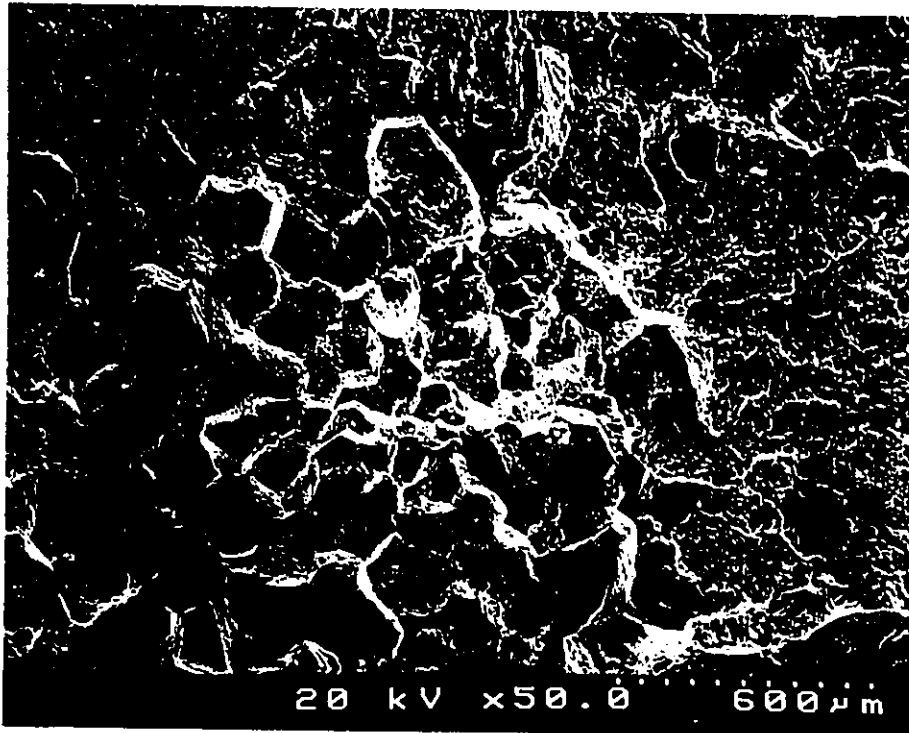


Figure 94. SEM Fractograph of Specimen 16

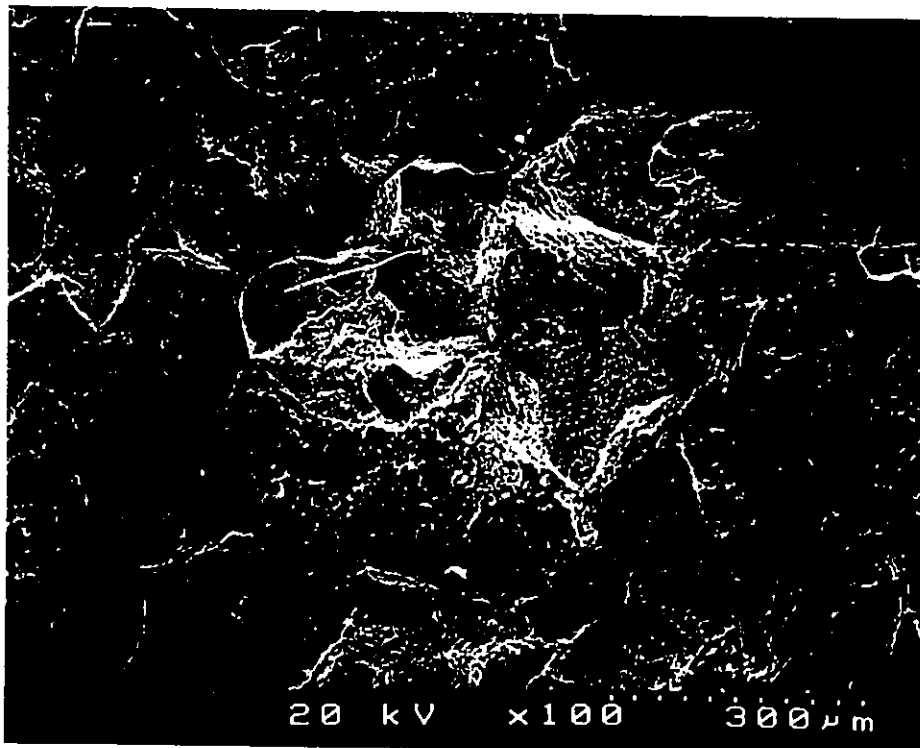


Figure 95. SEM Fractograph of Specimen 17

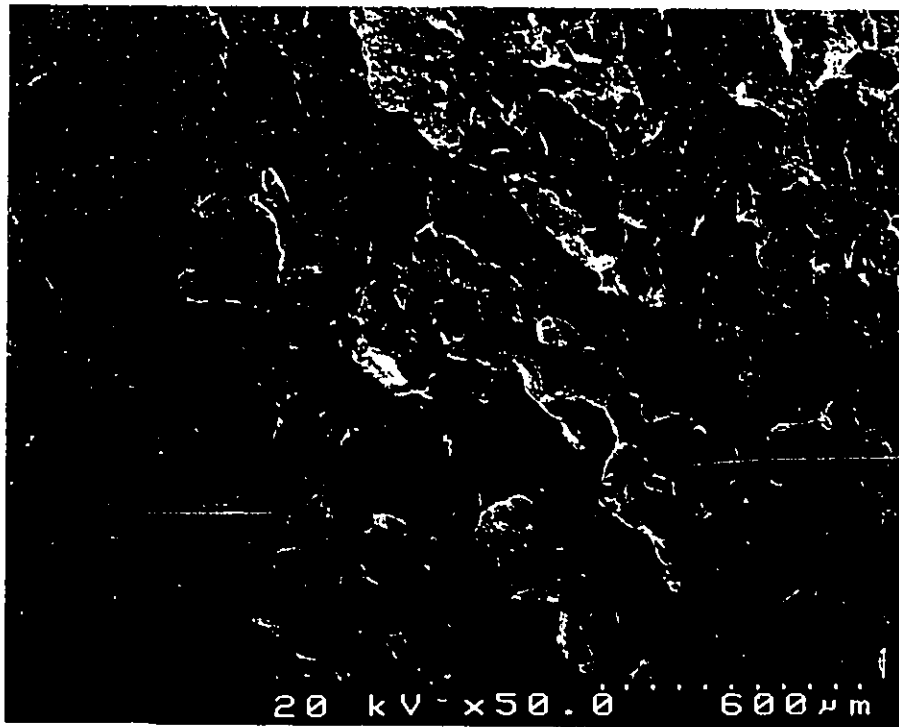


Figure 96. SEM Fractograph of Specimen 18



Figure 97. SEM Fractograph of Specimen 19

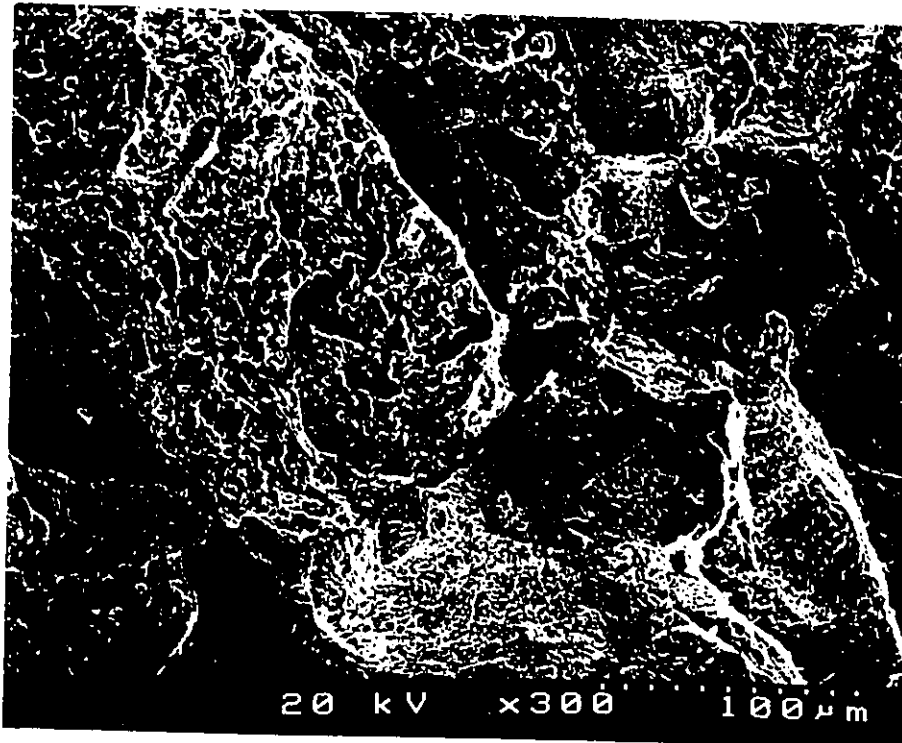


Figure 98. SEM Fractograph Shows the Quasicleavage and the Brittle Fracture

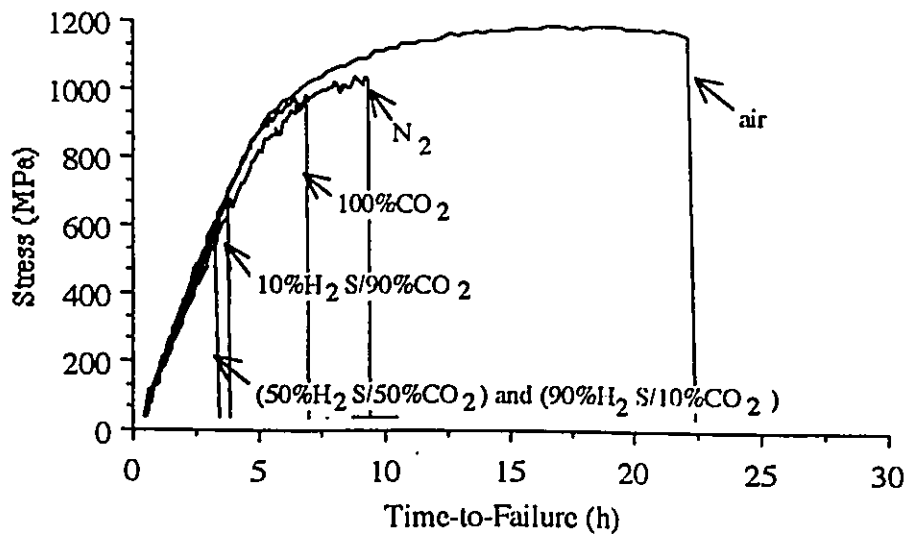


Figure 99. Stress versus Time Curves for 420 Stainless Steel Tempered at 650°C

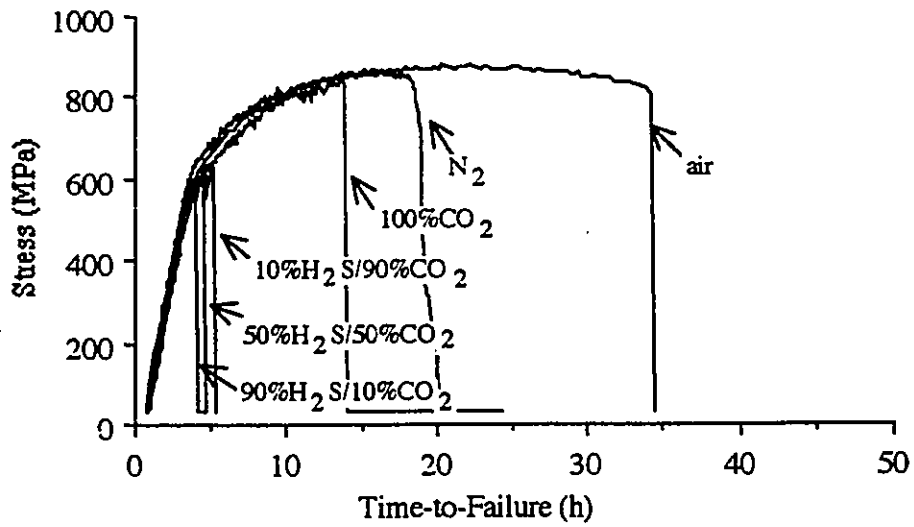


Figure 100. Stress versus Time Curves for 420 Stainless Steel Tempered at 750°C

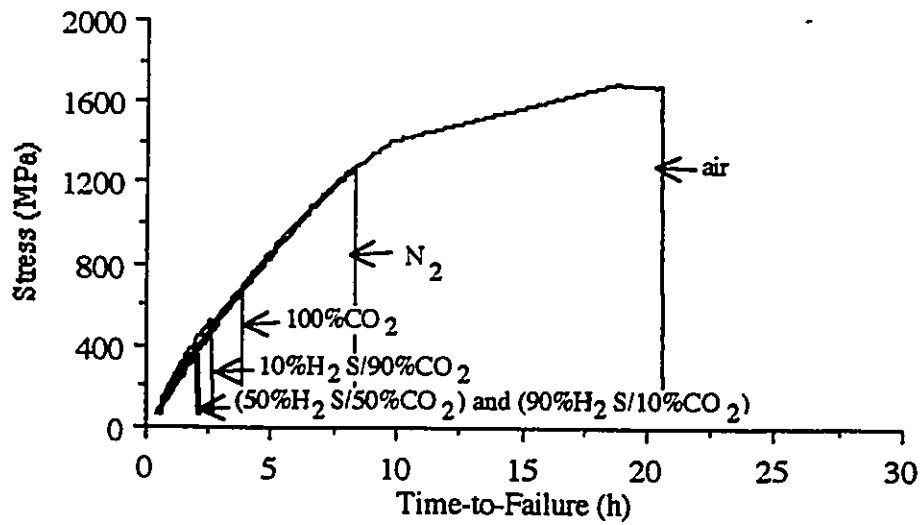


Figure 101. Stress versus Time Curves for 420 Stainless Steel Tempered at 850°C

Bibliography

1. A.I. Asphahani, Evaluation of Highly Alloyed Stainless Materials for CO₂/H₂S Environments, Corrosion, Vol. 37, No. 6, June (1981): p. 327.
2. A.K. Agrawal, W.N. Stiegelmeier, J.H. Payer, Corrosion and Cracking Behavior of a Martensitic 12Cr-3.5NiFe Alloy in Simulated Sour Gas Environments, Materials Performance, Vol. 26, No. 3, (1987): p. 24.
3. R.D. Kane, M. Watkins, J.B. Greer, The Improvement of Sulfide Stress Cracking Resistance of 12%Cr Stainless Steels Through Heat Treatment, Corrosion, Vol. 33, No. 7, (1977): p.231.
4. D.S. Burns, Laboratory Test for Evaluating Alloys for Hydrogen Sulfide Service, Materials Performance, Vol. 15, No. 1, (1976): p. 21.
5. S. Takeno, H. Zoka, T. Niihara, Metastable Cubic Iron Sulfide-With Special Reference to Mackinawite, American Mineralogist, Vol. 55, (1970): p. 1639.
6. P.R. Rhodes, Electrochemical Society Fall Meeting, Extended Abstract No. 107, (1976).
7. B.R.D. Gerus, Detection and Mitigation of Weight Loss Corrosion in Sour Gas Gathering Systems, Symposium on Sour Gas and Crude of the Society of Petroleum Engineers of AIME, Tyler, Texas, November 11-12, (1974).
8. T.A. Ramanarayanan, S.N. Smith, Corrosion of Iron in Gaseous Environments and Gas Saturated Aqueous Environments, Corrosion, January (1990): p. 66.

9. F.F. Lyle, E.B. Norris, Evaluation of Sulfide Stress Corrosion Cracking Resistance of High Strength Steels by The Constant Strain-Rate Method, Corrosion, Vol. 34, (1978): p.193.
10. R.D. Kane, Roles of H₂S in Behavior of Engineering Alloys, International Metals Reviews, Vol. 30, No. 6, (1985): p. 291.
11. B.J. Berkowitz, H.H. Horowitz, The Role of H₂S in the Corrosion and Hydrogen Embrittlement of Steel, Electrochemical Society Journal, Vol. 129, March (1982): p. 468.
12. R.R. Fessler, T.P. Groeneveld, A.R. Elsea, Stress Corrosion and Hydrogen Stress Cracking in Buried Pipelines, in Stress Corrosion Cracking and Hydrogen Embrittlement of Iron Base Alloys. Proceeding of NACE 5 Conference, June 12-16, (1973).
13. T. Taira, Y. Kobayashi, Development of Linepipe for Sour Gas Services, Proceeding Manuscript for 15th Anniversary of The Discovery of Vanadium, The Metal Society at London, October 21-23, (1981).
14. E.M. Moore, J.J. Warga, Factors Influencing The Hydrogen Cracking Sensitivity Of Pipeline Steels, Materials Performance, Vol. 15, No. 6, June(1976): p. 17.
15. J.F. Bates, Sulfide Cracking of High Yield Strength Steels in Sour Crude Oils, Materials Protection, Vol. 8, January (1969): p.33.
16. R.S. Treseder, Oil Industry Experience With Hydrogen Embrittlement and Stress Corrosion Cracking in Stress Corrosion Cracking and Hydrogen Embrittlement of Iron Base Alloys - Proceeding of Conference, NACE 5, June 12-16, (1973).

17. M. Kowaka, S. Nagata, Effects of Strength and Composition on Sulfide Corrosion Cracking of Low Alloy Steels, Metallic Materials, 12th Japanese Congress on Materials Research, March (1969).
18. G.J. Bieffer, M. Fichera, Examination of Steel From Two Failures in The Grizzly Sour-Gas Pipeline, Canmet Report, MRP/PMRL 82-3(GF), March (1982).
19. C.M. Hudgins, Practical Aspects of Hydrogen Damage at Atmospheric Temperature, Bulletin 145, Welding Research Council, October (1979).
20. H.W. Liu, Hu. Lung, P.J. Ficalora, The Control of Catalytic Poisoning and Stress Corrosion Cracking, Engineering Fracture Mechanics, Vol. 5, (1973): p. 281.
21. D.L. Sponseller, R. Carber, J.A. Straatmann, Effect of Microstructure on Sulfide Stress Cracking Resistance of High Strength Casing Steels, — Paper No. 5, Presented at The CIM Conference H₂S Symposium, Edmonton Alberta, August 21- 24, (1983).
22. G.C. Schmid, The Resistance of Nickel Containing Steels and Weld Metals to Sulfide Stress Corrosion Cracking, Corrosion/79, Paper No. 170, Atlanta, Georgia, March (1979).
23. R.S. Treseder, T.M. Swanson, Factors in Sulfide Corrosion Cracking of High Strength Steels, Corrosion, Vol. 24, No. 1, (1968): p. 31.
24. NACE, Materials Requirements; Sulfide Stress Cracking Resistance Metallic Materials for Oil Field Equipment, NACE Standard MR-01-75, Houston, Texas, (1984).

25. T.G. Gooch, Stress Corrosion Cracking of Ferritic Steel Weld Metal - The Effect of Nickel, Part 1 and Part 2, Metal Construction, Vol. 14, (1982): p. 29, 73.
26. A.K. Dunlop, Stress Corrosion Cracking of Low Strength, Low Alloy Nickel Steels in Sulfide Environments, Corrosion, Vol. 34, No. 3, (1978): p. 88.
27. J.B. Greer, Factors Affecting The Sulfide Stress Cracking Performance of High Strength Steels, Materials Performance, Vol. 14, March (1975): p.11.
28. H. Murayama, M. Sakashita, N. Sato, H₂S Catalyzed Hydrogen Absorption In Iron, Hydrogen in Metals, (1979): p. 297.
29. R.A. Oriani, J.P. Hirth, M. Smialowski, Hydrogen Degradation of Ferrous Alloys, Noyes Publications, Park Ridge, N. J., USA, (1985).
30. C.M. Hudgins, R.L. McGlasson, P. Mehdizadeh, W.M. Rosborough, Hydrogen Sulfide Cracking of Carbon and Alloy Steels, Corrosion, Vol. 22, (1966): p. 238.
31. L.M. Dvoracek, Sulfide Stress Corrosion Cracking of Steels, Corrosion, Vol. 26, (1970): p. 177.
32. Miller, Van Rosenberg, Humble Oil and Refining Company Proprietary Report, November (1970).
33. Y. Nakai, H. Kurahashi, N. Totsuka, Y. Wesug, Corrosion/82, Houston, Texas, NACE, Paper No. 132, March (1982).

34. R.D. Kane, J.B. Greer, Sulfide Stress Cracking of High-Strength Steels in Laboratory and Oil Field Environments, Journal of Petroleum Technology, Vol. 29, (1977): p. 1483.
35. C.M. Hudgins, The Effect of Temperature on The Aqueous Sulfide Stress Cracking Behavior of an N-80 Steel, Presented at The NACE Canadian Western Regional Conference, (1971).
36. H.E. Townsend, Hydrogen Sulfide Stress Corrosion Cracking of High Strength Steel Wire, Corrosion, Vol. 28, February (1972): p. 39.
37. R.L. McGlasson, W.D Greathouse, Stress Corrosion Cracking of Oil Country Tubular Goods, Corrosion, Vol. 15, (1959): p. 437t.
38. E.C Greco, W.F. Brickell, SAE 1020 Steel Exposed to H₂S-CO₂-H₂O - Hydrogen Penetration of Steel, Materials Protection, Vol. 15, October (1966): p. 29.
39. M. Hill, E.P. Kawasaki, G.E. Kronbach, Oil Well Casing : Evidence of The Sensitivity to Rapid Failure in an H₂S Environment, Materials Protection, Vol. 11, No. 1, January (1972): p. 19.
40. E. Snape, Roles of Composition and Microstructure in Sulfide Cracking of Steel, - Presented at The 24th Annual Conference, NACE, March 18-22, Cleveland, Ohio, (1968).
41. J.A. Straatman, P.J. Grobner, High Strength H₂S Resistance Steels and Alloys for Oil Field Tubular Products - From Molybdenum Containing Steels for Gas and Oil Industry Applications - A State-of-The-Art-Review-Climax Molybdenum, (1982).

42. W.F. Brickell, E.C. Greco, J.B. Sardisco, Corrosion of Iron in an H₂S-CO₂-H₂O System : Some Factors Affecting Hydrogen Penetration Rate Through 8640 Steel, Corrosion, Vol.21, (1965): p. 48.
43. E. Snape, Sulfide Stress Corrosion Cracking of Some Medium and Low Alloy Steels, Paper Presented to NACE South Central Regional Conference, Shreveport, Louisiana, October 17-20, (1966).
44. A.A. Omar, R.D. Kane, W.K. Boyd, Factors Affecting The Sulfide Stress Cracking Resistance of Steel Weldments, Paper No. 196, Presented at NACE Corrosion/81, Toronto, April 6-10, (1981).
45. P. Damie, M. Traisnel, J.C. Bavay, K. Quang, Corrosion Behavior of 13%Cr Steel in CO₂-H₂S Solutions, Bull. Cercle Etud. Metaux, Vol. 14, March (1980): p. 9.
46. M. Iino, N. Nomura, H. Takezawa, T. Takeda, Engineering Solutions to The H₂S Problems in Linepipes, Proceeding of The First International Conference on Current Solutions to Hydrogen Problems in Steels, Washington, D. C. November 1-5, (1982).
47. Y. Yuichi, Low Alloy Steels in Hydrogen Sulfide Environment, Corrosion, Vol. 38, No. 3, March (1982): p. 156.
48. R. Garber, Higher Hardenability Low Alloy Steels for H₂S Resistant Oil Country Tubulars, Corrosion , Vol. 39, No. 3, March (1983): p. 83.
49. D.D. McAusland, J.A. Webb, Development of Materials and Fabrication Requirements of Oilfield Production Valves in Sour (H₂S/Chloride) Service, The Chemical Engineer, May (1981): p. 229.

50. R.M. Hudson, K.J. Riedly, G.L. Stragand, Influence of Cold Work on Hydrogen Behavior in Steel, Corrosion, Vol. 16, (1966): p. 115t.
51. G.M. Pressouyre, Current Solutions to Hydrogen Problems in Steel, Proceeding of The First International Conference, American Society for Metals, Metals Park, Ohio, (1982): p. 212.
52. J.C. Turn, Jr., B.E. Wilde, C.A. Troiano, On The Sulfide Stress Cracking of Line-Pipe Steels, Corrosion, Vol. 39, No. 9, September (1983): p. 364.
53. A.P. Coldren, G. Tither, Metallographic Study of Hydrogen Induced Cracking in Linepipe Steels, Journal of Metals, Vol. 28, No. 5, May (1976).
54. G.J. Biefer, M.J. Fichera, Sulfide Stress Cracking and Stepwise Cracking Tests on Gas Transmission Linepipes, - Paper No. 4, Presented at CIM Conference - H₂S Symposium, Edmonton, Alberta, August 21-24, (1983).
55. T. Taira, Y. Kobayashi, Resistance of Pipeline Steels to Wet Sour Gas, - Paper Presented to The First International Conference on Current Solutions to Hydrogen Problems in Steel, Washington, D. C., November (1982).
56. E. Miyoshi, T. Tanaka, F. Terasaki, A. Ikeda, Hydrogen Induced Cracking of Steels Under Wet Hydrogen Sulfide Environment, Transactions of the ASME Journal of Engineering for Industry, Vol. 98, No. 4, November (1976): p. 1221-1230.
57. T. Taira, Y.K. Obayashi, Full Size Sulfide Stress Cracking Test Result of Linepipe Under Wet Sour Gas Environments, Paper No. 183, Presented at NACE Corrosion/81, Toronto, April 6-10, (1981).

58. M.G. Fontana, N.D. Greene, Corrosion Engineering, New York, McGraw-Hill, (1967): p. 111.
59. T.V. Bruno, R.T. Hill, Stepwise Cracking of Pipeline Steels - A Review of The Work of Task Group T-1F-20, Corrosion/80, Paper No. 6, NACE, Chicago, Illinois, March (1980).
60. A. Ikeda, T. Kaneko, T. Hashimoto, M. Takeyama, Y. Sumitomo, T. Yamura, Development of Hydrogen Induced Cracking (HIC) Resistant Steels and HIC Test Methods for Hydrogen Sulfide Services, Paper Session II H₂S Symposium at the CIM Conference, Edmonton, August 22-23, (1983).
61. H. Inagaki, M. Tanimura, I. Matsushima, T. Nishimura, Effect of Cu on The Hydrogen Induced Cracking of The Pipeline Steel, Transactions of The Iron and Steel Institute of Japan, Vol.18, No. 3, (1978): p.149.
62. A. Ikeda, T. Kaneko, F. Terasaki, Influence of Environmental Conditions and Metallurgical Factors on Hydrogen Induced Cracking of Linepipe Steel, - Paper No. 8, Presented at NACE Corrosion/80, Chicago, March 3-7, (1980).
63. Y. Nakai, H. Kurahashi, T. Emi, O. Haida, Development of Steels Resistant to Hydrogen Induced Cracking in Wet Hydrogen Sulfide Environment, Transactions of The Iron and Steel Institute of Japan, Vol.19, No. 7, July (1979).
64. T. Taira, Y. Kobayashi, H. Inagaki, T. Watanabe, Sulfide Corrosion Cracking of Linepipe for Sour Gas Service, - Paper No. 171, Presented at NACE Corrosion/79, Atlanta, Georgia, March 12-16, (1979).

65. F. Terasaki, A. Ikeda, M. Takeyama, S. Okamoto, The Hydrogen Induced Cracking Susceptibilities of Various Kinds of Commercial Rolled Steels Under Wet Hydrogen Sulfide Environment, The Sumitomo Search, No. 19, May (1978).
66. M.G. Hay, D.P. Douthett, Control of Hydrogen Induced Cracking in Low Strength Carbon Steel Exposed to Hydrogen Sulfide Environments, First International Conference on Current Solutions to Hydrogen Problems in Steels - ASM, Washington, November (1982).
67. A. Ikeda, S. Mukai, M. Ueda, CO₂ Corrosion Behavior of Carbon and Cr Steels, The Sumitomo Search, No. 31, November (1985): p.91.
68. M. Kowaka, S. Nagata, S., Transgranular SCC of Mild Steels and Low Alloy Steels in The H₂O-CO-CO₂ System, Corrosion, Vol. 24, (1968): p. 427.
69. W.E. Berry, How CO₂ Affects Corrosion of Linepipe, Oil and Gas Journal, Vol. 81, No.7, (1983): p. 160.
70. A. Ikeda, S. Mukai, M. Ueda, Corrosion Behavior of 9 to 25%Cr Steels in Wet CO₂ Environments, Corrosion, Vol. 41, No. 4, April (1985): p. 185.
71. I.L. Crolet, M.R. Bonis, pH Measurements in Aqueous CO₂ Solutions Under High Pressure and Temperature, Corrosion, Vol. 39, No. 2, (1983): p.39.
72. S. Mukai, H. Okamoto, T. Kudo, A. Ikeda, Corrosion Behavior of 25% Duplex Stainless Steel in CO₂-H₂S-Cl⁻ Environments, Journal of Materials for Energy Systems, Vol. 5 No.1, June (1983): p. 59.

73. J.R. Bryant, G.B. Chitwood, Corrosion Behavior of 1 to 22% Chromium Steels and Monel K-500 in CO₂/Brine Environments, Corrosion/83, Paper No. 58, NACE, Houston, Texas, (1983).
74. K. Masamura, S. Hashizuma, K. Nunomura, J. Sakai, I. Matsushima, Corrosion of Carbon and Alloy Steels in Aqueous CO₂ Environment, Corrosion/83, Paper No. 55, NACE, Houston, Texas, (1983).
75. A. Ikeda, S. Mukai, M. Ueda, Relationship Between Environmental Factors and Corrosion Product on CO₂ Corrosion, Transactions of The Iron and Steel Institute of Japan, Vol. 24, No. 12, B-104, (1984).
76. A. Ikeda, M. Ueda, S. Mukai, S., CO₂ Corrosion Behavior and Mechanism of Carbon Steel and Alloy Steel, Proceeding International Corrosion Forum, Corrosion/83 at Anaheim, Paper No. 45, NACE, (1983).
77. A. Ikeda, M. Ueda, S. Mukai, Proceeding International Corrosion Forum, Corrosion/85 at Boston, Paper No. 29, NACE, (1985).
78. A. Ikeda, T. Kudo, Y. Okada, S. Mukai, F. Terasaki, Proceeding International Corrosion Forum, Corrosion/84, at New Orleans, Paper No. 206, NACE, (1984).
79. T. Kudo, H. Miyuki, H. Okamoto, J. Murayama, T. Moroishi, Proceeding International Corrosion Forum, Corrosion/82 at Houston, Texas, Paper No. 127, NACE, 1982.
80. V. Kuznetsov, N. Ohermaya, The Mechanism of The Carbon Dioxide Corrosion of Carbon Steel, Korroz. Zashch, Vol. 8. (1980): p. 2.

81. R. Parkins, C. O'dell, R. Fessler, Factors Affecting The Potential of Galvanostatically Polarized Pipeline Steel in Relation to SCC in CO_3^{--} - HCO_3^- Solutions, Corrosion Science, Vol. 24, (1984): p. 343.
82. J.B. Sardisco, W.B. Wright, E.L. Greco, Corrosion of Iron in an H_2S - CO_2 - H_2O System: Corrosion Film Properties on Pure Iron, Corrosion, Vol. 19, October (1963): p. 354t.
83. Rogne, Norges Tekniske Hoegskole, Internal Corrosion of Offshore Pipelines. Aqueous Corrosion of Steel in $\text{H}_2\text{S}/\text{CO}_2$ Containing Solutions, DE 837 50703 (NTIS), January (1982): p. 43.
84. P. Rhodes, G. Welch, L. Abrego, Stress Corrosion Cracking Susceptibility of Duplex Stainless Steels in Sour Gas Environments, Journal of Materials for Energy Systems, Vol. 5, No.1, June (1983): p.3.
85. J. Oredsson, S. Bernhardsson, The Performance of High Alloyed Austenitic and Duplex Stainless Steels in Sour Gas and Oil Environments, Corrosion/82, Paper No. 126, NACE, Houston, (1982).
86. V.P. Koval, V.Ya. Zhukovskii, L.A. Kuslitskii, Influence of High Partial Pressures of Hydrogen Sulfide and Carbon Dioxide on The Corrosion-Mechanical Properties of Steels, Soviet Materials Science, Vol. 19, (1983).
87. H. Kurahashi, T. Kurisu, Y. Sone, K. Wada, Y. Nakai, Stress Corrosion Cracking of 13Cr Steels in CO_2 - H_2S - Cl^- Environments, Corrosion, Vol. 41, No. 4, April (1985).
88. B.J. Berkowitz, H.H. Horowitz, Journal of Electrochemical Society, Vol. 129, March (1982):p. 468.

89. R. Kane, High-Alloy Tubulars Hold Promise for Sour Service Tolerance, Petroleum Engineer International, Vol. 55, January (1983): p. 98.
90. A. Dunlop, H. Hassell, P. Rhodes, Corrosion/83, Paper No. 46, NACE, (1983).
91. American Society for Metals (ASM), Properties and Selection of Metals, Metals Handbook, 8th Edition.,1961.
92. G.Schmitt, Corrosion/ 83, Paper No. 43, NACE, (1983).
93. F.A. Prange, Mechanical Properties and Corrosion Resistance of Oil Well Tubing, Corrosion, Vol. 15, No. 2, (1959): p. 49t.
94. J. Combes, J. Kerr, L. Klein, 13Cr Tubulars Solve Corrosion Problems in The Tuscaloosa Trend, Petroleum Engineer International, March (1983): p. 50.
95. E.H. Phelps, Stress Corrosion of Ferritic- Martensitic Stainless Steels, Metals Engineering Quarterly, May (1973): p. 44.
96. F. Blount, B. Arnwine, R. Chandler, A Field Study Designed to Select a Tubing Program for Ellenberger Gas-Brown-Bassett Field, Texas, Materials Protection, Vol. 1, December (1962): p. 24.
97. Y. Ishizawa, T. Shimada, M. Tanimura, Effect of Microstructure on the Sulfide Stress Corrosion Cracking Resistance of AISI 410 and 420 Steels, Corrosion/82, Paper No. 124, NACE, Houston, Texas, (1982).
98. A. Ikeda, S.Mukai, Tetsu - to - Hugane, S4186, (1982).

99. S. Mukai, M. Ueda, T. Tsumura, A. Ikeda, Proceeding 4th Asian Pacific Corrosion Conference at Tokyo, May (1985): p. 664.
100. A.E. Durkin, Corrosion Cracking of Martensitic Stainless Steel, Metal Progress, Vol. 64, July (1953): p.72.
101. W.L. Badger, Stress Corrosion of 12%Cr Stainless Steel, SAE Transactions, Vol. 62, (1954): p. 307.
102. F.K. Bloom, Stress Corrosion Cracking of Hardenable Stainless Steels, Corrosion, Vol. 11, No. 4, (1955): p. 351t.
103. C.N. Bowers, W.J. McGuire, A.E. Wiehe, Stress Corrosion Cracking of Steel Under Sulfide Conditions, Corrosion, Vol. 8, October (1952): p. 333.
104. M. Watkins, J.B. Greer, Corrosion Testing of Highly Alloyed Materials for Deep, Sour Gas Well Environments, Journal of Petroleum Technology, Vol.28, June (1976): p. 698.
105. J.P. Fraser, R.S. Treseder, Cracking of High Strength Steels in Hydrogen Sulfide Solutions, Corrosion, Vol. 8, October (1952): p. 343.
106. J.B. Greer, Effect of Metal Thickness and Temperature on Casing and Tubing Design for Deep, Sour Wells, Journal of Petroleum Technology, April (1973): p. 499.
107. J. Prouheze, J. Vaillant, G. Guntz, B. Lefebvre, ASM Metals Congress, 8201-012, (1982).
108. R.W.K. Honeycombe, Steels Microstructure and Properties, Metallurgy and Materials Science Series, Edward Arnold Ltd, London, (1981): p.211.

109. American Society for Metals (ASM), Metallography, Structures and Phase Diagrams, Metals Handbook, Vol. 8, (1973): p. 98.
110. D.R.F. West, Ternary Equilibrium Diagrams, Second Edition, Chapman and Hall Ltd, London, (1981): p. 104.
111. American Society for Metals (ASM), Heat Treating, Cleaning, Metals Handbook, Ninth Edition, Vol. 4, (1973): p. 248.
112. J.G. Parr, A. Hanson, An Introduction to Stainless Steel, ASM, (1965): p. 32.
113. F. Mancina, The Effect of Environmental Modification on The SSC Resistance of 13%Cr Martensitic Stainless Steels in H₂S - CO₂ - Cl⁻ Systems, Corrosion Science, Vol.27, (1987): p. 1225.
114. L.J. Klein, Proceeding International Corrosion Forum, CORROSION 84, New Orleans, Paper No. 211, (1984).
115. J.P. Hirth, Effects of Hydrogen on the Properties of Iron and Steel, Metallurgical Transactions A, Vol. 11A, (1980): p. 861.
116. R.A. Oriani, B. Bunsenges, Journal of Physical Chemistry, Vol. 76, (1972): p. 848.
117. V. Strikrishnan, H.W. Liu, P.J. Ficalora, Selective Chemisorption and Hydrogen Embrittlement - The Role of H₂S, Scripta Metallurgica, Vol. 9, (1975): p. 1341.
118. V. Strikrishnan, H.W. Liu, P.J. Ficalora, Selective Chemisorption and Hydrogen Embrittlement, Scripta Metallurgica, Vol. 9, (1975): p. 663.

119. T. Rosengvist, Principles of Extractive Metallurgy, 2nd Edition, McGrawHill Book Co., New York, (1983): p. 497, 486.
120. J.B. Sardisco, R.E. Pitts, Corrosion of Iron in an H₂S-CO₂-H₂O System Composition and Protectiveness of The Sulfide Film as a Function of pH, Corrosion, Vol. 21, (1965): p. 350.
121. E.M. Moore, J.J. Warga, Factors Influencing The Hydrogen Cracking Sensitivity of Pipeline Steels, Corrosion/76, March 22-26, Houston, Texas, (1976).
122. A. Ikeda, M. Kowaka, Stress Corrosion Cracking of Low and High Strength Steels in Wet H₂S Environment, Chemical Economy and Engineering Review, Vol. 10, No. 5-6, No. 117, May/June (1978): p. 12.
123. J. Murali, 13Cr Stands Above Low-Alloy Steel OCTG, Part 1, Oil and Gas Journal, Vol. 82, July 9 (1984): p. 104.